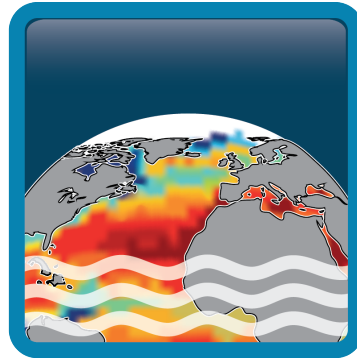


Climate Change Initiative+ (CCI+) Phase 1

Sea Surface Salinity



Product Validation and Intercomparison Report (PVIR)

Customer: ESA

Ref.: ESA-CCI-PRGM-EOPS-SW-17-0032

Version: v1.1

Ref. internal: AO/1-9041/17/I-NB_v1r2




Revision Date: 07/04/2020

Filename: SSS_cci-D4.1-PVIR-v1.1.docx

Deliverable code: D4.1



Signatures

	Name	Signature	Date
LEAD AUTHOR	Adrien Martin (NOC)		07/04/2020
APPROVED BY	Jacqueline Boutin (Science Leader) LOCEAN		07/04/2020
	Nicolas Reul (Science Leader) IFREMER		
	Rafael Catany (Project Manager) ARGANS		07/04/2020
ACCEPTED BY	Craig Donlon (Technical Officer) ESA		

DIFFUSION LIST
Sea Surface Salinity Team Members
ESA (Craig Donlon, Paolo Cipollini)

Amendment Record Sheet

Document Change Record		
Date / Issue	Description	Section / Page
15-Oct-2019/v1r1	Template	Whole document
24-Dec-2019/v1r2	Final draft distributed to the team involved in validation	Whole document
10-Jan-2020/v1.0	Final Distribution to ESA	
7-Apr-2020/v1.1	The document has been updated using ISAS at 5 m depth, using only data with PCTVAR<95%. Comparison between ISAS and CCI has been proceeded on CCI grid not to affect CCI uncertainty estimate.	Section 4 / 27-54
	Old section 5.4.1 about comparison between CCI and CMEMS in river plume has been removed from the PVIR and included in the CAR.	Section 5.4.1 / p 71
	section 5.5 about case study 5: comparing salinity variability between observations and models has been added to the document (originaly was in the CAR)	Section 5.5 / p.74
	Four figures from Pi-MEP match-up mooring report representing SSS power spectra have been included in Annex C.	Annex C / p.115
	Update of the executive summary	Section 2 / p. 19-21
	A sentence to summarize what specific improvements of SMOS in the Bay of Bengual has been added.	Section 5.3 / p. 64
	The document has been reviewed for spelling/grammar/typos errors	Whole document

Table of Contents

Signatures	iii
Amendment Record Sheet	v
List of figures	ix
List of tables	xiii
1 Introduction	14
1.1 Purpose and scope.....	14
1.2 Structure of the document	14
1.3 Applicable Documents.....	14
1.4 Reference Documents.....	15
1.5 Acronyms.....	16
2 Executive Summary	19
2.1 Main results from the systematic validation of CCI (section 4).....	19
2.2 Main validation results from case studies (section 5).....	20
2.3 Main results from Pi-MEP match-up reports (Annex A, B and C).....	20
2.4 Recommendations and caveats to use CCI+SSS dataset	21
3 Validation: Data & Methods	22
3.1 Dataset description	22
3.1.1 Argo	22
3.1.2 ISAS.....	23
3.2 Uncertainty validation.....	24
3.3 Quality metrics	26
4 Validation of products, long-term stability and product uncertainty estimates	27
4.1 Over global ocean.....	27
4.1.1 Products and long-term stability	27
4.1.2 Product uncertainty estimates	35
4.2 Regional Studies	38
4.2.1 Atlantic Ocean	38
4.2.2 Pacific Ocean	43
4.2.3 Indian Ocean	46
4.2.4 High-latitudes: Southern Ocean; Arctic Ocean	48
4.3 Over regions of high SSS variability	50
4.4 Over region of low SSS variability.....	51
5 Validation for climate case studies	54
5.1 Case Study 1: North Atlantic salinity anomaly (Adrien Martin, Simon Josey; NOC)	54
5.2 Case study 2: SSS and SSS error validation in the tropical Atlantic Ocean (Léa Olivier, Gilles Reverdin, J. Boutin, LOCEAN):	60
5.3 Case study 3: Water cycle in the Bay of Bengal (Jérôme Vialard; LOCEAN).....	63
5.4 Case study 4: Salinity stratification and small-scale variability (N. Reul, N. Kolodziejczyk, O. Houdegnonto, C. Maes and T. O’Kane; LOPS).....	65
5.4.1 SSS Mesoscale features in CCI+SSS products	65
5.4.2 Validation of SSS+CCI products in the Gulf of Guinea.....	69

5.5 Case study 5: Comparing salinity variability between observations and models (D. Stammer, J. Köhler, M. Sena-Martins, A. Köhl; UHAM)	73
<i>Annex A: Pi-MEP validation report againsts Argo</i>	79
<i>Annex B: Pi-MEP Satellite precision comparison against Argo</i>	113
<i>Annex C: Pi-MEP</i>	114

List of figures

Figure 1: SSS fields for the 15th of January 2015 for (top) CCI monthly product; (middle) Argo profiles top measurements; (bottom) ISAS at 1m depth. All subfigures share the same colourbar.

----- 28

Figure 2: Temporal median of SSS differences computed over the whole period (2010-2018) (in pss) between CCI and (top) Argo profiles are re-gridded on 3 x 3 under sampled 25 km EASE grid. Grid points with less than 5 observations are discarded and (bottom left) ISAS represented as the annual median difference. (bottom right) Annual median SSS error as percentage of the variance. The colourbar is not linear with levels at [0,50,80,90,95,100].

----- 29

Figure 3: Seasonal climatology of the CCI difference with ISAS calculated using the median.---

29

Figure 4: (bar plot) Normalised histogram of the SSS difference between CCI and Argo globally for the full time period. Statistics are indicated on the top left of the figure. (blue curve) Normal distribution computed from the mean and standard deviation. (orange curve) Normal distribution computed from the median and robust standard deviation based on IQR. Both normal distributions are adjusted to the peak.

----- 30

Figure 5: (top) Average of; (middle) standard deviation of; the SSS difference between CCI and (solid line) ISAS, (dotted line) Argo as function of time for the full open ocean where CCI products exist. Blue curves represent (top) the mean (middle) standard deviation. Orange curves represent (top) the median and (middle) the robust standard deviation based on IQR. (bottom) represents number of observations for collocation with Argo profiles for each time step.

----- 31

Figure 6: Global latitude-time Hovmöller of the CCI difference with (top) Argo with latitude bins of 4°, with monthly timestep. Each pixel represents the median value when there are more than 30 observations. Otherwise no value is shown. (bottom) median value at the same spatiotemporal scale as the ISAS field.

----- 33

Figure 7: Latitudinal band (20° wide) averaging (using median) of the salinity difference between CCI SSS and ISAS from (top) to (bottom) of [60°N;80°N] to [60°S;80°S]. Y-scale for the top panel is five time bigger than for other panels. Blue curves represent the median for the band in latitude and longitude for each time step. Orange curves are the anomaly after removing a median climatology calculated from blue curves. Green curves are an annual rolling mean of orange curves.

----- 34

Figure 8: (top) Number of Argo floats observations per satellite per uncertainty bins. (bottom) Distribution of the CCI difference with Argo floats observation for each bin of uncertainty including satellite random error and representativeness error. Vertical green bars represent the standard deviation. Red crosses represent the robust standard deviation. The green dashed lines is the theoretical relation between the measured uncertainty and the estimate. Bins are 0.05 pss wide starting from 0.05 pss.

----- 36

Figure 9: Measured standard deviation of the difference between (left) CCI and Argo; (right) CCI and ISAS for each uncertainty bins. Green dots are for standard deviation estimate; red dots for robust standard deviation.

----- 36

Figure 10: (top left) total estimated uncertainty error in pss from the satellite random error and the representativeness error. Uncertainty for the 15/01/2015. (top right) observed uncertainty as the standard deviation of the SSS difference between CCI and ISAS. (top) the colourbar is not

linear, steps are [0,0.1,0.2,0.3,0.5,1]. (bottom) Ratio of the observed over estimated total uncertainty.-----	37
Figure 11: As Figure 2 but only showing Atlantic Ocean (in pss). -----	38
Figure 12: As Figure 5 but for the area defined for the Atlantic Ocean (Figure 11). -----	39
Figure 13: As Figure 6 but for the area defined for the Atlantic Ocean (Figure 11) using ISAS.--	39
Figure 14: As Figure 7 but for the area defined for the Atlantic Ocean (Figure 11) -----	41
Figure 15: As Figure 2 but only showing Pacific Ocean (in pss). -----	43
Figure 16: As Figure 5 but for the area defined for the Pacific Ocean. -----	43
Figure 17: As Figure 6 but for the area defined for the Pacific Ocean using ISAS.-----	44
Figure 18: As Figure 7 but for the area defined for the Pacific Ocean.-----	45
Figure 19: As Figure 2 but only showing the Indian Ocean (in pss).-----	46
Figure 20: As Figure 5 but for the area defined for the Indian Ocean.-----	46
Figure 21: As Figure 6 but for the area defined for the Indian Ocean using ISAS. -----	47
Figure 22: As Figure 7 but for the area defined for the Indian Ocean.-----	48
Figure 23: As Figure 2 but zoomed over the high latitudes: (top) Southern Ocean; (bottom) Arctic Ocean. (middle) is the SSS error are percentage of the variance on. Indian Ocean. (top/bottom left) with Argo. Grid point with less than 5 observations are discarded. (top/bottom right) with ISAS.-----	49
Figure 24: Temporal correlation of SSS between CCI and ISAS on ISAS grid cell in colour from -1 to +1. (top) for the global ocean. (bottom left) for the portion of the ocean with highest SSS variability observed from CCI (absolute maximum departure from CCI climatology > 0.8 pss). (bottom right) histogram of the correlation limited to the area with highest variability.-----	50
Figure 25: In yellow, ocean area with low variability where the absolute maximum departure from CCI SSS climatology is below 0.4 pss. It corresponds to half the ocean surface. -----	51
Figure 26: As Figure 4 but for the area defined by its low variability as represented in Figure 25. -----	52
Figure 27: As Figure 5 but for the area defined by its low variability. -----	52
Figure 28: As Figure 7 but for the area defined by its low variability. -----	53
Figure 29: Annual mean of CCI climatology based on the 2012-onward time series. Boxes represent areas selected for time series comparison below. Violet for the equatorial box; white for the Caribbean box, red for the sub-tropical box and black for the sub-polar box. -----	54
Figure 30: Seasonal cycle represented as the anomaly from annual mean (top) for CCI, top four panels, (bottom) ISAS CMEMS, following 4 panels. Season are defined with first letter of each month. DJF for winter; MAM for spring, JJA for summer and SON for winter.-----	55

Figure 31: CCI anomaly from climatology (2012-2018) with season for the different columns and years for the rows.-----	56
Figure 32: Example of SSS field strongly affected by RFI from the Southern part of Greenland.	57
Figure 33: Time series for the four boxes defined above (one box per row). (Left column) for the time series averaged over the box for the different fields, CCI in green; ISAS CMEMS Delayed mode in orange; ISAS 2015 in red; on close-to-surface Argo measurements averaged over the box in blue. (Right column) Anomaly to the climatology computed over each box.-----	58
Figure 34: Climatology for the four boxes.-----	59
Figure 35: a) In blue are represented the CCI salinity gradients and in orange the ship ones for the 15th of October 2015. b) Same as a) but with an average on 5 pixels in longitude.-----	61
Figure 36: a) The blue curve represents the RMS of the errors given in the CCI product, while the orange curve presents the STD of the difference between the salinity CCI and the salinity from the ships. b) Same as a) but for the errors on the gradient (blue) and the standard deviation of the salinity gradient's difference (orange). c,d) same as a,b) for the monthly product.-----	62
Figure 37: Comparison of the CCI+SSS product to co-located in situ SSS data in the Bay of Bengal, over the common observational sample with (a) SMOS, (b) Aquarius and (c) SMAP data. The CCI SSS has a higher correlation, smaller root-mean square difference and smaller bias relative to observations than all the other datasets.-----	63
Figure 38: CCI+SSS on 30 June 2011. 88 SSS TSG transects in the Subtropical North Atlantic (dashed) and 26 SSS TSG transect in the Tropical Atlantic. All SSS transects have been carried out between 2011-2016.-----	66
Figure 39: Upper panel: Density spectra from from 88 co-located TSG(black)/CCI+SSS(red) SSS transects in Subtropical North Atlantic. Vertical thick black bar is the level of confidence at 95%. Lower panel: Coherency between the TSG and CCI+SSS SSS transects. Dashed line is the level of significance at 95%.-----	67
Figure 40: Upper panel: Density spectra from 26 colocated TSG(black)/CCI+SSS(red) SSS transects in Tropical Atlantic. Vertical thick black bar is the level of confidence at 95%. Lower panel: Coherency between the TSG and CCI+SSS SSS transects. Dashed line is the level of significance at 95%.-----	68
Figure 41: Upper panel: scatter plot of TSG SSS measurements (left) and Argo/CTD data (right) with the CCI+SSS products in the Gulf of Guinea (15°S-10°N/10°W-15°E) over the period 2011-2017. Lower panel: distribution of the difference of co-located in situ/CCI+SSS (in pss) as a function of the distance from the coast.-----	70
Figure 42: Signal to noise ratio (SNR) by assuming random white noise for the CCI+SSS product. The higher the value, the larger the signal. SNR<1 means that noise is higher than signal.-----	73
Figure 43: (left) Correlation of seasonal satellite SSS and uppermost EN4 salinity and (right) ratio of the annual amplitude of the difference between satellite CCI+SSS and EN4 uppermost salinity and the annual amplitude of the EN4 uppermost salinity. High values indicate that the annual cycle of differences between satellite and EN4 uppermost salinities is larger than the annual salinity cycle. This could be due to salinity stratification but also due to land-ice-contamination,	

RFI or sample errors in the in situ fields. The ratio shows high values in high latitudes, but also in subtropical/mid-latitude regions, where the amplitude of the annual cycle is generally low.--- 74

Figure 44: STD in high-pass (<3 months) filtered time series of each grid point in the EN4 data (top), the high-pass filtered CCI data (middle); the high-pass filtered model SSS data (bottom).
----- 76

Figure 45: Pi-MEP comparison of satellite precision (standard deviation) against Argo of a wide range of satellite products.-----113

Figure 46: Pi-MEP CCI comparison report with moorings. Power spectrum of SSS from moorings, CCI (top; weekly), (bottom; monthly) products, ISAS and Mercator for the TAO mooring/match-up time series at 2°S; 140°W. -----114

Figure 47: Pi-MEP CCI comparison report with moorings. Average of all SSS power spectra for all moorings/match-up from moorings, CCI (top; weekly), (bottom; monthly) products, ISAS and Mercator.-----115

List of tables

Table 1 – Applicable documents (as seen in CCI+SSS website, http://cci.esa.int/salinity) -----	14
Table 2 – Reference documents -----	15
Table 3: Statistics from in situ/CCI+SSS products difference for co-localisation in the Gulf of Guinea over the period 2011-2017. -----	71



1 Introduction

1.1 Purpose and scope

The purpose of this document (D.4 Product Validation and Intercomparison Report, PVIR, document version v1.0) is to describe the results of the validation of the Sea Surface Salinity (SSS) products obtained during the ESA CCI+ SSS project when compared with other data sources. The PVIR is a requirement of the Statement of Work (Task 3 SoW ref. ESA-CCI-PRGM-EOPS-SW-17-0032). The PVIR contains a list of all reference datasets used for validation of each SSS product.

Two products are assessed, the level 4 (1) monthly and (2) weekly products based on a temporal optimal interpolation of SSS data measured by SMOS, Aquarius-SAC and SMAP satellite missions. Both gridded products have a resolution of ~25 km on an EASE 2 grid.

1.2 Structure of the document

This document is composed of six sections:

Section 1 introduces the purpose and scope of the document. Section 2 provides an executive summary of the results presented. Section 3 presents the data and methods used for the systematic validation presented in Section 4. Section 5 presents validation results obtained for each case study. Annex A reproduces the global ocean Argo Pi-MEP report. Annex B compares the precision against Argo of a wide range of satellite products (including the CCI monthly and weekly products).

1.3 Applicable Documents

PSD	Product Specification Document	SSS_cci-D1.2-PSD-v1r6
PUG	Product User Guide	SSS_cci-D4.3-PUG-v1.1
PVP	Product Validation Plan	SSS_cci-D2.5-PVP-v1.1
SoW	CCI+ Statement of Work	SOW

Table 1 – Applicable documents (as seen in CCI+SSS website, <http://cci.esa.int/salinity>)



Climate Change Initiative+ (CCI+)
Phase 1
Product Validation and
Intercomparison Report

Ref.: ESA-CCI-PRGM-EOPS-SW-17-0032
Date: 07/04/2020
Version : v1.1
Page: 15 of 115

1.4 Reference Documents

ID	Document	Reference
RD01	Product Validation Plan	
RD02	Pi-MEP consortium, March 2019; Match-up database Analyses report, CCI-L4-ESA-MERGED-OI-V1.5-MONTHLY Argo Global Ocean: pimep-mdb-report_GO_cci-l4-esa-merged-oi-v1.5-1m_argo_20190315.pdf	
RD03	G. Reverdin, S. Morisset, L. Marié, D. Bourras, G. Sutherland, B. Ward, J. Salvador, J. Font, Y. Cuyppers, L.R. Centurioni, V. Hormann, N. Koldziejczyk, J. Boutin, F. D’Ovidio, F. Nencioli, N. Martin, D. Diverres, G. Alory & R. Lumpkin (2015). Surface salinity in the North Atlantic subtropical gyre during the STRASSE/SPURS summer 2012 cruise. <i>Oceanography</i> 28 (1): 114-123	
RD04	N. Hoareau, A. Turiel, M. Portabella, J. Ballabrera-Poy & J. Vogelzang (2018). Singularity Power Spectra: A Method to Assess Geophysical Consistency of Gridded Products - Application to Sea-Surface Salinity Remote Sensing Maps. <i>IEEE Transactions on Geosciences and Remote Sensing</i> 56, 5525-5536	

Table 2 – Reference documents



Climate Change Initiative+ (CCI+)
Phase 1
Product Validation and
Intercomparison Report

Ref.: ESA-CCI-PRGM-EOPS-SW-17-0032
Date: 07/04/2020
Version : v1.1
Page: 16 of 115

1.5 Acronyms

CAR	Climate Assessment Report
CCI	The ESA Climate Change Initiative (CCI) is formally known as the Global Monitoring for Essential Climate Variables (GMECV) element of the European Earth Watch programme
CCI+	Climate Change Initiative Extension (CCI+), is an extension of the CCI over the period 2017–2024
CDR	Climate Data Record
CMEMS	Copernicus Marine Environmental Monitoring Service
CMIP	Coupled Model Intercomparison Project
CMUG	Climate Modelling User Group
CRDP	Climate Research Data Package
CRG	Climate Research Group
DARD	Data Access Requirements Document
EASE-2	Cylindrical Equal Area Scalable Earth grid 2.0
ECMWF	European Centre for Medium Range Weather Forecasts
ECV	Essential Climate Variable
FRM	Fiducial Reference Measurements
ISAS	In-Situ Analysis System
ISDB	in situ database (of Fiducial Reference Measurements and satellite measurements)
MDB	Match-up DataBase
Pi-MEP	Pilot Mission Exploitation Platform
PMP	Project Management Plan
PSD	Product Specification Document



Climate Change Initiative+ (CCI+)
Phase 1
**Product Validation and
Intercomparison Report**

Ref.: ESA-CCI-PRGM-EOPS-SW-17-0032

Date: 07/04/2020

Version : v1.1

Page: 17 of 115

PUG	Product User Guide
PVIR	Product Validation and Intercomparison Report
PVP	Product Validation Plan
QA4EO	Quality Assurance Framework for Earth Observation
RFI	Radio Frequency Interference
SISS	Satellite and In situ [Working Group]
SMAP	Soil Moisture Active Passive [mission of NASA]
SMOS	Soil Moisture and Ocean Salinity [satellite of ESA]
SoW	Statement of Work
SSS	Sea Surface Salinity
TSG	ThermoSalinoGraph
UCR/CECR	Uncertainty Characterisation Report (formerly known as the Comprehensive Error Characterisation Report)
UNFCCC	United Nations Framework Convention on Climate Change
URD	User Requirements Document



2 Executive Summary

The products validated are:

- Monthly: ESACCI-SEASURFACESALINITY-L4-SSS-MERGED-OI-Monthly-CENTRED-15Day-25km-xxxxxxx-fv1.6
- Weekly: ESACCI-SEASURFACESALINITY-L4-SSS-MERGED-OI-Weekly-CENTRED-1Day-25km-xxxxxxx-fv1.6

The different CCI products from versions 1.5 to 1.8 have identical values for all variables and only differ by their metadata. Full description of the dataset can be found in the Product User Guide (PUG). The products follow recommendations of the Product Specification Document (PSD). Both products cover all open water seas with a spatial resolution of 25 km.

2.1 Main results from the systematic validation of CCI (section 4)

- In situ references data are Argo floats upper salinity measurement between 0 m and 10 m and ISAS at 5 m;
- Need to take robust estimator (median, standard deviation based on IQR, ...) to be robust to non-normal distribution and fairly representative of the behaviour of more than 50% of the observations;
- No systematic bias against reference data;
- Global precision against reference data is of 0.16 pss (0.10 pss in areas with low variability)
- Good agreement between CCI and reference data, including long-term stability, differences within ± 0.05 pss for:
 - Atlantic Ocean for the latitudinal band [40°S-20°N];
 - Pacific Ocean for the latitudinal band [40°S-20°N];
 - Indian Ocean for the latitudinal band [40°S-0°].
- Strong seasonal oscillation of CCI SSS differences against references:
 - CCI are fresher/saltier in Winter/Summer than references;
 - Amplitude is maximum at high latitudes ($>60^\circ$) reaching 1 pss peak-to-peak;
 - Seasonal amplitudes of more than 0.2 pss are observed in the Atlantic Ocean for the latitudinal band [40°N-60°N]; in the Pacific Ocean [20°N-60°N] and the Indian Ocean between 0°-20°N.
- CCI SSS is higher than reference data in the beginning of the time series (2010) up to 2012 with an amplitude up to 0.1 pss;
- CCI data in the Arctic and Southern Ocean have not been properly validated as there are limited suitable in situ references;
- Good agreement between CCI uncertainties estimate plus spatial representativeness error with observation of the error distribution.



2.2 Main validation results from case studies (section 5)

- North Atlantic:
 - Strong impact of RFI on CCI SSS before 2012;
 - Good agreement between CCI and in situ observations in three out of four Case Study regions (Equatorial, Caribbean, sub-tropical gyre) for both intra- and inter-annual variability
 - Sub-polar gyre: weak agreement for the intra-annual variability between CCI and in situ measurements; opposite trend between CCI and references.
- SSS and SSS errors validation in the tropical Atlantic Ocean
 - Good agreement between CCI and TSG data in the intertropical convergence zone
 - Uncertainty for CCI weekly product overestimated by approximately 40%
- Water cycle in the Bay of Bengal
 - Improved performance of CCI products compared to previous state of the art satellite products
- SSS mesoscale features in CCI products
 - TSG and CCI spectra show good agreement, i.e. comparable spectral slopes between 50-1000 km are observed.
 - Subtropical Atlantic: CCI+SSS products resolve wavelengths of ~300 km (150 km eddy)
- Gulf of Guinea
 - very good agreement between CCI and in situ measurements;
 - insignificant bias (~0.01 pss) against in situ measurements (TSG, Argo and ship based CTD);
 - RMSD ranging from 0.43 pss for the comparison with TSG data and 0.35 pss for the comparison with the Argo and CTD data.
- Salinity variability in observations and models
 - Magnitude of SSS variability is 1.5 times higher for CCI than EN4 observations;
 - Larger differences in the gulf stream region, Amazon outflow, eastern tropical Pacific, north-eastern Indian Ocean and around the maritime continent.
 - High-frequency and sub-seasonal variability is enhanced in a band around the equator and in regions of river outflow.

2.3 Main results from Pi-MEP match-up reports (Annex A, B and C)

- No global bias against Argo except for filtered collocations where:
 - SSS less than 33 pss (CCI saltier by 0.06 pss);
 - Mixed layer depth shallower than 20m (CCI saltier by 0.04 pss);
 - SST lower than 5°C (CCI saltier by 0.02 pss);
 - SSS higher than 37 pss (CCI fresher by 0.04 pss);



**Climate Change Initiative+ (CCI+)
Phase 1
Product Validation and
Intercomparison Report**

Ref.: ESA-CCI-PRGM-EOPS-SW-17-0032
Date: 07/04/2020
Version : v1.1
Page: 21 of 115

- Global precision against Argo of 0.16 pss
 - Decreasing to 0.13 pss for optimal region (>800 km from the coast; area with temporal standard deviation smaller than 0.2 pss)
 - Increasing to 0.27 pss for area closer than 150 km from the coast
 - Increasing to 0.20 pss for area characterised by one of the following conditions: rain and low wind; mixed layer depth <20m; area with temporal standard deviation >0.2pss; SSS < 33 pss.
- Comparison with other 29 satellite SSS products against Argo
 - CCI products have the best precision (and no bias) except for Aquarius L4 IPRC v5 products.
 - Same precision for the monthly and weekly products.
- SSS power spectra at mooring position are similar with in-situ and Mercator up to a period of:
 - About 14 days for the weekly CCI product
 - About 50 days for the monthly CCI product

2.4 Recommendations and caveats to use CCI+SSS dataset

Below are the caveats mentioned with the distribution of the public version 1.8 of the CCI+SSS phase 1 data: <https://catalogue.ceda.ac.uk/uuid/9ef0ebf847564c2eabe62cac4899ec41>

CAVEATS

- The SSS random error in the weekly product is overestimated by a factor ~1.4.
- The number of outliers is wrongly set to 'NaN' in the case where it is equal to zero.
- Products have not yet been not optimised for some issues encountered at high latitudes (i.e. ice, RFI, biases due to land-sea contamination and dielectric constant in cold waters).
- The criteria for flagging data close to land (including islands) are conservative and likely to be too restrictive in places.
- There is a systematic global underestimation (-0.08) of SSS starting at the beginning of the dataset, and gradually disappearing at the end of 2010.
- There is a seasonal varying bias (~0.1, peaking in the middle of the year) north of 25°N in the Pacific.



3 Validation: Data & Methods

This section describes the Data and Methods used for the main validation results given in section 4. Data and methods used for the case studies (presented in section 5) are described in the corresponding sections of section 5.

Following PVP [RD1] recommendations, the reference dataset used for product validation consists of:

- In situ measurements of close-to-surface (<10 m) Argo from Pi-MEP
- Interpolated maps of ISAS Near Real Time (NRT) product available on Copernicus Marine Environment Service

The reason for these choices of reference dataset are as follows:

- In the list of acceptable Fiducial Reference Measurements (FRM) referred to in PVP [RD1], the Argo dataset has been selected as it is the only dataset to have a nearly homogeneous spatial sampling of global open water ocean. The temporal distribution from 2010 is also homogeneous [Pi-MEP – RD2].
- To cover the longest possible time series concomitant with the CCI+SSS products with a single dataset of interpolated maps, the NRT ISAS product has been chosen.

In the following, both datasets are described with their collocation criteria along with the method to estimate uncertainties and representativeness errors. A summary of the spatial representativeness error of in situ measurement, as described in the PVP [RD1], is given here. Finally, quality metrics to assess CCI products are presented.

3.1 Dataset description

3.1.1 Argo

The Argo floats used for validation have been taken from Pi-MEP which performed quality control checks. Annex A provides a copy of the Pi-MEP report [RD2] of CCI+SSS data compared against Argo floats. The text below is an extract of the detailed description of the Argo dataset and of the collocation (Match-ups Data Base - MDB) with CCI+SSS products.

Argo is a global array of 3,000 free-drifting profiling floats that measures the temperature and salinity of the upper 2000 m of the ocean. This allows continuous monitoring of the temperature and salinity of the upper ocean, with all data being relayed and made publicly available within hours after collection. The array provides around 100,000 temperature/salinity profiles per year distributed over the global open water oceans at an average of 3-degree spacing. Only Argo salinity and temperature float data with a quality



Climate Change Initiative+ (CCI+)
Phase 1
Product Validation and
Intercomparison Report

Ref.: ESA-CCI-PRGM-EOPS-SW-17-0032
Date: 07/04/2020
Version : v1.1
Page: 23 of 115

index set to 1 or 2 and data mode set to real time (RT), real time adjusted (RTA) or delayed mode (DM) are considered in Pi-MEP. Argo floats that may have problems with one or more sensors appearing in the grey list maintained at the Coriolis/GDACs are discarded. Furthermore, Pi-MEP provides an additional list of ~1000 "suspicious" Argo salinity profiles that are also removed before analysis. The upper ocean salinity and temperature values recorded between 0 m and 10 m depth are considered as Argo sea surface salinities (SSS) and sea surface temperatures (SST). These data were collected and made freely available by the international Argo project and the national programs that contribute to it [Argo (2000)].

The Argo MDB is produced from the previously described cleaned Argo dataset. For the monthly CCI+SSS product, the match-up temporal window radius is 7.5 days around the central date of each satellite time step (bi-weekly, monthly averaged), and 12.5 km for the spatial window radius for each grid nodes centre of a 25 km spatial resolution product. If several satellite pixels are found to meet these criteria, the final satellite SSS match-up point is the closest in time from the in situ data measurement date. The final spatial and temporal lags between the in situ and satellite data are stored in the MDB files. A wide range of collocated auxiliary information are also provided in the MDB.

All the data are freely available as NetCDF files at:

- <https://pimep.ifremer.fr/diffusion/data/cci-l4-esa-merged-oi-v1.5-1m/argo/>
- <ftp://ftp.ifremer.fr/ifremer/cersat/pimep/diffusion/data/cci-l4-esa-merged-oi-v1.5-1m/argo>

3.1.2 ISAS

The In Situ Analysis System (ISAS), as described in Gaillard et al. (2016) is a re-analysis of temperature and salinity fields over the global ocean. It was initially designed to synthesise the temperature and salinity profiles collected by the Argo program. It has been extended to accommodate all type of vertical profile as well as time series. ISAS gridded fields are entirely based on in situ measurements. The methodology and configuration have been conceived to preserve as much data as possible. ISAS is developed and produced by LOPS in close collaboration with Coriolis (one of the Argo Global Data Assembly Centres) and unique data provider for the Mercator operational oceanography system. The gridded fields are produced over the global ocean on a $\frac{1}{2}^\circ$, monthly grid with data downloaded from the Coriolis data centre (for more details on ISAS see Gaillard et al., 2009 and Szekely et al., 2019).

The product used is the INSITU_GLO_TS_OA_NRT_OBSERVATIONS_013_002_a with links for Copernicus data access and documentation as:



- http://marine.copernicus.eu/services-portfolio/access-to-products/?option=com_csw&view=details&product_id=INSITU_GLO_TS_OA_NRT_OBSERVATIONS_013_002_a
- <http://marine.copernicus.eu/documents/PUM/CMEMS-INS-PUM-013-002-ab.pdf>

ISAS covers the period from 15 January 2010 to date. The major contribution to the data set is from the Argo array of profiling floats, reaching an approximate resolution of one profile every 10-days and every 3-degrees over the satellite SSS period. In the chosen version, SSS from ships of opportunity thermosalinographs are not used. The ISAS optimal interpolation involves a structure function modelled as the sum of two Gaussian functions, each associated with specific time and space scales, resulting in a smoothing over typically 3 degrees. The smallest scale which can be retrieved with ISAS analysis is between 300–500 km (Kolodziejczyk et al., 2015). For validation purpose, it is recommended to use the ISAS monthly SSS fields at 5 m depth. Indeed, most Argo floats turn off their CTD pump around 5 m on their way up to the surface. In addition, the "percentage of variance" field (PCTVAR) contained in the ISAS analyses provides information on the local variability of in situ SSS measurements within half degree boxes. ISAS SSS values are loosely filtered for data quality based on PCTVAR < 95% (recommendations vary between 80% and 95%). For these validation studies, ISAS has been re-gridded on the refined CCI+SSS 25km Equal Area EASE grid using the nearest value.

3.2 Uncertainty validation

To validate satellite uncertainty estimates, the approach is to compare the distribution of the difference of satellite SSS minus reference SSS ($\Delta SSS = CCI - ref$). In an ideal scenario, the ΔSSS standard deviation equals the satellite uncertainty (σ_{sat}):

$$\sigma_{\Delta SSS=CCI-ref} = \Delta\sigma_{sat}$$

However, as stated in the PVP [RD1] the geophysical variability of reference SSS data over the time-space scale of remote sensing products depends not only on the particular spatial resolution and time window defining the remote sensing products, but also on the region at which this variability is estimated (inter-regional variability being quite significant [RD3]). Consequently, the ΔSSS standard deviation is a combination of both the satellite SSS uncertainty and the uncertainty in the reference SSS ($\Delta\sigma_{ref}$):

$$\sigma_{\Delta SSS} = \sqrt{\Delta\sigma_{sat}^2 + \Delta\sigma_{ref}^2}$$

In the reference uncertainty all the following terms are included:

- $\Delta\sigma_{meas.}$: Measurement uncertainty (direct instrument error);



- $\Delta\sigma_{space}$: Spatial representativeness error (difference in spatial sampling of a point measurement versus a surface measurement defined by a grid cell);
- $\Delta\sigma_{time}$: Time representativeness error;
- $\Delta\sigma_{vertical}$: Vertical representativeness error (difference in depth of the measurements).

The reference uncertainty corresponds to the following combination:

$$\Delta\sigma_{ref} = \sqrt{\Delta\sigma_{space}^2 + \Delta\sigma_{time}^2 + \Delta\sigma_{vertical}^2 + \Delta\sigma_{meas}^2}$$

In the following, we assume the measurement uncertainty to be negligible ($\Delta\sigma_{meas} = 0$). This is true at first order as we consider all poor measurements to have been discarded with the quality control and filtering methods applied by Pi-MEP.

The vertical representativeness error, although sometimes important, is neglected for now ($\Delta\sigma_{vertical} = 0$), because it is difficult to estimate [RD1]. Strong vertical stratification on the scale of a few centimetres (making a difference between satellite SSS and close-to-surface salinity from buoys) can happen due to persistent weak winds or the presence of freshwater lenses. However, trying to characterize this stratification will require having very detailed information about surface wind stress and ocean currents, which is exceedingly complex as so far no dedicated product exists.

The time representativeness error ($\Delta\sigma_{time} = 0$) is considered to be negligible as Argo measurements have been selected in a ± 7.5 days range around the central date of each satellite time step with a 30 days/monthly running mean.

The spatial representativeness error is the only remaining reference uncertainty considered in this uncertainty assessment. This error is fully described in the PVP [RD1], a summary is provided below.

The spatial power spectra of SSS consistently exhibits a spectral slope of -2.4 ($S(k)=\beta k^{-2.4}$) in a range going from a few kilometres to basin scale ($\sim 10,000$ km) [RD4]. The variance contained between the spatial frequency k_L and k_I (respectively, between the scales l and L , with $l < L$) is given by the double integral:

$$\sigma^2(k_L, k_I) = \iint_{k_L < k < k_I} d\mathbf{k} S(\mathbf{k}) = B \int_{k_L}^{k_I} k dk k^{-2.4}$$



Assuming three spatial scales: g for the ground truth measurements, r for the remote sensing product and L for the basin scale, $g \ll r \ll L$, $\sigma_0 = \sigma(r)$ the standard deviation of SSS contributed by all scales as measured by remote sensing, we obtain the following relationship:

$$\Delta\sigma^2(g, r) \approx \sigma_0^2 \left(\frac{r}{L}\right)^{0.4} \approx \sigma^2(r) \left(\frac{r}{L}\right)^{0.4}.$$

Assuming $L = 5000$ km, with $r = 25$ km for the SSS product, the spatial representativeness is estimated as follow:

$$\Delta\sigma_{space} = \sigma_0 * 0.35$$

With $\sigma_0 = \sigma(r)$ the CCI SSS field standard deviation in time for each grid cell.

3.3 Quality metrics

Two types of quality metrics have been used throughout this document:

- Standard statistics: **mean** and **standard deviation**. It assumes the central limit theorem can be relied on to produce normally distributed estimates;
- Robust statistics based on ranking which are robust against deviation from a normal distribution assumption: **median** and a robust standard deviation (**std IQR: σ_{IQR}**) scaled from the InterQuartile Range (IQR) ($\sigma_{IQR} = IQR * \frac{27}{20}$) assuming a normal distribution.

As recommended in the PVP [RD1], statistics with less than 30 samples have been discarded. For readability, the number of figures has been restricted and limited, if necessary, to the robust statistics (median and robust standard deviation based on IQR) which are more representative of the majority of the distribution.



4 Validation of products, long-term stability and product uncertainty estimates

In this section, we present a systematic validation, first for the global ocean including validation of uncertainty estimates, then for the main ocean basins (Atlantic, Pacific and Indian Ocean and then for high latitudes in the Southern and Arctic Oceans).

4.1 Over global ocean

4.1.1 Products and long-term stability

SSS observations are presented in Figure 1 for the 15th of January 2015 for the CCI+SSS monthly product, Argo profiles top measurements and ISAS field. The three fields show good agreement in resolved patterns. CCI patterns are sharper and resolved smaller resolution than ISAS's. To further assess the agreement between datasets, Figure 2 presents differences of CCI field with references (Argo and ISAS).

The SSS differences between CCI and Argo have been re-gridded on a 75 km Equal Area EASE grid. The temporal median has been calculated over the full time period 2010-2018 (cells with less than 5 observations have been discarded). The field represented for ISAS (Figure 2 bottom) corresponds to the annual median of the median climatology (median for every given month) over 2010-2018. At large scale (open ocean), there is a good agreement between the CCI and both references as confirmed by the very pale colour indicating low amplitude of systematic spatial bias.

In the central Pacific Ocean, CCI is slightly fresher (blue) than ISAS/Argo and it tends to be the opposite for the rest of the ocean. Closer to the coast, river plumes appear fresher (blue) in CCI.

The seasonal climatology (Figure 3), calculated using the median for each season over the full time series, highlights fresher CCI SSS than ISAS in the Northern hemisphere in Winter (DJF) and Spring (MAM) but saltier in Summer (JJA) and Fall (SON). This is particularly clear around Japan and in the northern North-Atlantic.

Looking at the distribution of differences between CCI and references (Figure 4 with Argo as reference) highlights the non-normal distribution of the data (longer tails). There are no systematic biases (versus Argo lower than 0.003 pss in absolute value; versus ISAS lower than 0.002 pss, not shown). The robust standard deviations are of 0.16 pss and 0.13 pss using Argo or ISAS as reference respectively. Using the simple standard deviation, the estimates are much higher with 0.30 pss and 0.32 pss using Argo or ISAS as reference.

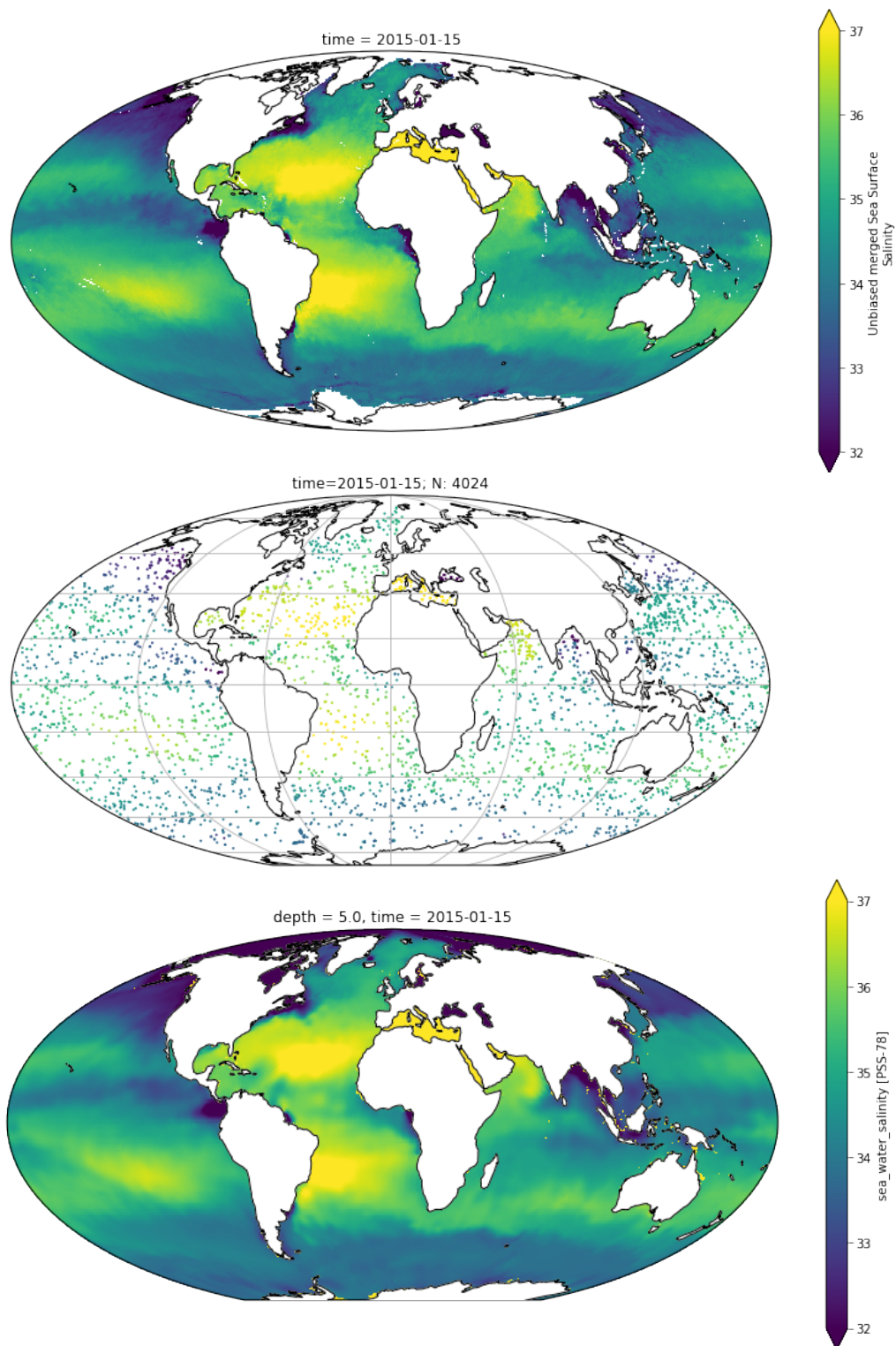


Figure 1: SSS fields for the 15th of January 2015 for (top) CCI monthly product; (middle) Argo profiles top measurements; (bottom) ISAS at 1m depth. All subfigures share the same colourbar.

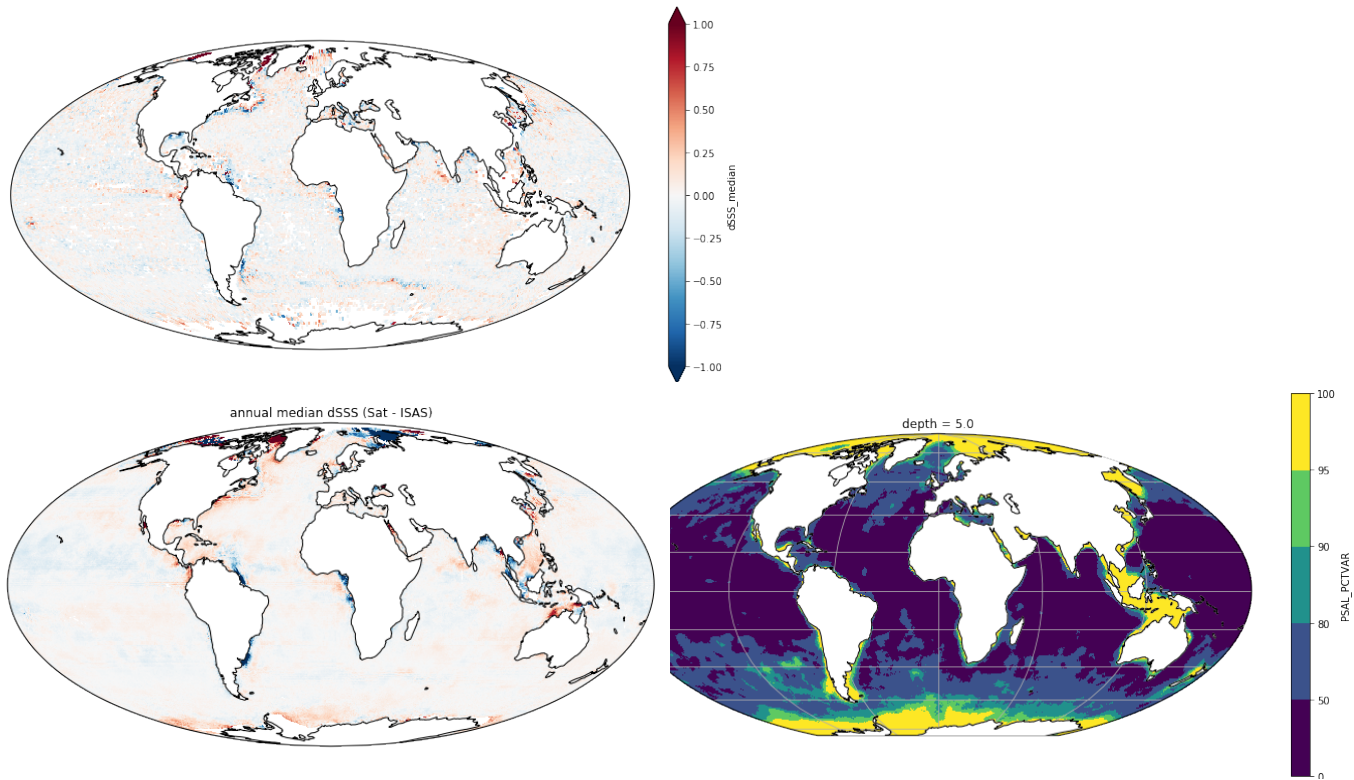


Figure 2: Temporal median of SSS differences computed over the whole period (2010-2018) (in pss) between CCI and (top) Argo profiles are re-gridded on 3 x 3 under sampled 25 km EASE grid. Grid points with less than 5 observations are discarded and (bottom left) ISAS represented as the annual median difference. (bottom right) Annual median SSS error as percentage of the variance. The colourbar is not linear with levels at [0,50,80,90,95,100].

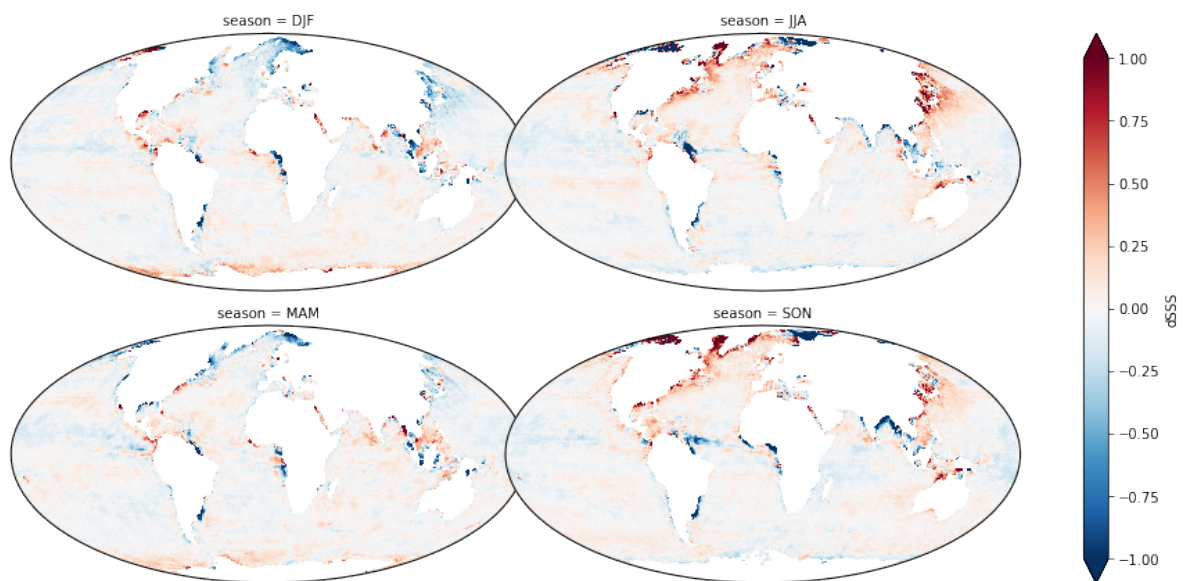


Figure 3: Seasonal climatology of the CCI difference with ISAS calculated using the median.

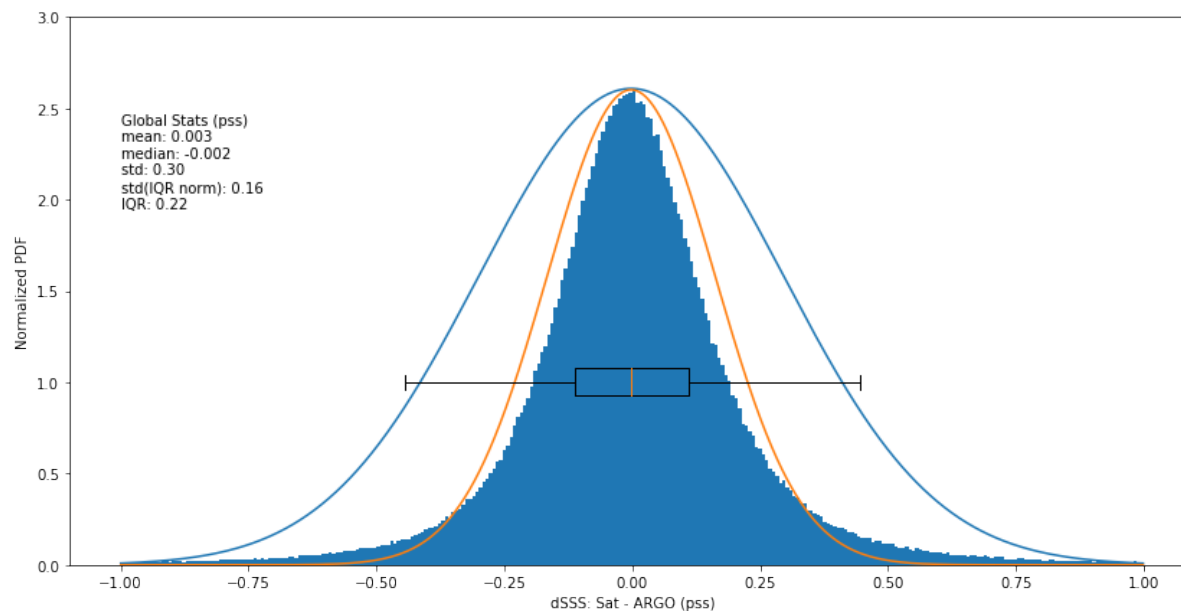


Figure 4: (bar plot) Normalised histogram of the SSS difference between CCI and Argo globally for the full time period. Statistics are indicated on the top left of the figure. (blue curve) Normal distribution computed from the mean and standard deviation. (orange curve) Normal distribution computed from the median and robust standard deviation based on IQR. Both normal distributions are adjusted to the peak.

The time series in Figure 5 represents the temporal evolution of: the CCI differences with references (dotted line for Argo, solid line for ISAS); the bias (mean and median); and the precision (standard deviation, simple or robust). As shown in Figure 4, standard statistics are not very helpful in interpreting the data distributions (but are kept for completeness) and we will focus only on the description of robust statistics results (in orange). There is very good agreement using either Argo or ISAS reference, which makes sense as Argo is the main source of observation for ISAS. The global, temporal difference remains within ± 0.05 pss. There is a small trend in 2010 with the CCI product fresher than reference datasets, at the beginning of the time series. There is a small but appreciable global seasonal cycle with a minimum at the beginning of each year. The amplitude decreases with time, in particularly since 2015 suggesting a link to the demise of Aquarius (end of mission June 2015) or inception of SMAP (mission start in February 2015) data in the CCI dataset or potentially to a better representativity of SSS by reference datasets, ISAS and Argo (Argo salinity measurements closer to the sea surface after 2015-2016).

The precision stays rather constant over the full time series with minima in 2014 and early 2015.

We have further assessed the temporal variability of the CCI difference against reference using latitude-time (Hovmöller) plots over the global ocean (Figure 6). The Hovmöller plot using Argo data does not have enough data at high latitudes (< 30 observations per pixel) even after having reduced the Hovmöller plot pixel resolution to 4° in latitude and using

monthly fields (instead of bi-weekly). In both Argo and ISAS based Hovmöller plot, there is a strong oscillating signal with stronger amplitude at higher latitude. The oscillation is in phase opposition between Northern and Southern hemisphere. This means the CCI data are fresher in winter than references. In addition, we note the CCI freshening occurring at the beginning of the time series is particularly important in the Northern hemisphere at high latitudes.

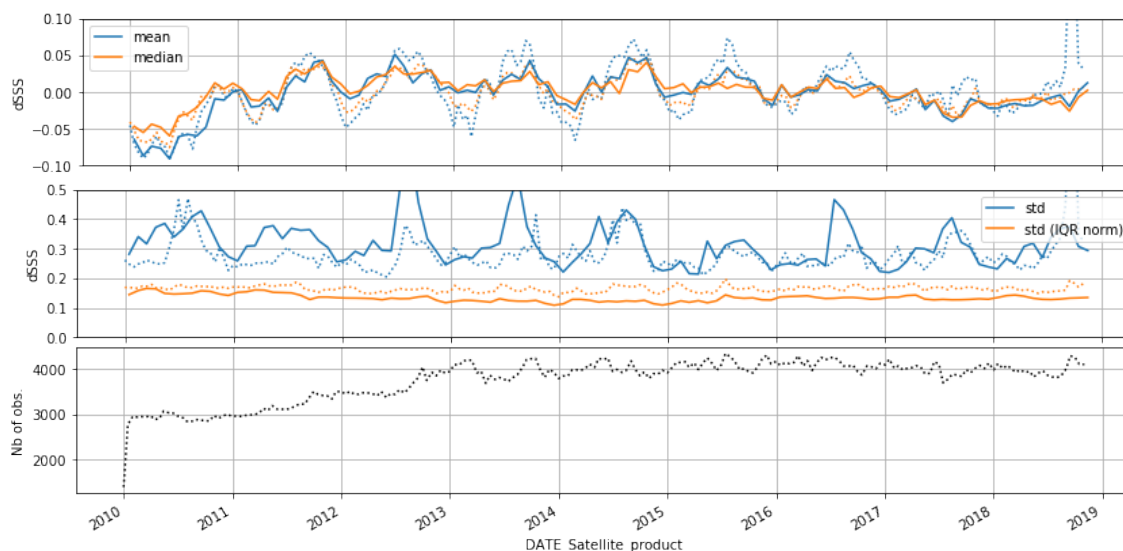


Figure 5: (top) Average of; (middle) standard deviation of; the SSS difference between CCI and (solid line) ISAS, (dotted line) Argo as function of time for the full open ocean where CCI products exist. Blue curves represent (top) the mean (middle) standard deviation. Orange curves represent (top) the median and (middle) the robust standard deviation based on IQR. (bottom) represents number of observations for collocation with Argo profiles for each time step.

To have a more quantitative estimate, Figure 7 represents 20° latitudinal median averaging of the CCI difference against ISAS for each time step (blue lines). A median climatology is removed (orange curve) and an annual moving window mean is then applied (green curve) and indicates the long-term stability. The oscillation of the CCI SSS against ISAS for the band 60°N-80°N (top panel) presents a seasonal cycle of ± 0.3 pss with differences between consecutive minimum/maximum of up to 1 pss (e.g. 2013). After removing the seasonal cycle, the period after 2012 is smoother than the original blue curve, but with a degradation for the earlier period (2010-2012). The yearly running mean (green curve) highlights a quasi-linear positive trend from -0.5 pss to +0.2 pss (i.e. CCI starting fresher than reference then becoming saltier) from 2010 to January 2016.

Other latitudinal bands have a much smaller seasonal cycle in the difference between CCI SSS and ISAS. Among the most significant are: band 80°S-60°S with +0.15;-0.07 pss; band 40°N-60°N with ± 0.10 pss and band 20°N-40°N with -0.03;+0.06 pss. In terms of long-term stability, bands 60°S-40°S; 40°S-20°S; 20°S-0°; 10°S-10°N; 0°-20°N; 20°N-40°N stays within a ± 0.04 pss range. They tend all to have a positive trend for about the first 18 months. The variation in long term stability is much stronger for band 60°N-80°N as discussed above. The variations for



Climate Change Initiative+ (CCI+)
Phase 1
**Product Validation and
Intercomparison Report**

Ref.: ESA-CCI-PRGM-EOPS-SW-17-0032

Date: 07/04/2020

Version : v1.1

Page: 32 of 115

other bands have a minimum <0.10 pss in 2010 at 40°N - 60°N and maximum of $+0.07$ pss in Fall 2015; and for band 80S-60S with a minimum in 2010 <-0.05 pss, maximum in Southern summer 2011-2012 $>+0.05$ and slowly decreasing since then.

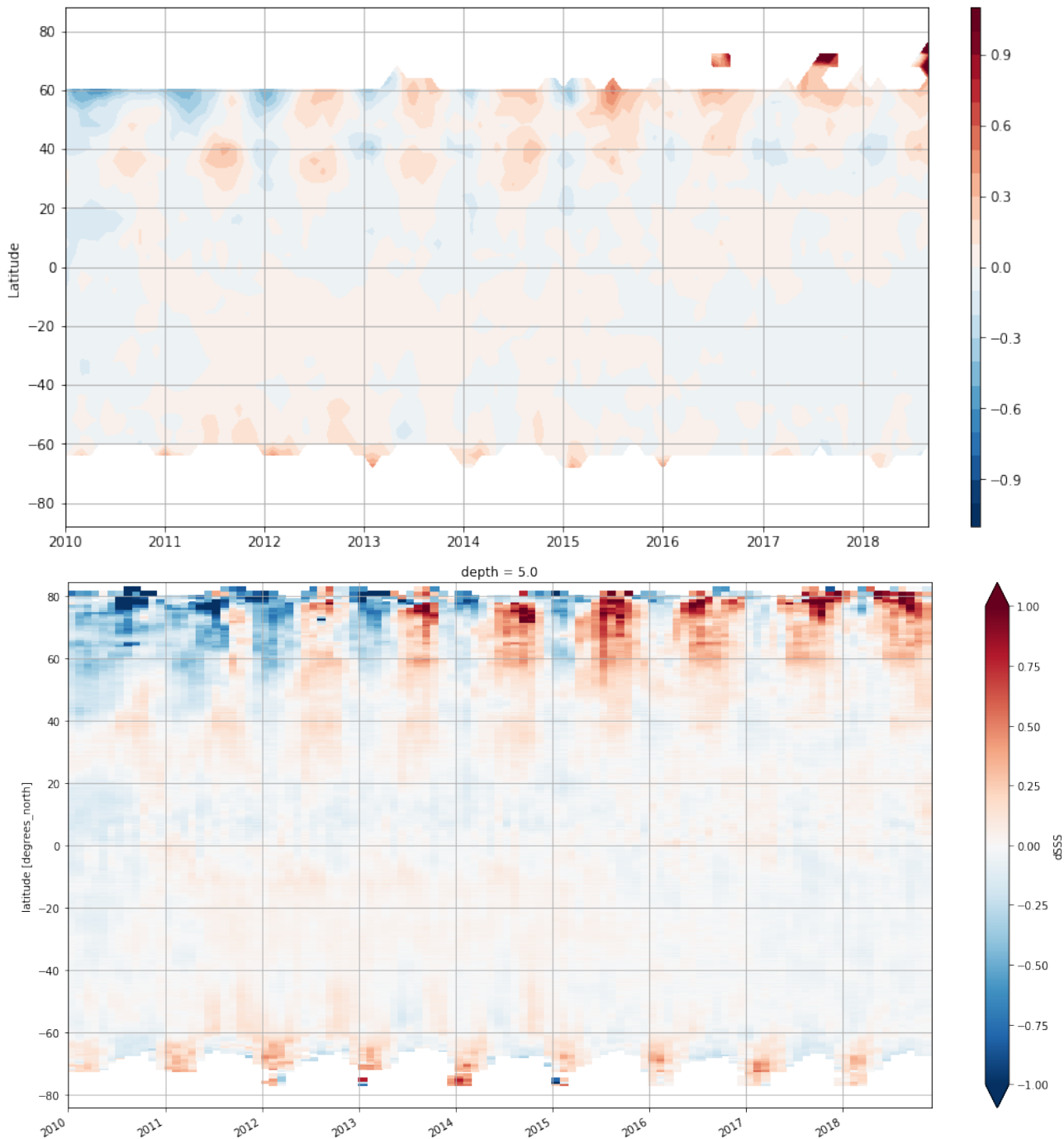


Figure 6: Global latitude-time Hovmöller of the CCI difference with (top) Argo with latitude bins of 4°, with monthly timestep. Each pixel represents the median value when there are more than 30 observations. Otherwise no value is shown. (bottom) median value at the same spatiotemporal scale as the ISAS field.

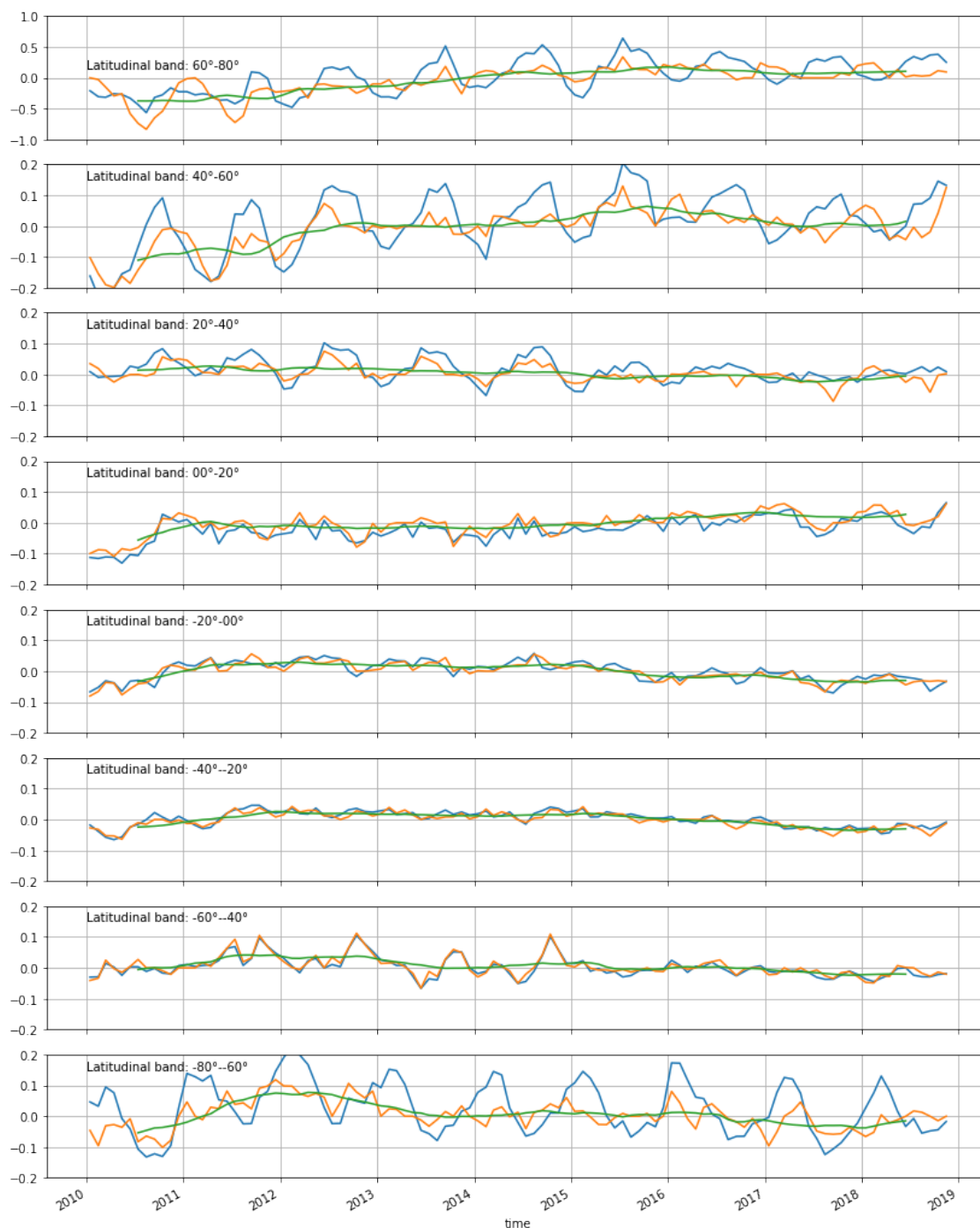


Figure 7: Latitudinal band (20° wide) averaging (using median) of the salinity difference between CCI SSS and ISAS from (top) to (bottom) of [60°N;80°N] to [60°S;80°S]. Y-scale for the top panel is five time bigger than for other panels. Blue curves represent the median for the band in latitude and longitude for each time step. Orange curves are the anomaly after removing a median climatology calculated from blue curves. Green curves are an annual rolling mean of orange curves.



4.1.2 Product uncertainty estimates

As explained in section 3.2 above, to validate satellite uncertainty estimates, the approach is to compare the distribution of the differences of satellite SSS minus reference SSS ($\Delta SSS = CCI - ref$) with the satellite CCI product estimates of uncertainty. However, it is necessary to take into account the uncertainty of the reference itself leading to:

$$\sigma_{\Delta SSS} = \sqrt{\Delta\sigma_{sat}^2 + \Delta\sigma_{ref}^2}$$

Figure 8 represents the distribution (pale blue violin) of the CCI SSS difference with Argo per uncertainty bin of 0.05 pss wide. This is computed over the full time series. There are more than 1000 observations per bin as long as the total uncertainty (satellite + reference) is lower than 0.8 pss and covers the vast majority of the globe. There is a very good agreement between the standard deviation of the difference and the estimated uncertainty. This is true using both the 'simple' and robust standard deviation particularly up to 0.4 pss (Figure 9 left) suggesting the behaviour of the difference distribution for low total uncertainty bins is close to normal. For higher total uncertainty, there is nearly a one to one relation between the difference standard deviation and the estimate uncertainty as long as we use the robust standard deviation (Figure 9 left). Using ISAS as a reference for the difference with CCI SSS field (Figure 9 right), the behaviour is very similar to (Fig 9 left) up to 0.6 pss (corresponding to most of the open ocean, well sampled by Argo). It diverts from the one-to-one line above a total uncertainty of 0.6 pss. This means, above this value, the difference is higher than expected. This might be explained with the SSS temporal variability which is not well captured by ISAS or in areas where there are few observations.

Figure 10 represents, estimated total uncertainty on the left and observed uncertainty using ISAS as reference on the right. As highlighted in Figure 9 right and Figure 10, the total uncertainty is overestimated for most of the ocean by more than 25%. On the other hand, total uncertainty is underestimated in area with high-variability like river plumes (Amazon, Congo, Bay of Bengal) and gulf stream. This is potentially due to an underestimation of the reference representativeness error.

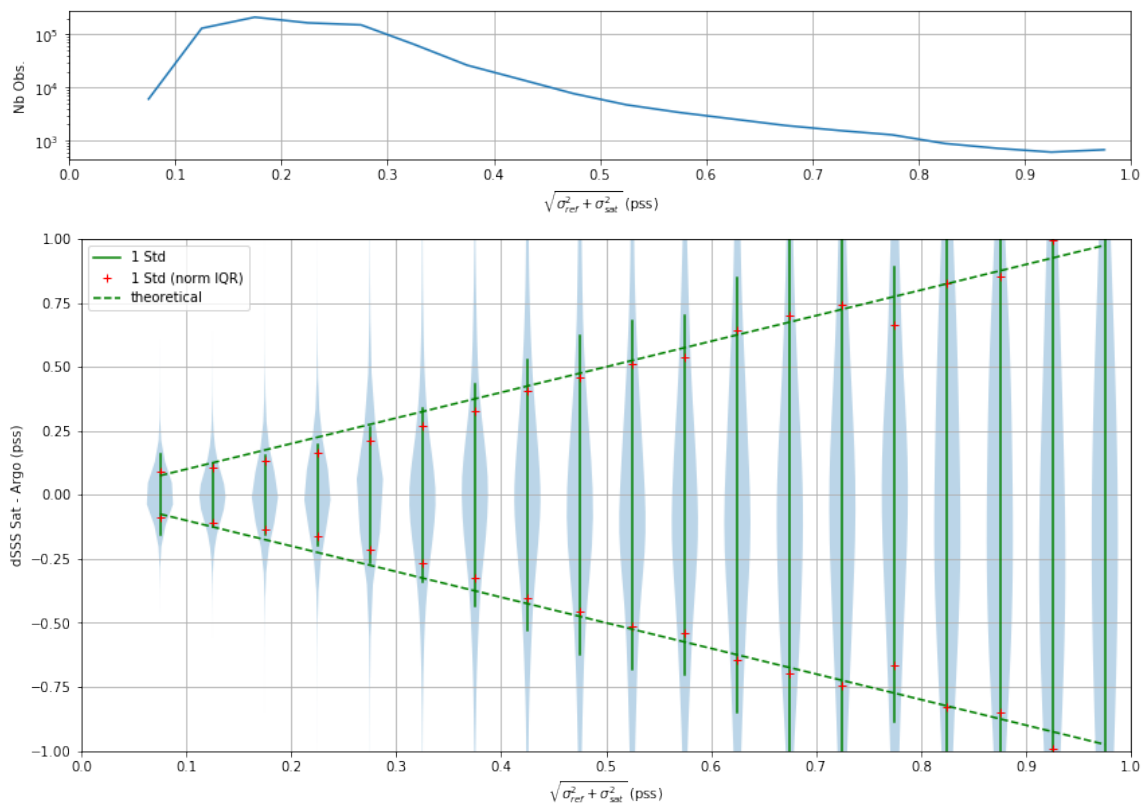


Figure 8: (top) Number of Argo floats observations per satellite per uncertainty bins. (bottom) Distribution of the CCI difference with Argo floats observation for each bin of uncertainty including satellite random error and representativeness error. Vertical green bars represent the standard deviation. Red crosses represent the robust standard deviation. The green dashed lines is the theoretical relation between the measured uncertainty and the estimate. Bins are 0.05 pss wide starting from 0.05 pss.

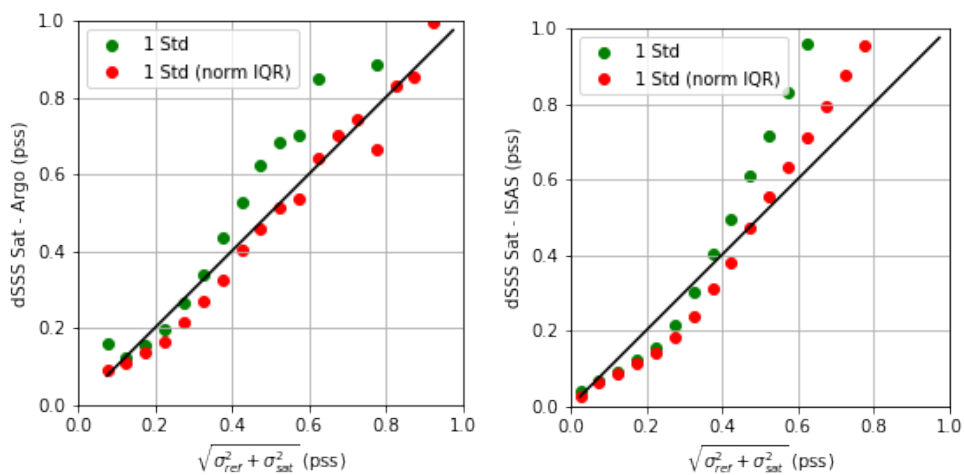


Figure 9: Measured standard deviation of the difference between (left) CCI and Argo; (right) CCI and ISAS for each uncertainty bins. Green dots are for standard deviation estimate; red dots for robust standard deviation.

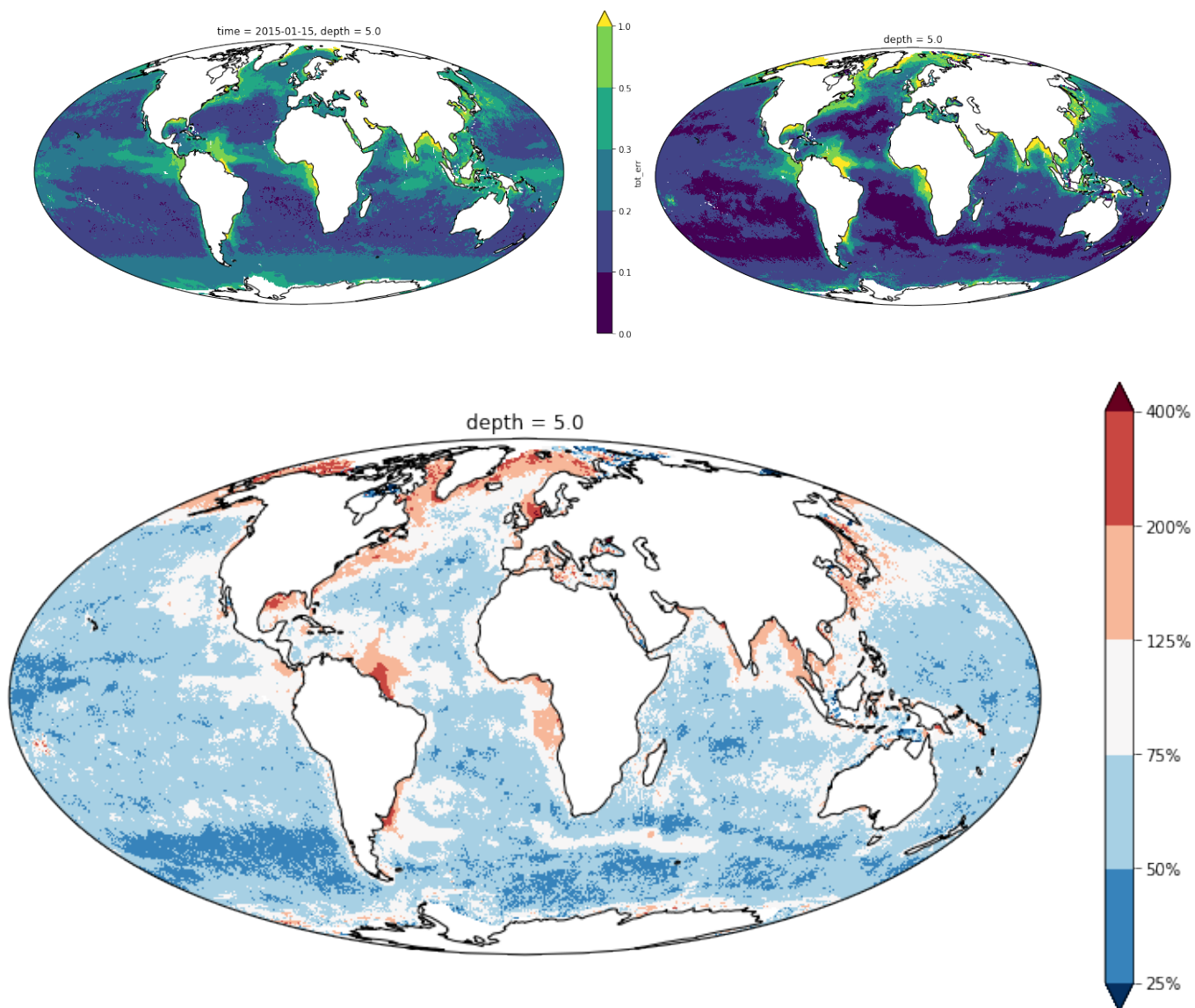


Figure 10: (top left) total estimated uncertainty error in pss from the satellite random error and the representativeness error. Uncertainty for the 15/01/2015. (top right) observed uncertainty as the standard deviation of the SSS difference between CCI and ISAS. (top) the colourbar is not linear, steps are [0,0.1,0.2,0.3,0.5,1]. (bottom) Ratio of the observed over estimated total uncertainty.

4.2 Regional Studies

In this section, we provide the same results as given above but for specified ocean basins (Atlantic, Pacific, Indian, Southern and Arctic).

4.2.1 Atlantic Ocean

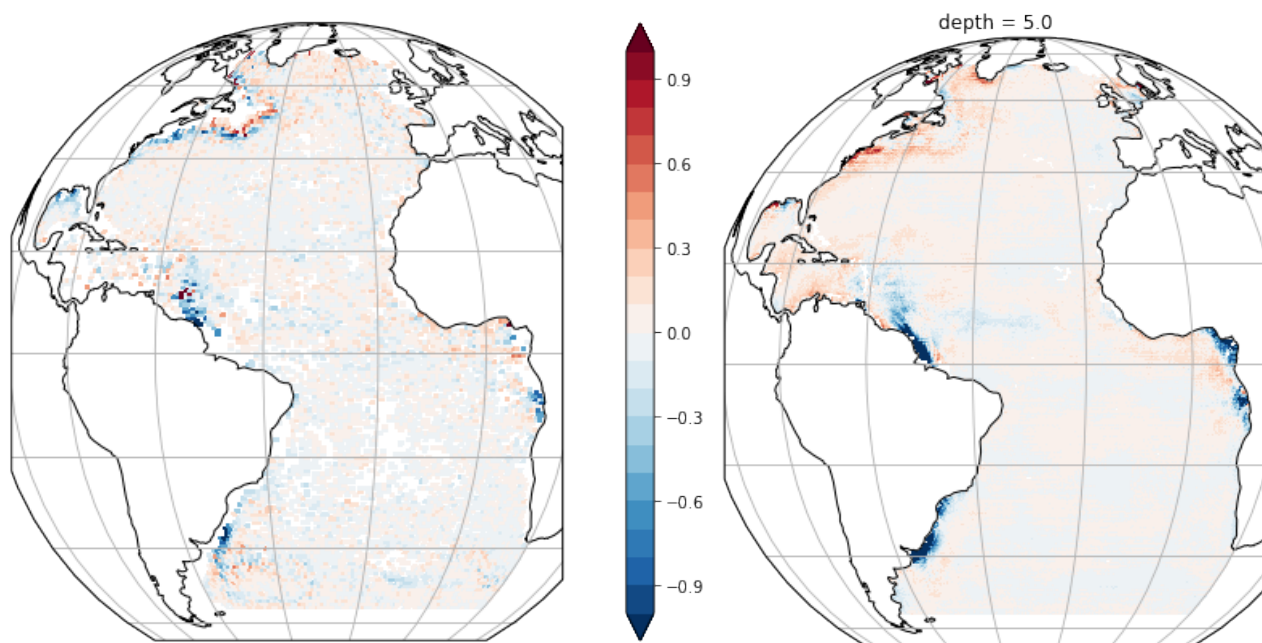


Figure 11: As Figure 2 but only showing Atlantic Ocean (in pss).

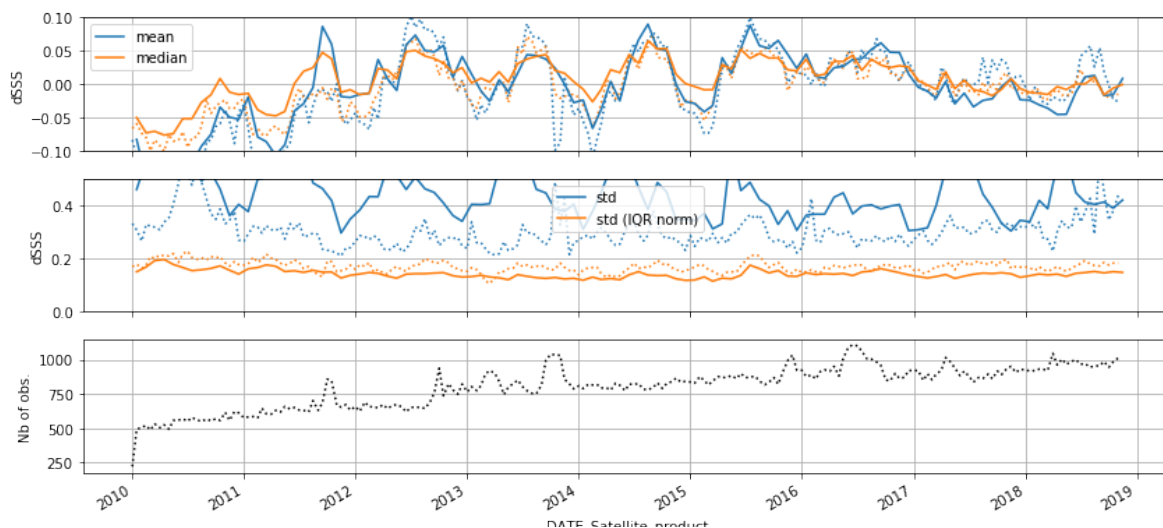


Figure 12: As Figure 5 but for the area defined for the Atlantic Ocean (Figure 11).

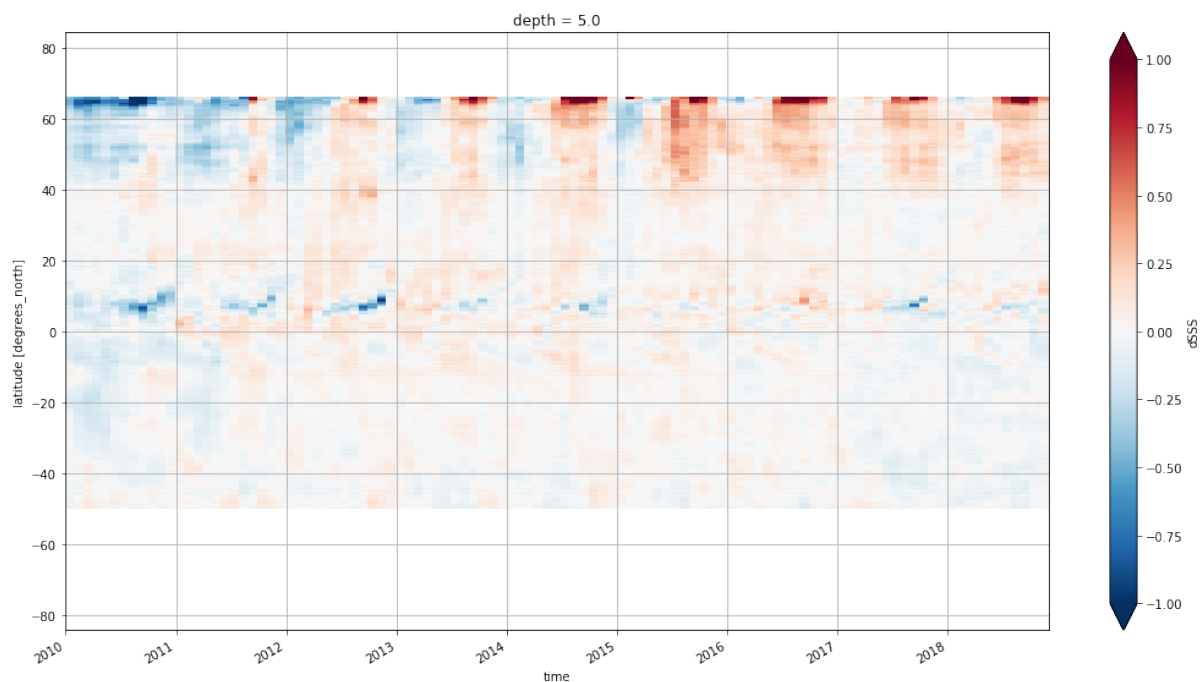


Figure 13: As Figure 6 but for the area defined for the Atlantic Ocean (Figure 11) using ISAS.

There is a good agreement of the two fields of SSS CCI difference with the reference datasets (gridded Argo or ISAS, Figure 11). The CCI product is fresher than the reference datasets in major river plumes (e.g. Amazon, Orinoco, Congo, Mississippi). This is probably due to a better ability of satellite products to resolve sharp gradients in salinity and higher spatial resolution



Climate Change Initiative+ (CCI+)
Phase 1
Product Validation and
Intercomparison Report

Ref.: ESA-CCI-PRGM-EOPS-SW-17-0032
Date: 07/04/2020
Version : v1.1
Page: 40 of 115

compared to either ISAS or in situ measurements. In addition, freshening is stronger at the surface (satellite $\sim 1\text{cm}$) than at the depth sampled by Argo ($\sim 5\text{m}$). In the vicinity of the Gulf Stream above 40°N , Argo indicates strong positive/negative differences which are probably due to in situ measurements not being representative of surrounding areas where there are very strong salinity gradient and many mesoscale structures (eddies). At the large scale (open ocean), there is a good agreement between the CCI and both references as confirmed with the pale colour indicating the low amplitude of systematic spatial bias.

As for the global oceans (Figure 5), we will focus our analysis on the robust quality metrics (median, robust standard deviation based on IQR). Except for the beginning of the period, the time series of the CCI difference with references (Figure 12) remains within ± 0.05 pss. As for the global ocean, there is a small but apparent seasonal cycle with a minimum at the beginning of each year. The amplitude decreases with time, in particular since 2015 suggesting, as before, a link to the absence of Aquarius (end of mission June 2015) or presence of SMAP (mission start in February 2015) data in the CCI dataset.

The precision stays fairly constant over the full time series with minima in 2014 and early 2015 and a local peak in mid-2015.

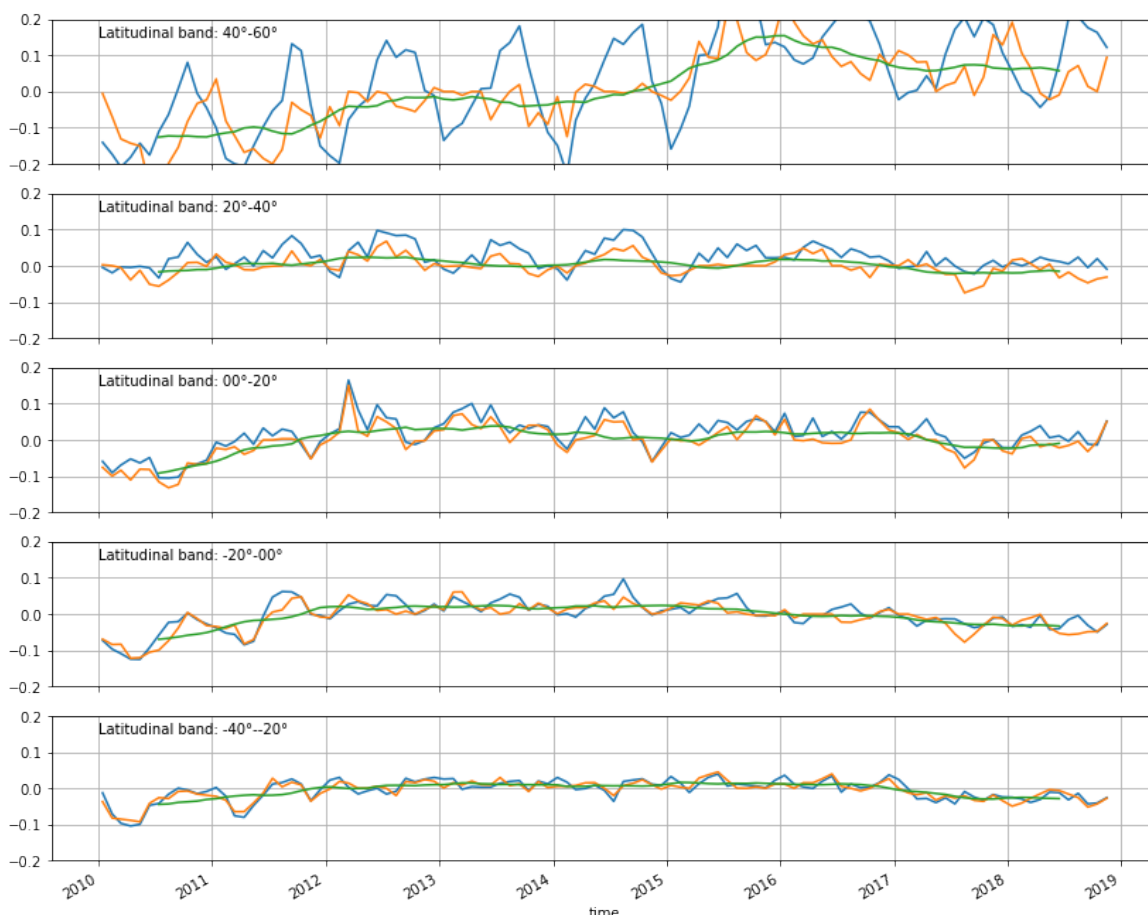


Figure 14: As Figure 7 but for the area defined for the Atlantic Ocean (Figure 11)

We have further assessed the temporal variability of the CCI difference against reference using a latitude-time Hovmöller diagram over the Atlantic Ocean using ISAS field (Figure 13). As for the Hovmöller for the global ocean (Figure 6), the Atlantic presents a strong oscillating signal with stronger amplitudes at higher latitudes. The oscillation is in phase opposition between Northern and Southern hemisphere. This means the CCI data are fresher in winter than ISAS. In addition, we note the CCI freshening occurring at the beginning of the time series is particularly noticeable in the Northern hemisphere at high latitude.

To have a more quantitative estimate, similarly to Figure 7, Figure 14 represents 20° latitudinal median averaging of the CCI difference against ISAS for each time step (in blue). A median climatology is removed (orange curve) and a yearly moving-window mean is then applied (green curve) and indicates the long-term stability. The strongest oscillation for the Atlantic concerns again the northernmost band (although this time that band is 40N-60N) which presents a seasonal cycle of ± 0.15 pss (not shown) with differences between consecutive minimum/maximum of up to 0.4 pss (e.g. 2014). There is a significant intra-annual variation, with a positive trend from 2010 to 2016 which levels off around 2013 and



Climate Change Initiative+ (CCI+)
Phase 1
**Product Validation and
Intercomparison Report**

Ref.: ESA-CCI-PRGM-EOPS-SW-17-0032

Date: 07/04/2020

Version : v1.1

Page: 42 of 115

onwards. This long term variation indicates CCI is fresher (up to -0.1 pss) than reference in the early period (2010-2014), and saltier (up to >0.1 pss) in more recent years (after 2015).

Other latitudinal bands present much smaller variations with small seasonal cycle (<0.05 pss; not shown). After removing the seasonal cycle, variations are much smaller than for the 40N-60N band and stay generally within ± 0.05 pss except for the early period (2010- Jan. 2012) which is characterised by a fresher CCI signal up to 0.1 pss. All bands are affected except band 20N-40N.

4.2.2 Pacific Ocean

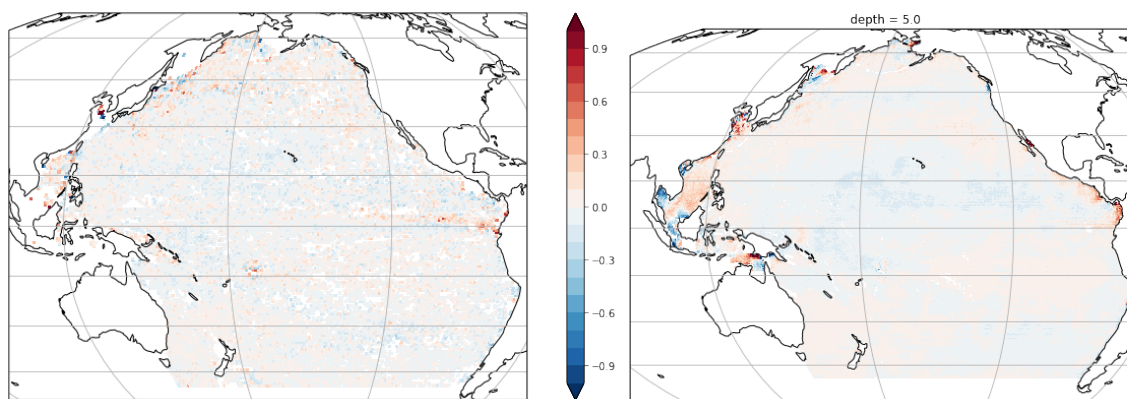


Figure 15: As Figure 2 but only showing Pacific Ocean (in pss).

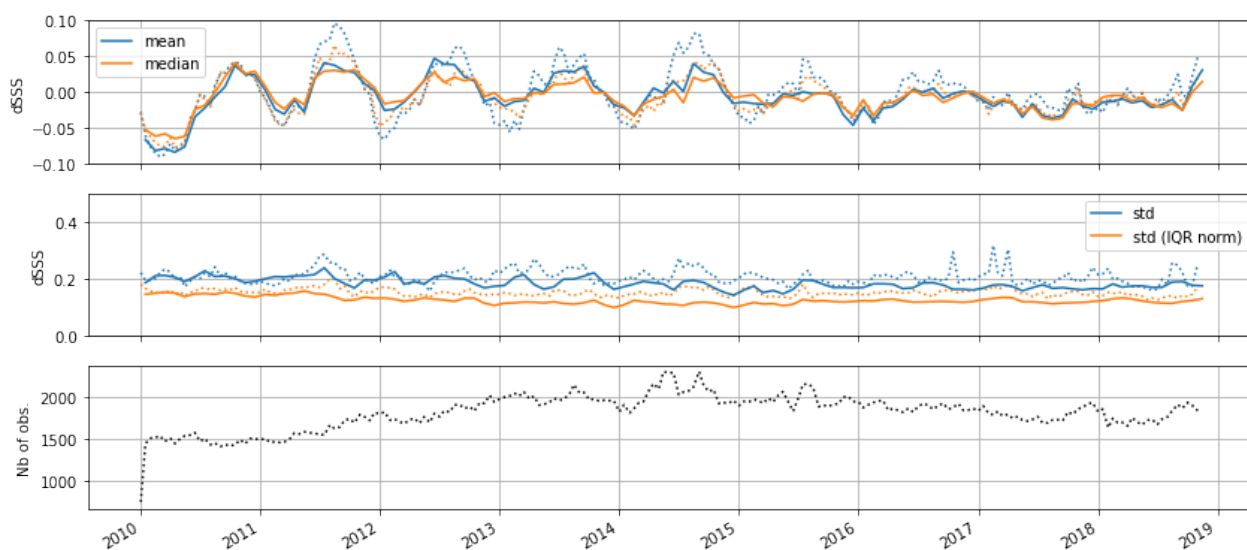


Figure 16: As Figure 5 but for the area defined for the Pacific Ocean.

There is a very good agreement for the two fields of SSS CCI difference with references (gridded Argo and ISAS, Figure 15) with no strong systematic bias either at large or small spatial scales.

As with the study of the global oceans (Figure 5), we will focus our analysis using the robust quality metrics (median, robust standard deviation based on IQR). Except for the beginning of the period, the time series of the CCI difference with references (Figure 16) remains within ± 0.05 pss. As before with the global ocean, there is a small but apparent seasonal cycle with a minimum at the beginning of each year. The amplitude decreases with time, in particular

since 2015 suggesting a link to the absence of Aquarius (end of mission June 2015) or presence of SMAP (mission start in February 2015) data in the CCI datasets.

The precision is fairly constant over the full time series with a slight decrease from 2012 onwards.

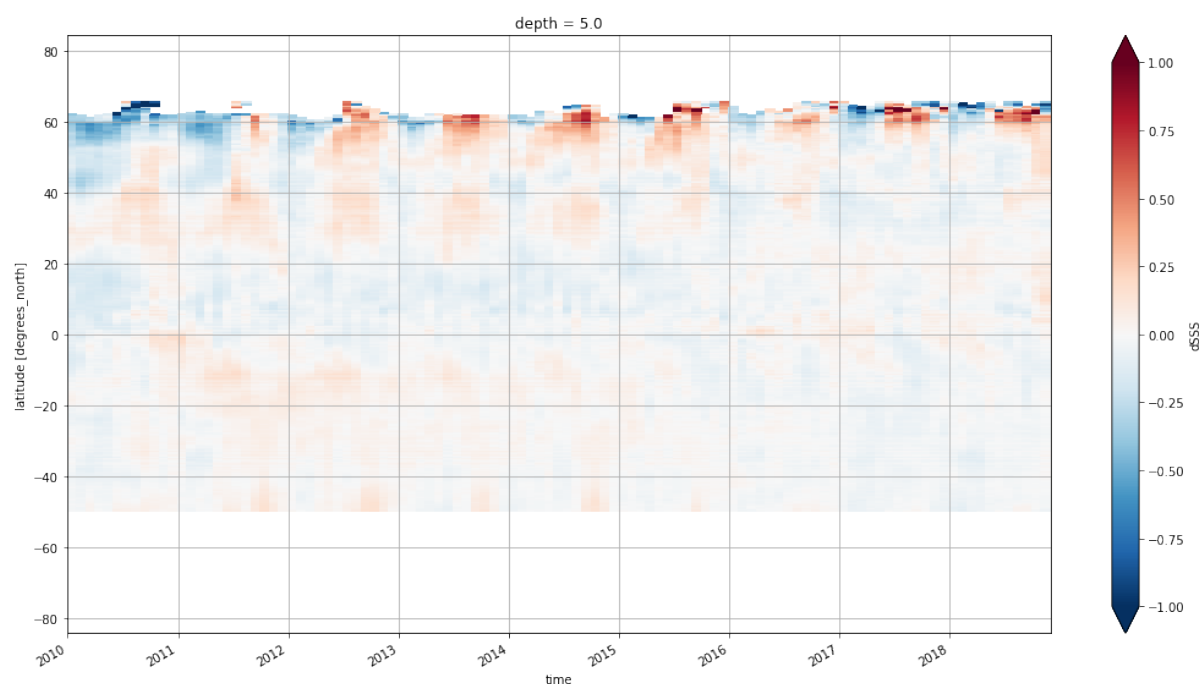


Figure 17: As Figure 6 but for the area defined for the Pacific Ocean using ISAS.

We have further assessed the temporal variability of the CCI difference against reference using a latitude-time Hovmöller over the Pacific Ocean using ISAS field (Figure 17). As with the Hovmöller for the global ocean (Figure 6), the results for the Pacific show a strong oscillation with an increased amplitude at higher latitudes (particularly in the Northern Hemisphere). The oscillation is in phase opposition between Northern and Southern hemispheres. This suggests the CCI data are fresher in winter than ISAS. In addition, we note that the CCI freshening occurring at the beginning of the time series is particularly important in the Northern Hemisphere at high latitude.

To have a more quantitative estimate, similar to Figure 7, Figure 18 represents 20° latitudinal median averaging of the CCI difference against ISAS for each time step. Bands 40N-60N and 20N-40N present the strongest oscillation for the Pacific Ocean with a seasonal cycle of ± 0.10 pss and ± 0.07 pss respectively and with differences between consecutive minimum/maximum of up to 0.3 pss (e.g. 2012) and ~ 0.2 pss (e.g. winter 2013-2014). There is a significant intra-annual variation for the northernmost band, with a positive trend from 2010 to 2013 followed by a plateauing and then a slight decrease from 2015 onwards. This

long term variation indicates CCI is fresher (up to -0.1 pss) than reference in the early period (2010-2011).

Other latitudinal bands present much smaller variations with decreased seasonal cycles (<0.05 pss; not shown). After removing the seasonal cycle, variations are small and stay generally within +/-0.05 pss.

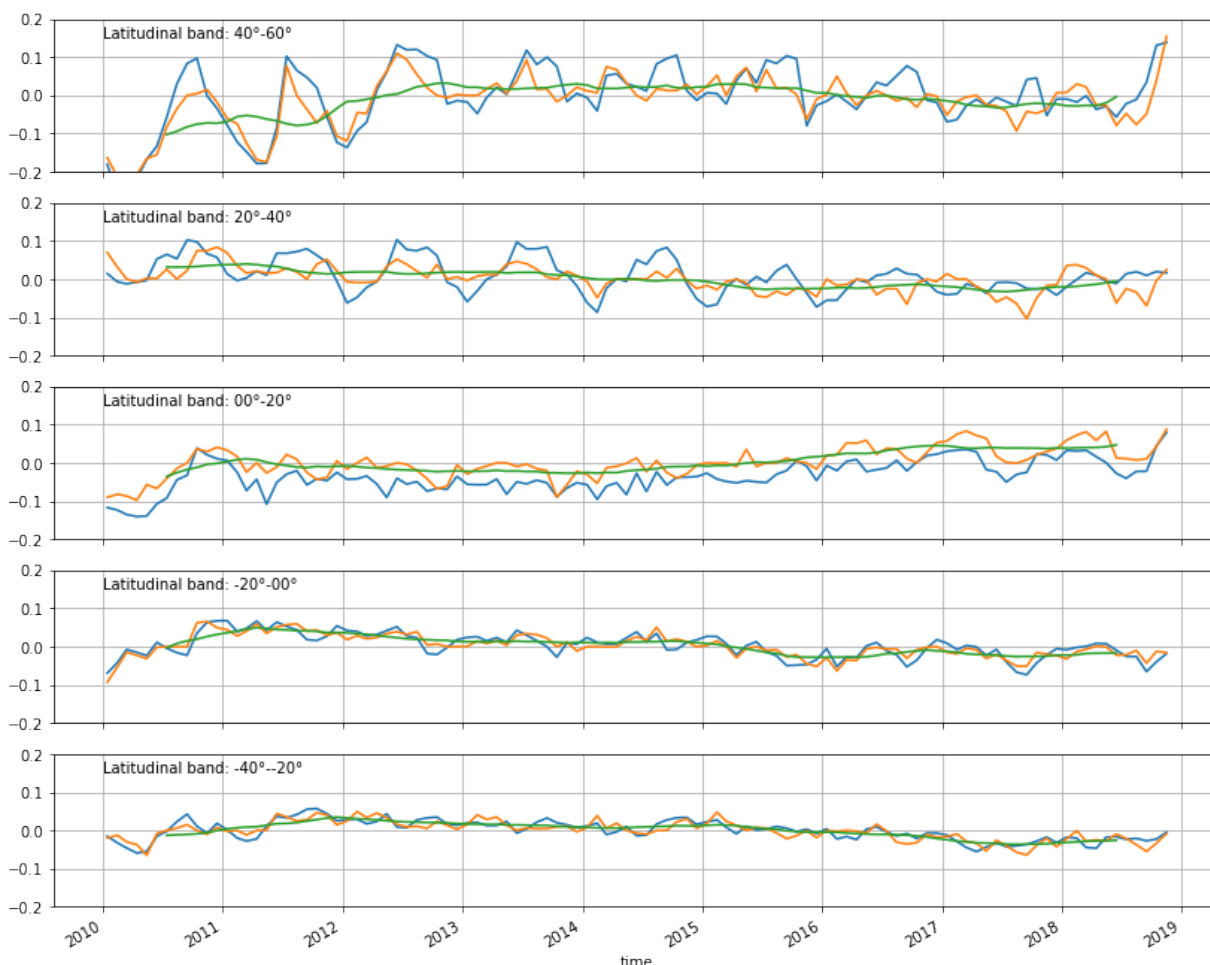


Figure 18: As Figure 7 but for the area defined for the Pacific Ocean.

4.2.3 Indian Ocean

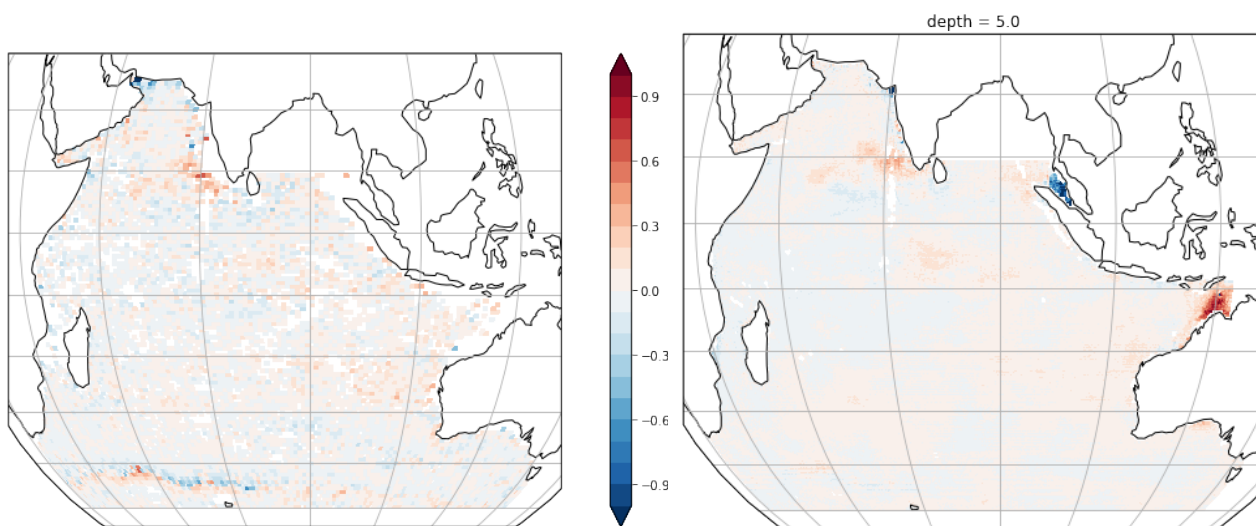


Figure 19: As Figure 2 but only showing the Indian Ocean (in pss).

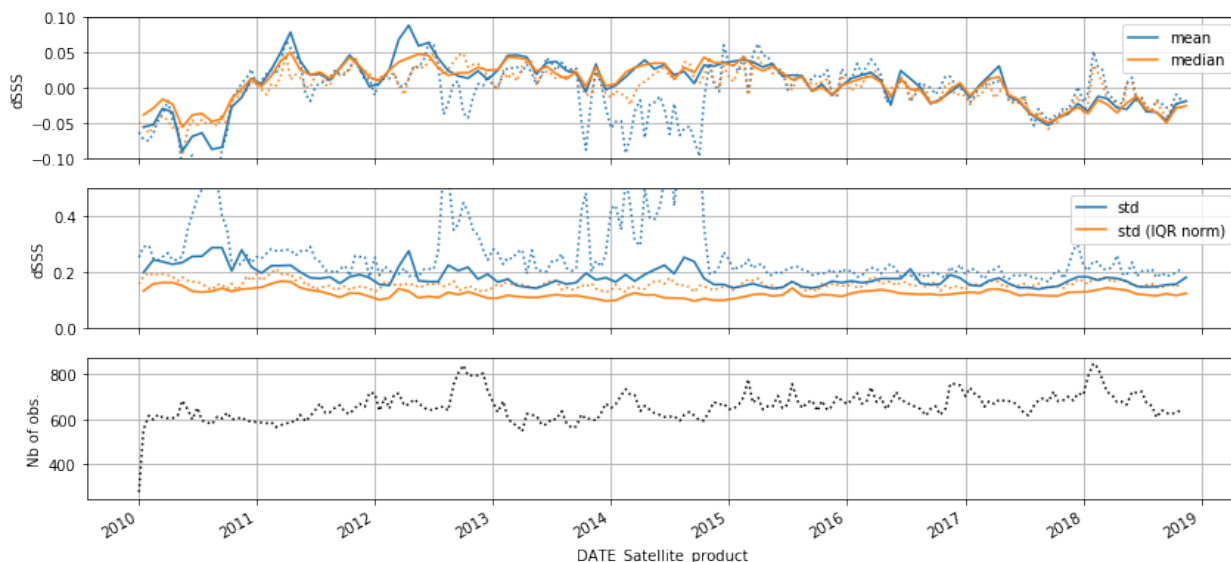


Figure 20: As Figure 5 but for the area defined for the Indian Ocean.

There is a very good agreement for the two fields of SSS CCI difference with references (re-grid Argo or ISAS, Figure 19) with no strong systematic bias either at large or small spatial scales. In the vicinity of the sub-polar front near Kerguelen Island, the difference from Argo shows strong positive/negative values which are probably due to in situ measurements not representative of surrounding area as it is an area with a strong salinity gradient and high mesoscale activity (eddies).

As with the global oceans (Figure 5), the following analyses focus on robust quality metrics (median, robust standard deviation based on IQR). Contrary to previous similar figures for the global ocean and Atlantic and Pacific oceans, the time series of the CCI difference with reference datasets for the Indian Ocean (Figure 20) does not present any obvious seasonal cycle. There is long-term variation with a rapid increase between 2010 and 2011 and a recent decrease. Variations remains within ± 0.05 pss and the precision stays rather constant over the full time series.

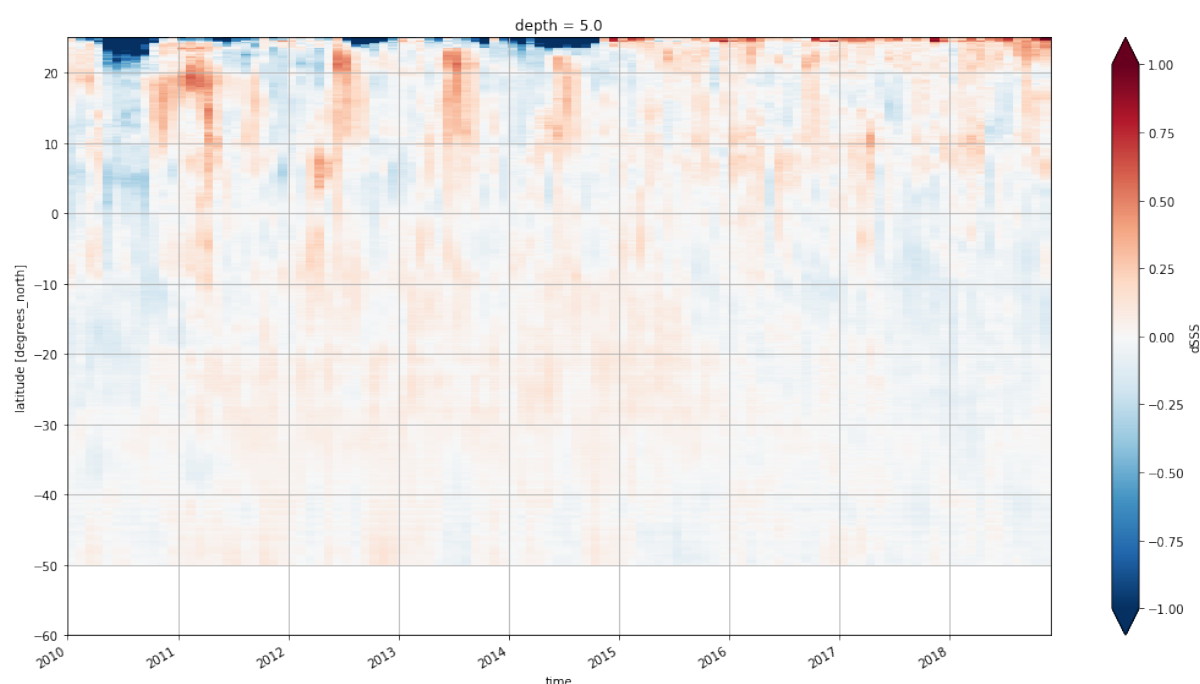


Figure 21: As Figure 6 but for the area defined for the Indian Ocean using ISAS.

We have further assessed the temporal variability of the CCI differences with reference data using a latitude-time/Hovmöller plot over the Pacific Ocean using ISAS field (Figure 21). There are some relatively strong oscillations in the 10N-20N latitudinal band. These oscillations are more noticeable prior to 2015. No oscillations are visible for the South Indian Ocean.

To have a more quantitative estimate, similar to Figure 7, Figure 22 represents 20° latitudinal median averaging of the CCI difference against ISAS for each time step. Band 0N-20N presents some oscillation, particularly in the early period before 2015. There is no significant seasonal cycle as the signal is not strongly periodic. Also, there are differences between consecutive minimum/maximum of 0.2 to 0.4 pss. There is a strong trend for the first year. Other latitudinal bands present much smaller variations with no significant seasonal cycle (no agreement of the mean and median seasonal cycle). The long-term stability is fairly smooth and generally remains within ± 0.05 pss with minima at the beginning and end of the time series.

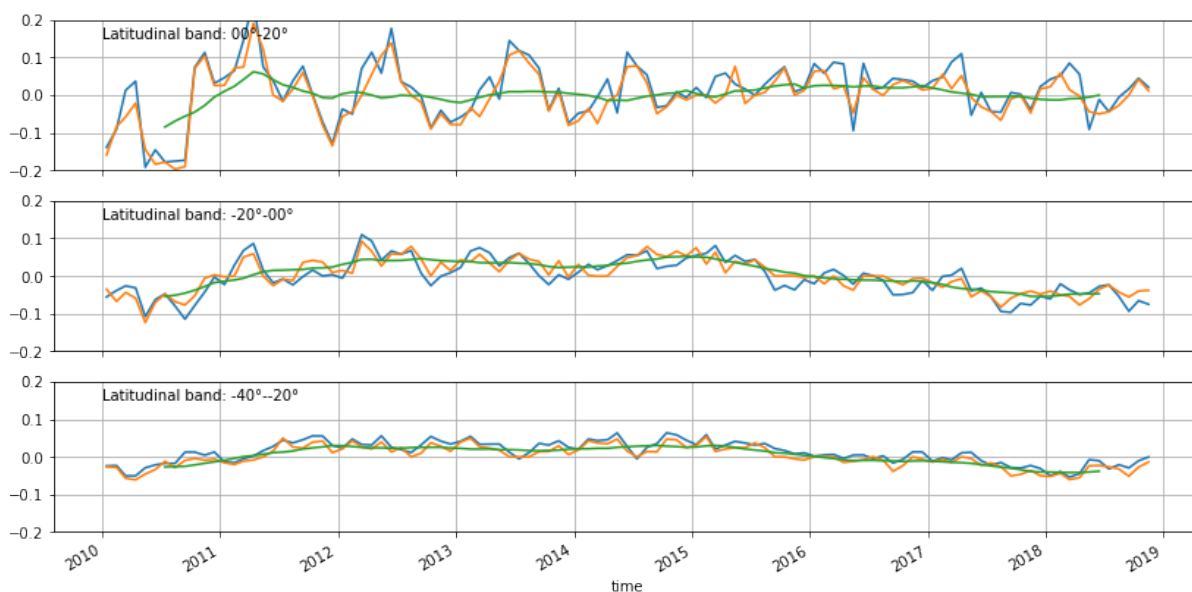


Figure 22: As Figure 7 but for the area defined for the Indian Ocean.

4.2.4 High-latitudes: Southern Ocean; Arctic Ocean

In this section, the systematic bias as observed from re-gridded Argo and ISAS for the Southern and Arctic Oceans is presented. In the Southern Ocean, most of the ocean close to the continent is not sampled sufficiently with Argo (less than 5 samples over the full time series, Figure 23 top-left). The portion towards the Pacific ocean is better sampled. Despite comparison between CCI and ISAS shows a positive bias for CCI close to the continent, we have little confidence in this feature as the error estimated in ISAS through the error in percentage of variance is over 95% (ISAS SSS with a PCTVAR > 95% have not been used when computing the difference with CCI). This means much of ISAS data corresponds to the climatology. For all these reasons we have not further characterised the region.

Over the Arctic Ocean, there is a similar issue of insufficient observations from Argo over most regions. Only the Nordic Seas are well sampled by Argo, which are also characterised by low value of the error in percentage of variance in ISAS. Over most of the Arctic Ocean, CCI differences with ISAS shows strong differences but for which we have no confidence (error in percentage of variance higher than 95%). For these reasons we have not further characterised the region.

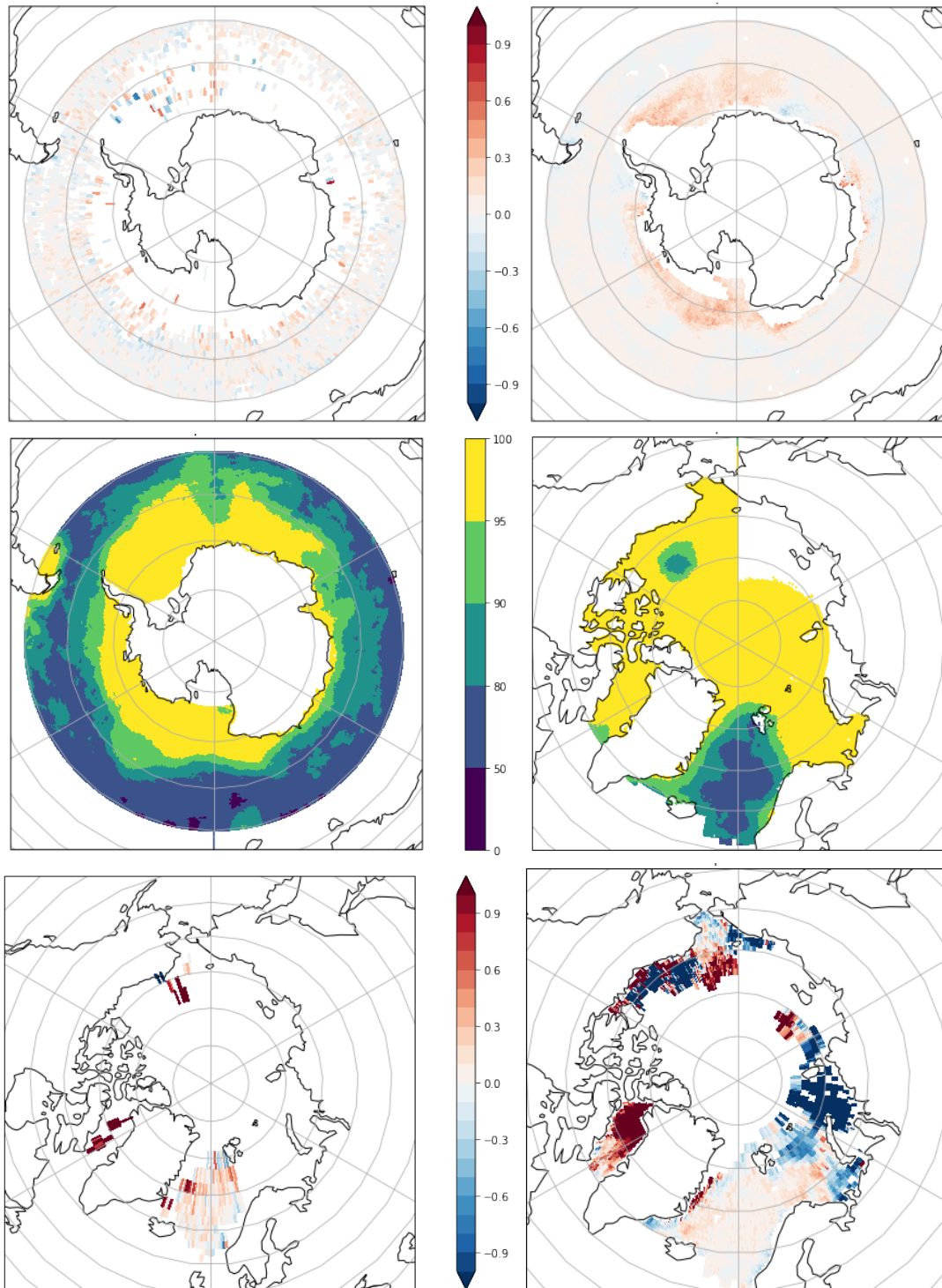


Figure 23: As Figure 2 but zoomed over the high latitudes: (top) Southern Ocean; (bottom) Arctic Ocean. (middle) is the SSS error are percentage of the variance on Indian Ocean. (top/bottom left) with Argos. Grid point with less than 5 observations are discarded. (top/bottom right) with ISAS.

4.3 Over regions of high SSS variability

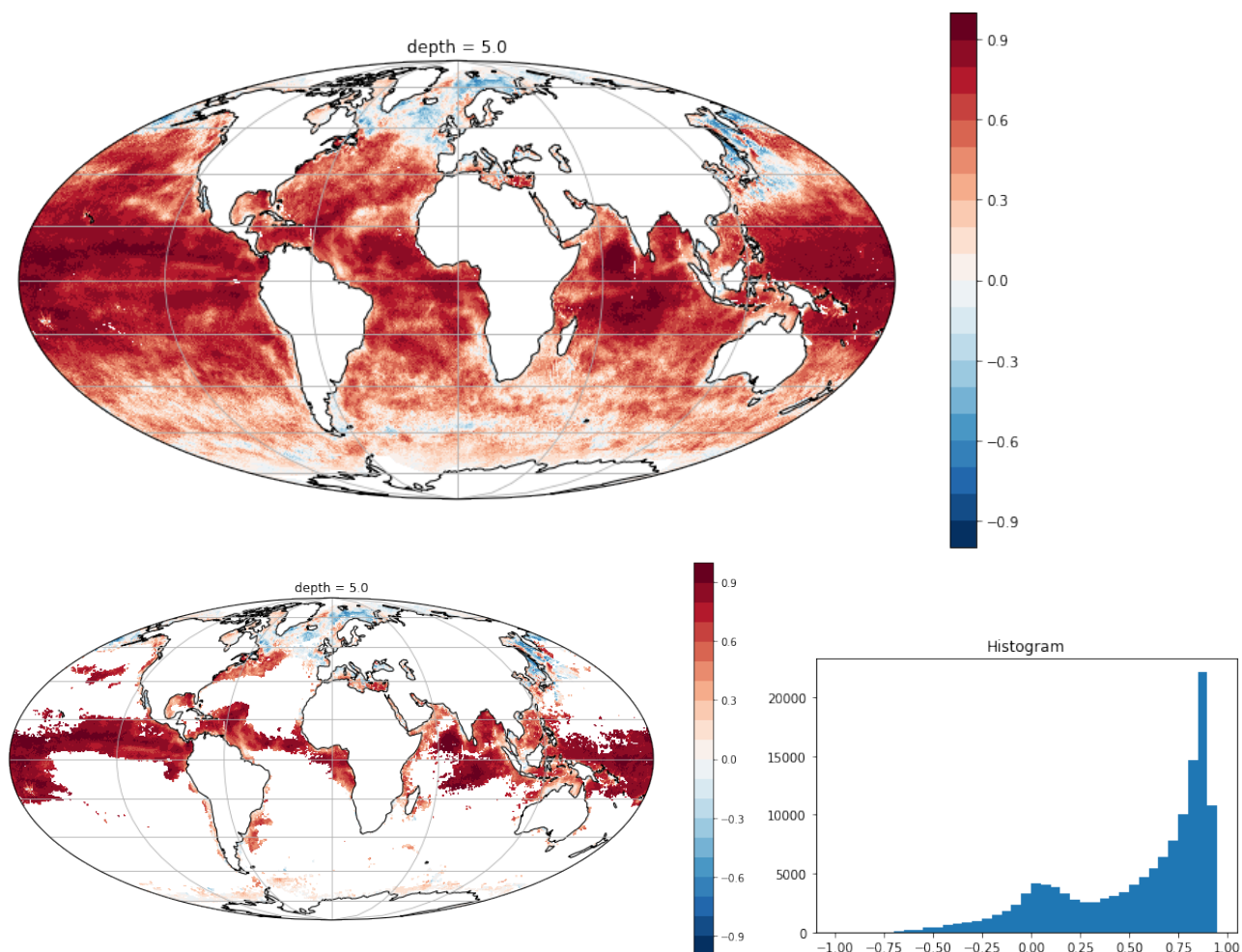


Figure 24: Temporal correlation of SSS between CCI and ISAS on ISAS grid cell in colour from -1 to +1. (top) for the global ocean. (bottom left) for the portion of the ocean with highest SSS variability observed from CCI (absolute maximum departure from CCI climatology > 0.8 pss). (bottom right) histogram of the correlation limited to the area with highest variability.

Figure 24 represents the temporal correlation of CCI with ISAS over the full time series 2010-2018. The correlations are generally positive and above ~0.5 over much of the open ocean, particularly over low latitudes. We have selected from the CCI dataset areas where the absolute maximum departure from the climatology over the full time period is higher than 0.8 pss. Correlations for these areas are reproduced on the bottom left of the above figure. A histogram of these correlations are given on the bottom right of the figure. This highlights the correlation is above 0.8 for a large part of the ocean corresponding to the tropical regions, and the lower correlations close to 0 concern areas at high latitudes. As the CCI signal has been selected based on a high amplitude, there is an important difference between the time-series over these high latitude areas.

4.4 Over region of low SSS variability

In this section, we have selected from the CCI dataset areas where the absolute maximum departure from the climatology is less than 0.4 pss.

The distribution of differences between CCI and Argo (Figure 26) is narrower than the global difference distribution (Figure 4). The distribution is quasi normal with very small differences between the two standard deviation estimates (0.15 pss for the 'simple' and 0.12 for the robust).

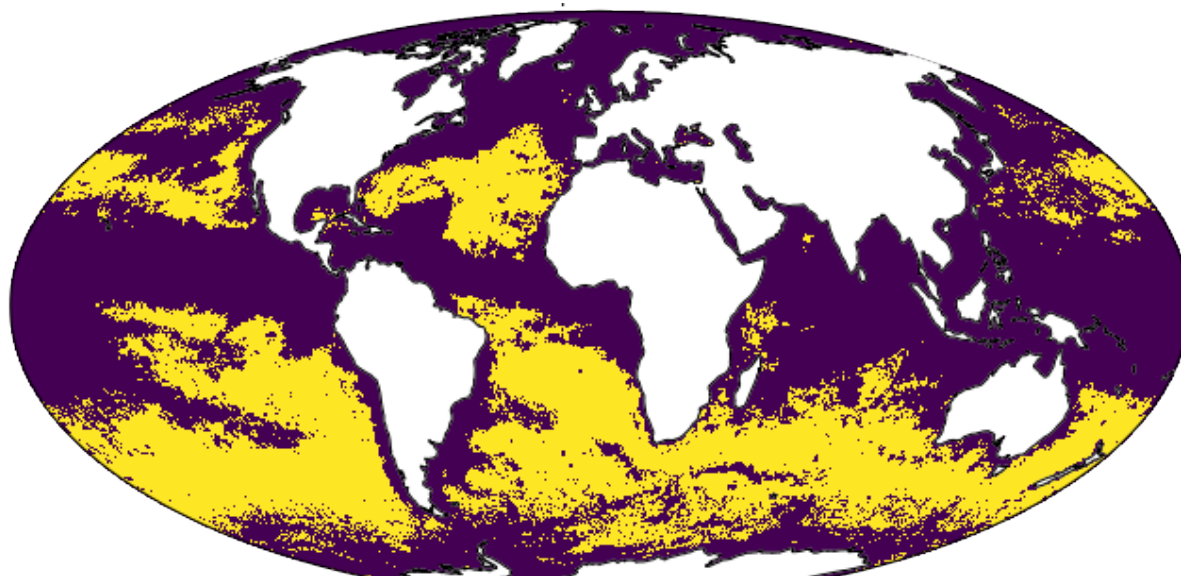


Figure 25: In yellow, ocean area with low variability where the absolute maximum departure from CCI SSS climatology is below 0.4 pss. It corresponds to half the ocean surface.

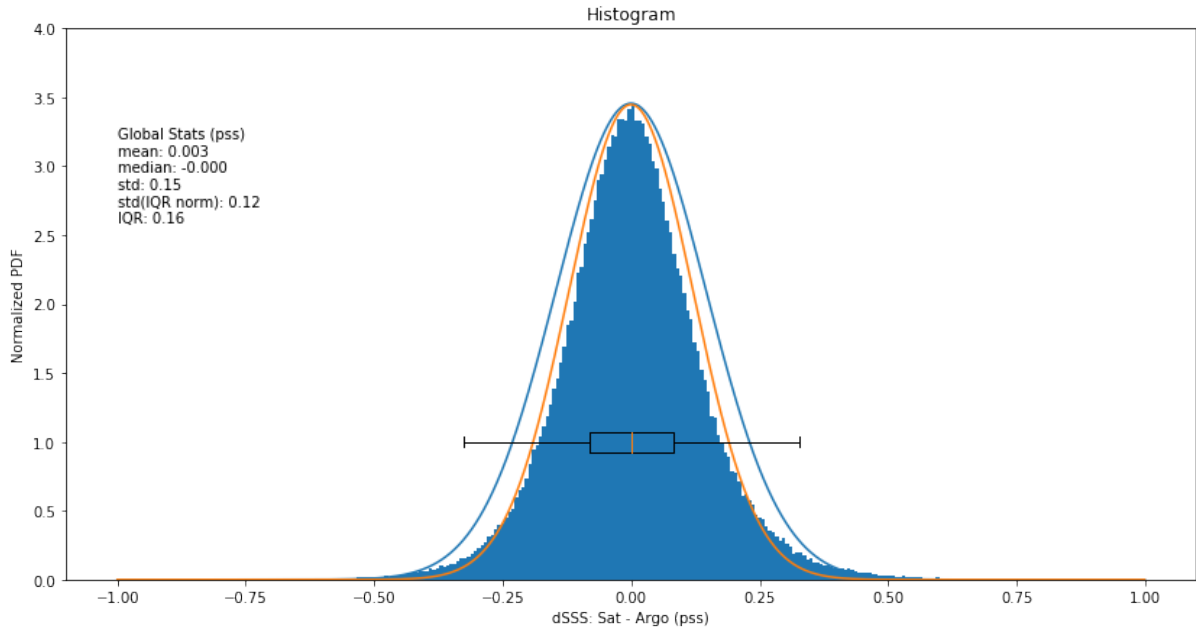


Figure 26: As Figure 4 but for the area defined by its low variability as represented in Figure 25.

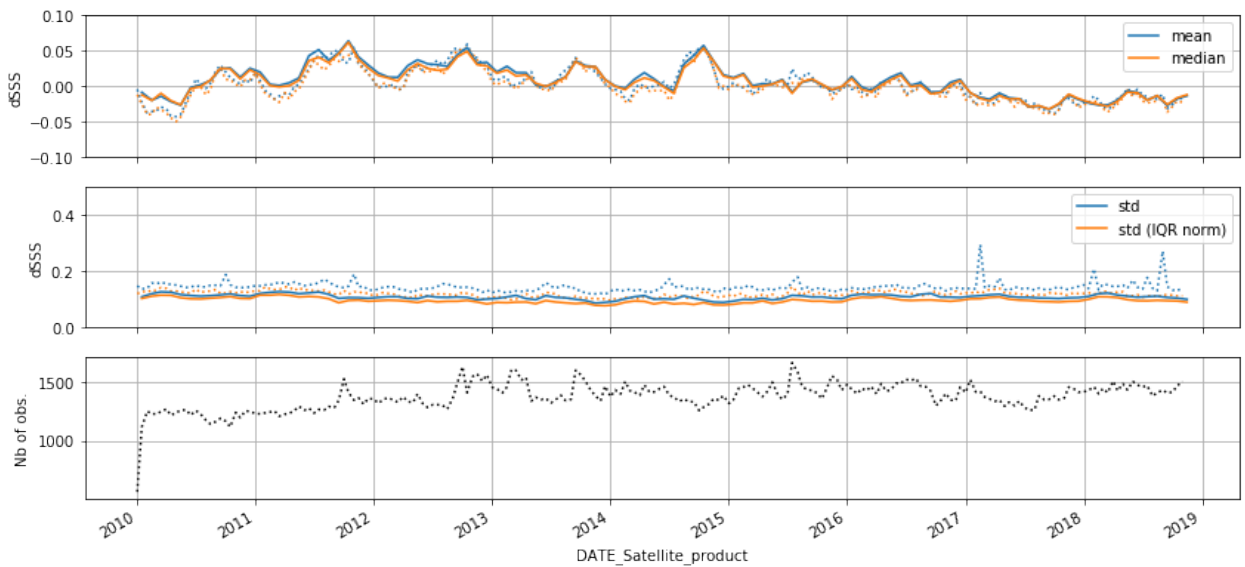


Figure 27: As Figure 5 but for the area defined by its low variability.

The time series in Figure 27 highlights that differences between CCI and reference datasets remains generally within ± 0.05 pss. There is an oscillation of more than 0.05 pss between 2011 and 2015 associated with a positive bias (CCI saltier than references). There is a positive trend in 2010-2011 and from 2016 onwards there is a small negative trend.

The precision is around 0.1 pss for the full time series with very small differences between the robust estimates and the ‘simple’.

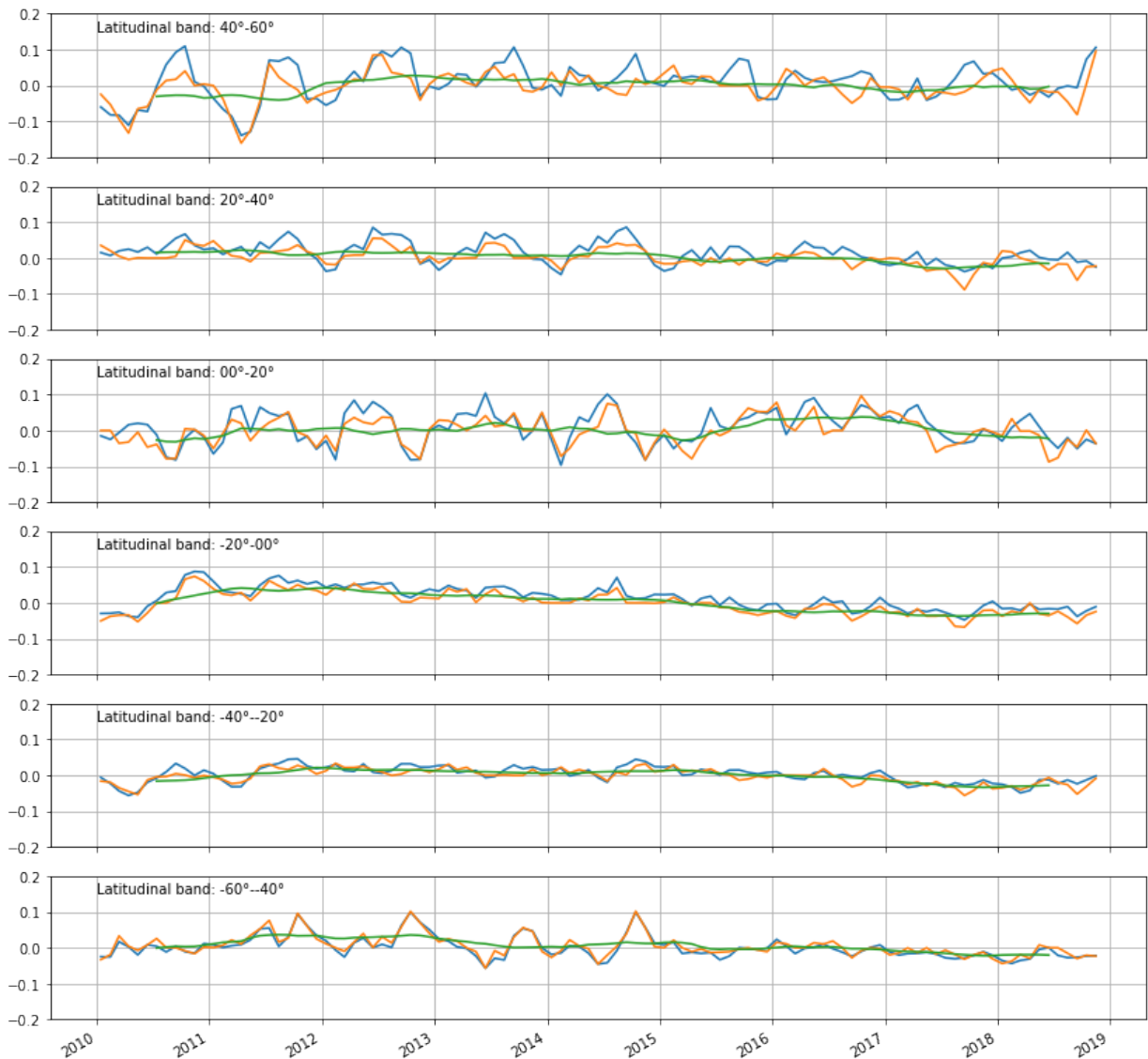


Figure 28: As Figure 7 but for the area defined by its low variability.

The latitudinal band averaging of the difference between CCI and ISAS over 20° bands (Figure 28) shows similar oscillation than the un-filtered global dataset (Figure 7), but with a smaller amplitude. Band 40N-60N presents a smaller seasonal cycle of -0.03,0.07 pss; versus +/-0.10 pss for the un-filtered.

Band 40N-60N and 20S-0° present a trend at the beginning of the period but smaller than that in Figure 7. Otherwise the long-term stability is very good and stays below +/-0.05 pss.

5 Validation for climate case studies

5.1 Case Study 1: North Atlantic salinity anomaly (Adrien Martin, Simon Josey; NOC)

We have evaluated CCI SSS capability to reproduce inter-annual variability in the North Atlantic with a focus on the subpolar gyre, where strong evidence for anomalous cold waters have been suggested (Josey et al., 2018). This case study aims to determine whether there is any corresponding signal in salinity using the ESA CCI SSS product and alternative sources of salinity data e.g. Argo. In this section, the ESA CCI SSS product is assessed using other in situ SSS products over areas of similar surface conditions (10° in latitude, 9° to 15° in longitude as a function of latitude; Figure 29).

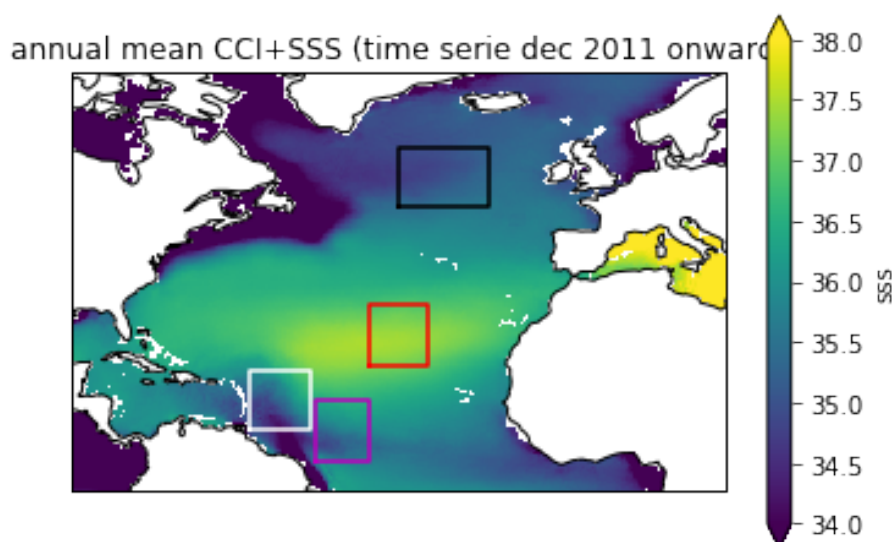


Figure 29: Annual mean of CCI climatology based on the 2012-onward time series. Boxes represent areas selected for time series comparison below. Violet for the equatorial box; white for the Caribbean box, red for the sub-tropical box and black for the sub-polar box.

In situ dataset are ISAS 2015; ISAS/CORA Delayed mode (ISAS CMEMS) and close-to-surface Argo measurements downloaded from Pi-MEP.

Figure 29 shows the CCI SSS annual mean field whereas the climatology seasonal cycle is shown in Figure 30 (top four panels, anomaly to the annual mean). The lower four panels in Figure 30 show the same for ISAS CMEMS. There is a very good agreement between the two data sources. There are some differences including CCI fields are sharper than ISAS demonstrating the effective higher spatial resolution. Close to the mouth of the Amazon there are discrepancies for Boreal Spring (MAM) and Autumn (SON) between CCI and ISAS. On the larger scale, the seasonal cycle is opposite for Winter (DJF) and Summer (JJA) between CCI and ISAS. In the Labrador Sea, there is a stronger seasonal cycle in ISAS than CCI.

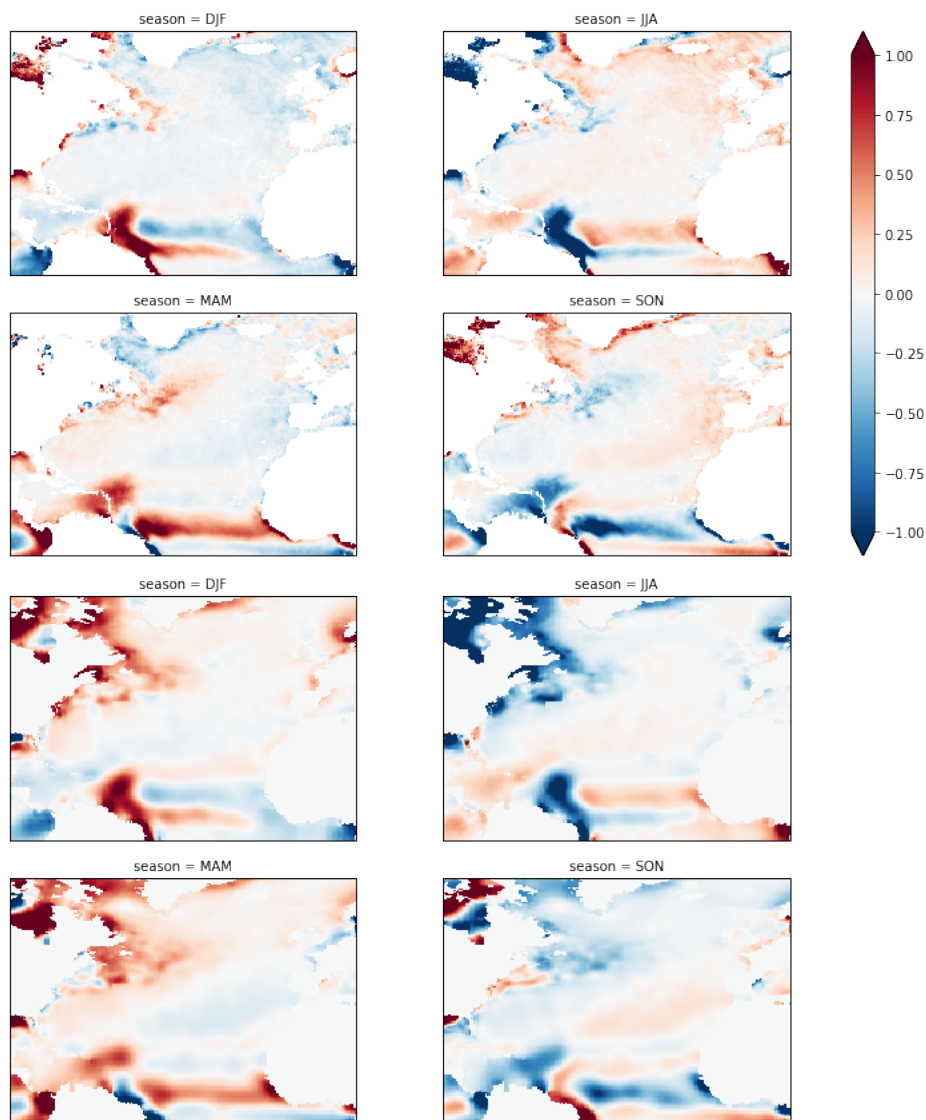


Figure 30: Seasonal cycle represented as the anomaly from annual mean (top) for CCI, top four panels, (bottom) ISAS CMEMS, following 4 panels. Season are defined with first letter of each month. DJF for winter; MAM for spring, JJA for summer and SON for winter.

The inter-annual anomalies (Figure 31) for the period 2012-2018 highlight a trend from fresh to saltier affecting most parts of the basin and for all seasons (signal smaller in Summer JJA). We have ignored the first two years of the CCI dataset due to the strong impact of RFI centred around Southern Greenland (Figure 32). This RFI results in a freshening in the northern part of the North Atlantic, but was switched off in late 2011.

A more quantitative assessment is undertaken for the study regions shown as the boxes in Figure 29. Two of these regions sample the Amazon plume (equatorial and Caribbean boxes),

another corresponds to the sub-tropical gyre (SPURS) and the last samples the sub-polar gyre (Figure 33 and Figure 34).

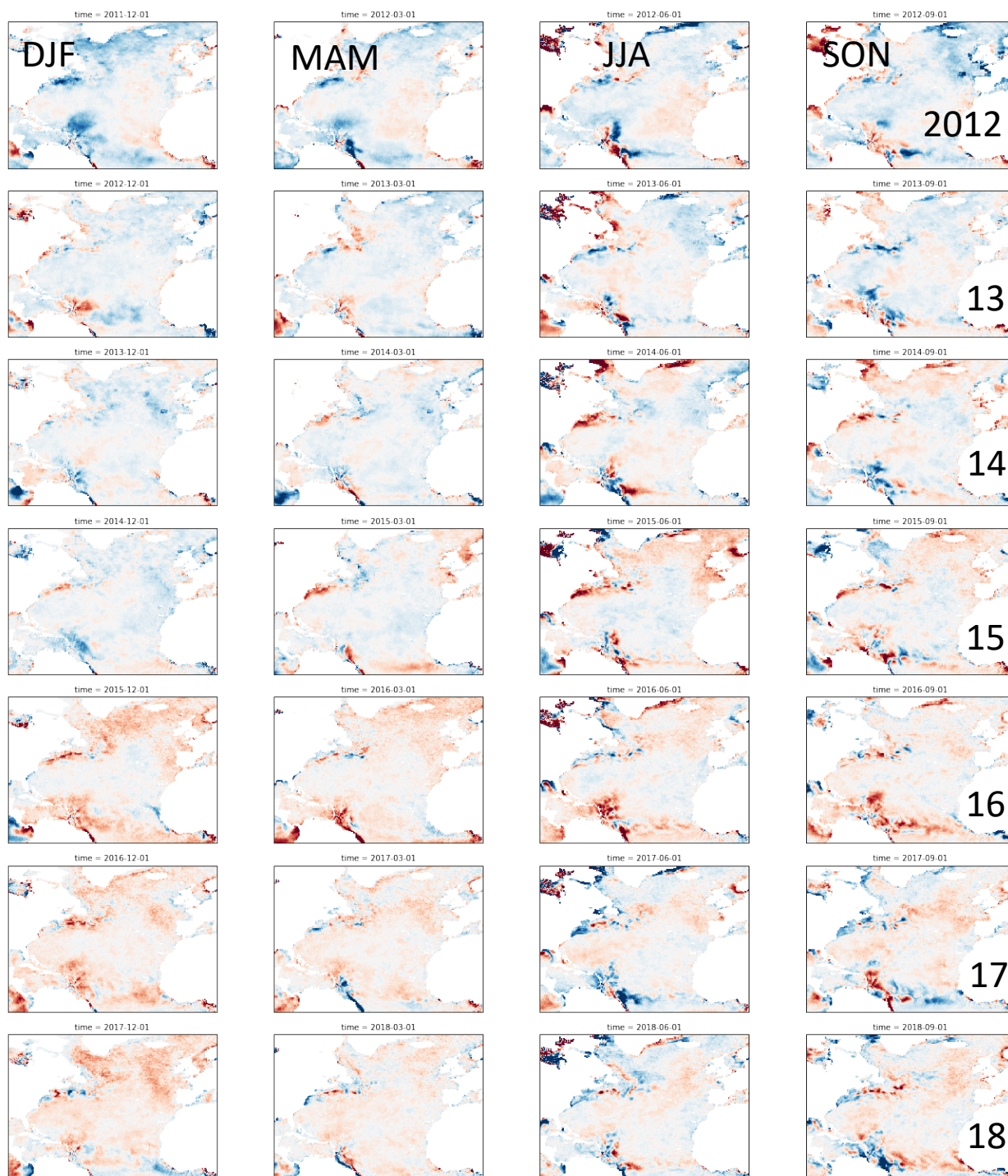


Figure 31: CCI anomaly from climatology (2012-2018) with season for the different columns and years for the rows.

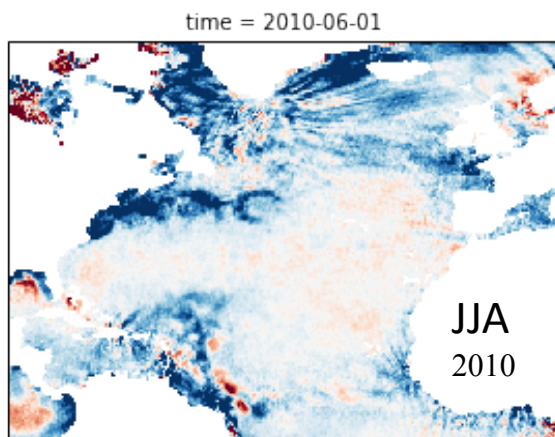


Figure 32: Example of SSS field strongly affected by RFI from the Southern part of Greenland.

Both boxes sampling the Amazon plume present a strong seasonal cycle of 1 pss or more (Figure 33 left two last rows and Figure 34 bottom row). There is a very good agreement between the different products. Freshening tend to be stronger with CCI than with ISAS, and is stronger with the top quality ISAS 2015 product than for the routine ISAS CMEMS product.

Concerning the inter-annual variability, there is a good agreement between products (Figure 33 right). For the Equatorial box, CCI product presents some strong peaks corresponding to minima in the seasonal cycle. Same for ISAS CMEMS in 2015 and 2016. This indicates in this area, the anomaly in the climatology cycle does not affect equally the different products. The Caribbean box is characterised by a strong intra-annual variability (> 0.4 pss) with oscillations of two to three years. All products agree on this variability.

The two other boxes (sub-tropical and subpolar) are characterised by a much smaller intra/inter-annual variability. The seasonal cycles are of 0.2 pss (Figure 34 top row). In the sub-tropical box, there is a good agreement in seasonal cycle between products despite an apparent bias for the average computed using Argo. For the sub-polar box, there is a rough agreement on the position of the maximum (Spring) and minimum (Fall) but there are discrepancies of the order of 0.1 pss.

Concerning the inter-annual variability, the sub-tropical box presents a variability up to 0.2 pss with a good agreement between all products, whereas the sub-polar presents opposite trends between CCI and both ISAS products. CCI trend is about 0.2 pss over (2012-2018) six years period.

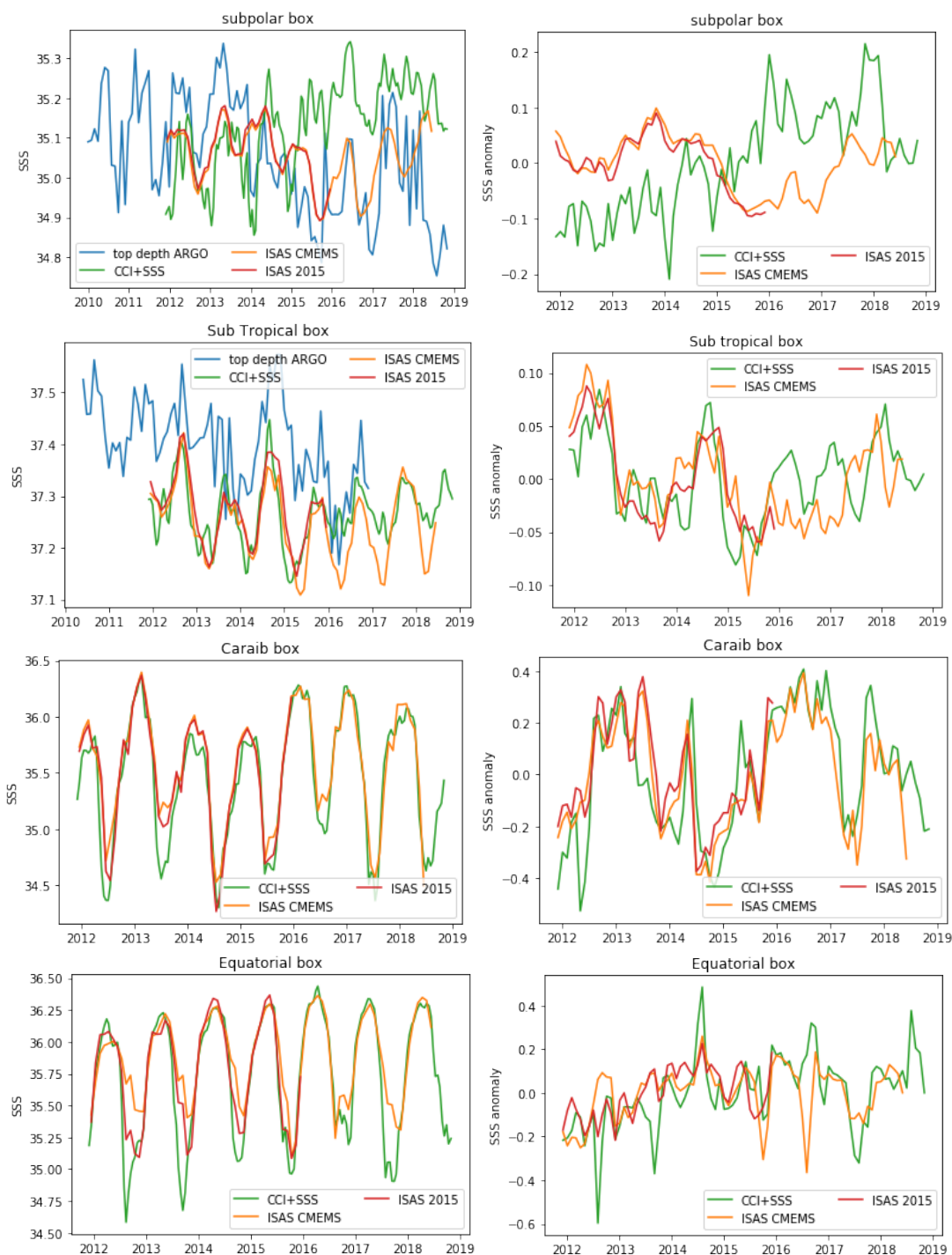


Figure 33: Time series for the four boxes defined above (one box per row). (Left column) for the time series averaged over the box for the different fields, CCI in green; ISAS CMEMS Delayed mode in orange; ISAS 2015 in red; on close-to-surface Argo measurements averaged over the box in blue. (Right column) Anomaly to the climatology computed over each box.



**Climate Change Initiative+ (CCI+)
Phase 1**
Product Validation and
Intercomparison Report

Ref.: ESA-CCI-PRGM-EOPS-SW-17-0032
Date: 07/04/2020
Version : v1.1
Page: 59 of 115

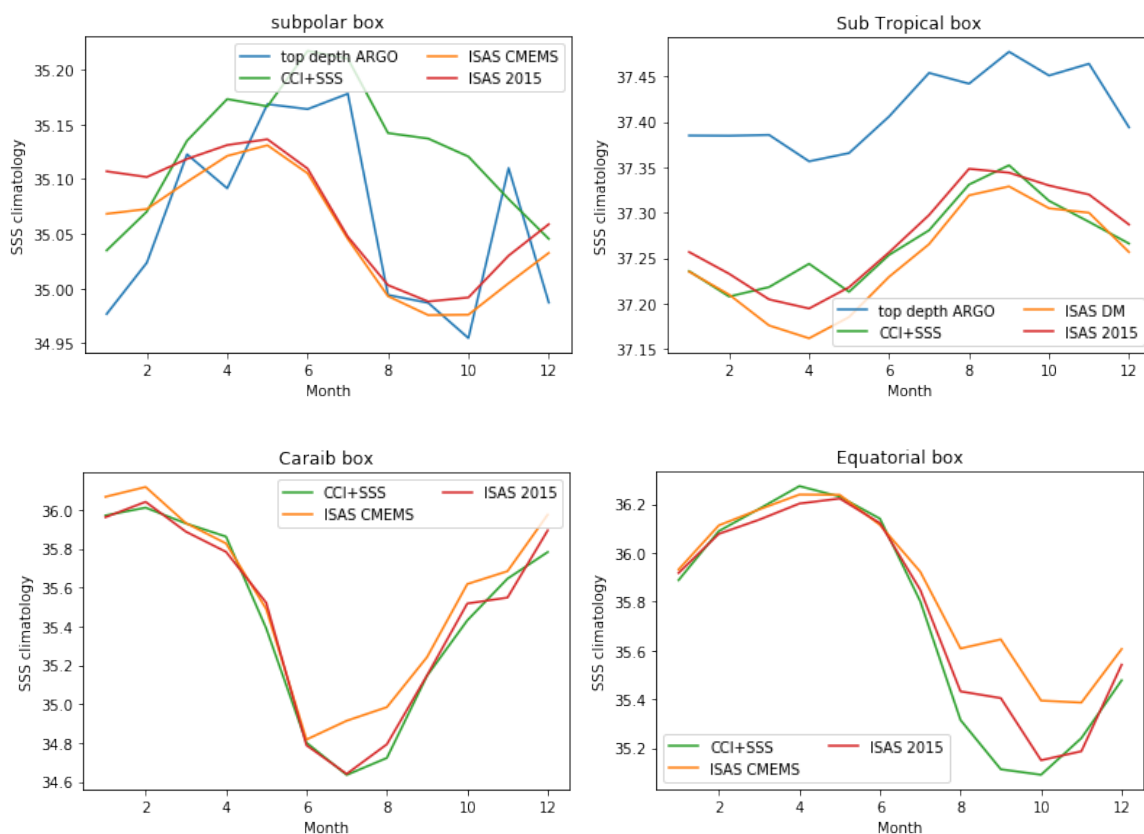


Figure 34: Climatology for the four boxes.



5.2 Case study 2: SSS and SSS error validation in the tropical Atlantic Ocean (Léa Olivier, Gilles Reverdin, J. Boutin, LOCEAN):

To evaluate the capacity of the satellite derived product to reproduce the SSS, we compare it to in situ SSS measurements from ship mounted thermosalinographs (TSG).

In-situ salinity data from the CAP LORENZO ship of opportunity thermosalinograph from 2015 to 2018 are used. The CAP LORENZO cargo ship travels back and forth from Europe to Brazil/Argentina six times a year. The along-track sea surface salinity data set was made freely available by the French Sea Surface Salinity Observation Service (<http://www.legos.obs-mip.fr/observations/sss/>) (Alory et al., 2015). Every satellite SSS data (thereafter called CCI) grid point is collocated with the ship track. To take into account the fact that the actual resolution of the CCI product is of 50 km, a Gaussian smoothing where 95% of the 50 km information is contained in the Gaussian (standard deviation $\sigma = 50/4$) is applied to the TSG data. Then, all of the ship TSG data points contained in a CCI grid point are averaged.

The aim of this study is to take advantage of the high resolution and good spatial resolution of the SMAP and SMOS combined SSS products. The comparison is then focused on the April 2015 - January 2018 period, where both satellites are operational and data are combined in the CCI product. Since we are mainly interested in SSS gradients, we compare the CCI SSS gradient to the TSG SSS gradient. An example obtained with CCI products is shown in Figure 35a. The satellite data being quite noisy, we decide to average the CCI SSS on 5 pixels in longitude (50 km on each side of the 25 km pixel). In the equatorial region, structures are mainly zonal and gradients mainly meridional, so not much information should be lost in such a process. The signal to noise ratio is then expected to increase, as confirmed by Figure 35b. Most of the noise has been reduced, and strong gradients are still very well represented by the CCI data. For the example of the 15th of October 2015, the gradient associated with the intertropical convergence zone (ITCZ) between 6° and 8° North, is very well represented by the CCI data, in shape and intensity. When the gradient is weak, data should be cautiously interpreted. However, in order to analyse the main gradients in the central equatorial Atlantic, the CCI product is very faithful to the in-situ observations.

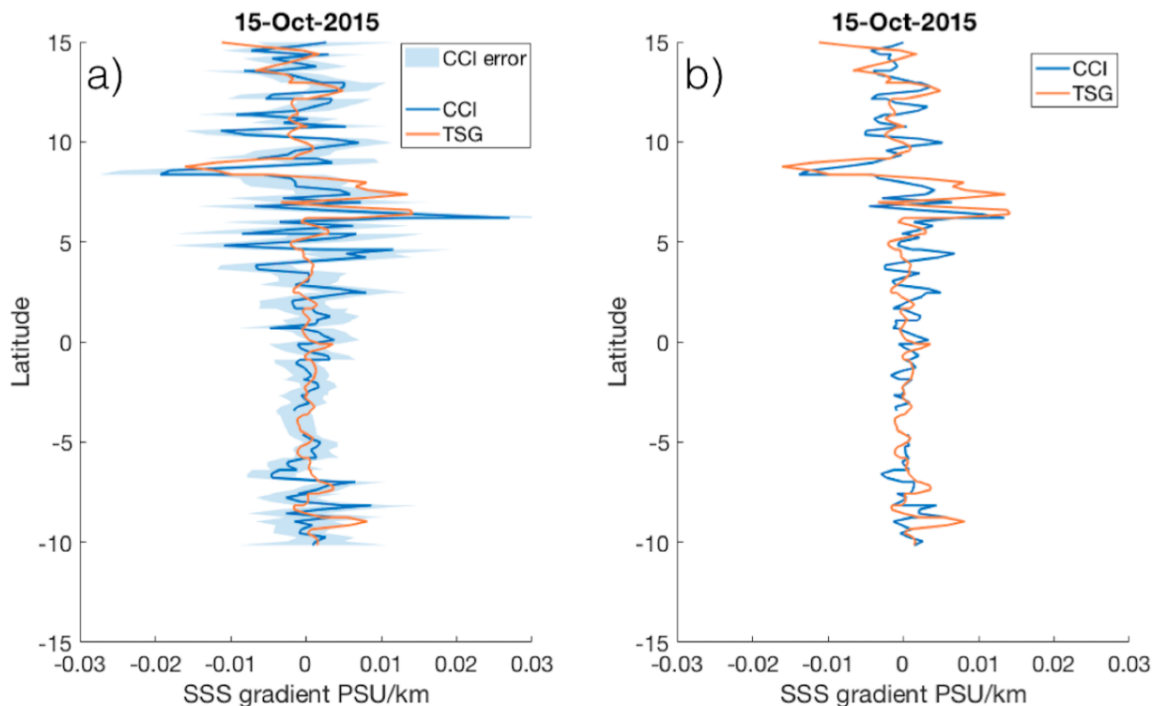


Figure 35: a) In blue are represented the CCI salinity gradients and in orange the ship ones for the 15th of October 2015. b) Same as a) but with an average on 5 pixels in longitude.

One of the objectives of the climate change initiative project is to provide well defined uncertainties for each data point. The CCI dataset is then supplying SSS errors at each grid point. By comparing the root mean square (RMS) of the CCI errors on the 33 transects to the standard deviation (STD) of the difference between the SSS measured by satellite and the one observed by ships, one finds that the CCI errors of the weekly fields seems to be overestimated by approximately 40% (Figure 36). This test points out a flaw in the propagation of errors between monthly and weekly CCI products that is going to be corrected in future CCI versions. For the error on the salinity gradient, we consider that it can be calculated as :

$$Err_{grad} = \sqrt{(Err_{SSS}(i + 1))^2 + (Err_{SSS}(i - 1))^2} / dist$$

Comparing the RMS of this error to the STD of the difference between the CCI SSS gradient and the TSG SSS gradient, we find that CCI gradient error is overestimated by roughly a factor 2. This suggests that errors in pixels at 50 km distance are correlated, possibly due to elongation of the SMOS measurements lobes at the front of its field of view. This will require further investigation in the future. The errors of the 30 days CCI files are more consistent with the STD of the salinity CCI and salinity TSG. Indeed, we find that the RMS of the CCI errors over all the transects is 20% lower than the STD difference, which is coherent with the fact that given the temporal smoothing of the 30 days CCI product, some fluctuations by the ships

are not seen on the CCI. The correlation at 50km is still present and of the same order as in the 7 days CCI product.

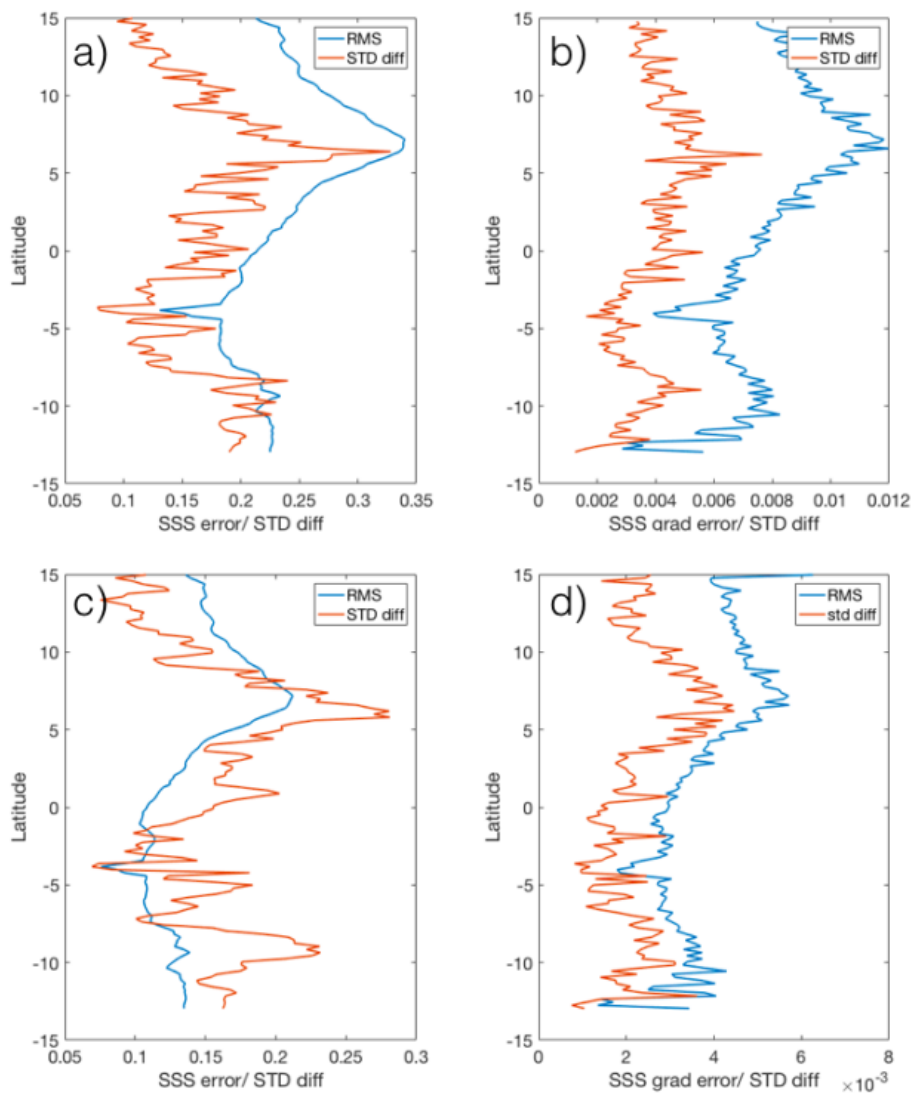


Figure 36: a) The blue curve represents the RMS of the errors given in the CCI product, while the orange curve presents the STD of the difference between the salinity CCI and the salinity from the ships. b) Same as a) but for the errors on the gradient (blue) and the standard deviation of the salinity gradient's difference (orange). c,d) same as a,b) for the monthly product.

5.3 Case study 3: Water cycle in the Bay of Bengal (Jérôme Vialard; LOCEAN)

The Bay of Bengal (hereafter, BoB) has large, seasonal freshwater inputs and an energetic circulation, including narrow coastal currents such as the EICC (East India Coastal Current) and a strong eddy variability. This creates large horizontal salinity gradients, which were previously difficult to study from available in situ data, sometimes resorting to fishermen collecting water samples on the beach to monitor the seasonal expansion of the fresh, southward-flowing EICC (Chaitanya et al. 2014). While SMOS initially performed poorly in the Bay of Bengal (Akhil et al. 2016a), a reprocessing of the data correcting for systematic differences created by land-sea contamination and radio-frequency interferences has allowed major improvements (Boutin et al. 2018), yielding a better performance than Aquarius and almost equivalent performance to that of SMAP (Akhil et al. submitted).

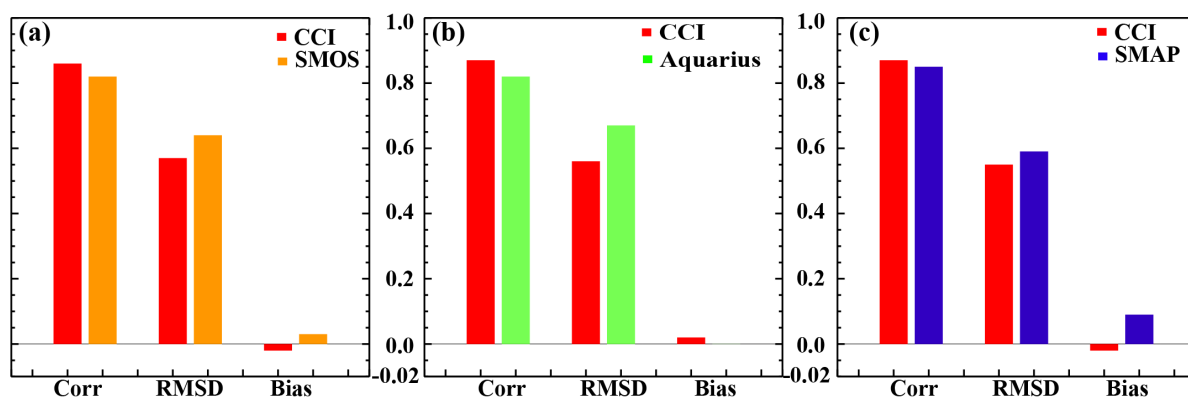


Figure 37: Comparison of the CCI+SSS product to co-located in situ SSS data in the Bay of Bengal, over the common observational sample with (a) SMOS, (b) Aquarius and (c) SMAP data. The CCI SSS has a higher correlation, smaller root-mean square difference and smaller bias relative to observations than all the other datasets.

We have started by repeating some of the validations that we had previously performed on the SMOS, Aquarius and SMAP projects to the CCI SSS. The CCI product reveals a slightly better performance than any of the other products over their common periods (Figure 37).

Publication

Akhil, V.P., J. Vialard, M. Lengaigne, M.G. Keerthi, J. Boutin, J-I. Vergely and F. Papa, 2019: Bay of Bengal Sea Surface Salinity variability using 8-years of improved SMOS re-processing, Rem. Sens. Envir., submitted.

References

Akhil, V.P., F. Durand, M. Lengaigne, J. Vialard, M.G. Keerthi, V.V. Gopalakrishna, C. Deltel, F. Papa and C. de Boyer Montégut, 2014: A modeling study of the processes of surface salinity seasonal cycle in the Bay of Bengal, J. Geophys. Res. Oceans, 119, doi:10.1002/2013JC009632.



Climate Change Initiative+ (CCI+)
Phase 1
Product Validation and
Intercomparison Report

Ref.: ESA-CCI-PRGM-EOPS-SW-17-0032
Date: 07/04/2020
Version : v1.1
Page: 64 of 115

Akhil, V. P., M. Lengaigne, J. Vialard, F. Durand, M. G. Keerthi, A. V. S. Chaitanya, F. Papa, V. V. Gopalakrishna, and C. de Boyer Montégut, 2016a: A modeling study of processes controlling the Bay of Bengal sea surface salinity interannual variability, *J. Geophys. Res. Oceans*, 121, 8471–8495, doi:10.1002/2016JC011662.

Akhil, V.P., M. Lengaigne, F. Durand, J. Vialard, V.V. Gopalakrishna, C. de Boyer Montégut and J. Boutin, 2016b: Validation of SMOS and Aquarius remotely-sensed surface salinity in the Bay of Bengal, *IJRS*, 37, doi: 10.1080/01431161.2016.1145362

Chaitanya, A.V.S., M. Lengaigne, J. Vialard, V.V. Gopalakrishna, F. Durand, Ch. Krantikumar, V. Suneel, F. Papa and M. Ravichandran, 2014: Fishermen-operated salinity measurements reveal a “river in the sea” flowing along the east coast of India, *Bull. Am. Met. Soc.*, 95, 1897–1908.

Fournier, S., Vialard, J., Lengaigne, M., Lee, T., Gierach, M. M., & Chaitanya, A.V. S., 2017: Modulation of the Ganges-Brahmaputra river plume by the Indian Ocean dipole and eddies inferred from satellite observations. *Journal of Geophysical Research: Oceans*, 122, 9591–9604. <https://doi.org/10.1002/2017JC013333>



5.4 Case study 4: Salinity stratification and small-scale variability (N. Reul, N. Kolodziejczyk, O. Houdegnonto, C. Maes and T. O’Kane; LOPS)

5.4.1 SSS Mesoscale features in CCI+SSS products

The surface mixed layer thermohaline structures at meso-scale to submesoscale (smaller than the local radius of deformation, *Chelton et al.*, 1998) are ubiquitous features in the global ocean. They contribute to horizontal and vertical heat and salt exchange, and vertical re-stratification (*Fox-Kemper et al.*, 2008). They have a global impact on ocean circulation and climate since they contribute to the cascade of energy from large scale toward the smallest scales of diffusive mixing (*Callies and Ferrari*, 2013). Eventually, they have a major impact on biogeochemistry and ecosystems. The submesoscale processes are characterized by very intense vertical velocities that allow strong exchanges of carbon, oxygen and nutrient between surface and subsurface ocean (*Lévy and Martin*, 2013).

Until early 2010, satellite capabilities for observing surface thermohaline variability have mainly relied on the observation of Sea Surface Temperature (SST) only, resolving horizontal small scale features such as 10 km (*Kilpatrick et al.*, 2015). In contrast, synoptic image of Sea Surface Salinity (SSS) were not available and in situ SSS at high resolution are only available from a few high resolution transects from Thermosalinograph (TSG) survey from ship of opportunity or cruise campaign (*Kolodziejczyk et al.*, 2015b). Since 2010, thanks to ESA SMOS mission, then NASA Aquarius and SMAP missions, 4-7 days global maps of SSS at resolution between 40-100 km are now available, permitting the observation of larger mesoscale features in subtropical and tropical regions (*Reul et al.*, 2014; *Kolodziejczyk et al.*, 2015a).

In order to check the effective capability of the new CCI-SSS product (7 day) to monitor the mesoscale features of SSS in the subtropical and tropical regions, the CCI product’s SSS were systematically co-localized and compared with TSG SSS along existing repeated transect in Subtropical North Atlantic and Tropical Atlantic. An effective metric to assess the SSS horizontal variance and scale content of both products is to compute the spectra and coherency spectra between co-located TSG SSS and CCI+SSS transects (*Boutin et al.*, 2018).

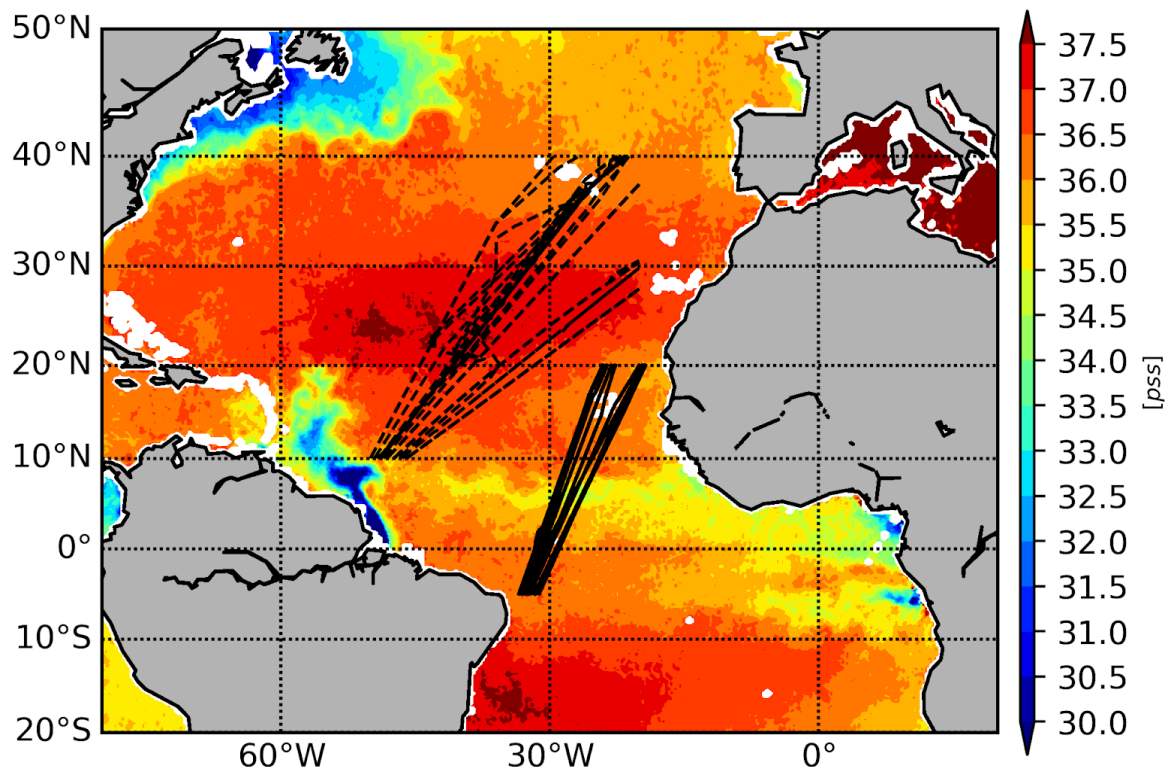


Figure 38: CCI+SSS on 30 June 2011. 88 SSS TSG transects in the Subtropical North Atlantic (dashed) and 26 SSS TSG transect in the Tropical Atlantic. All SSS transects have been carried out between 2011-2016.

SSS TSG transects were collected from ships of opportunity (representative of salinity at 10 m depth), resolving horizontal SSS features around 2-3 km (Alory *et al.*, 2015). Two regions were chosen for the present study (Figure 38): i) the North Atlantic subtropical SSS maximum (50-20°W/10-40°N), where 88 transects over 2011-2016 are available; and ii) the Tropical Atlantic (40-10°W/5°S-20°N) where 26 transects over 2014-2016 are available. Individual transects were visually inspected and suspicious transects were discarded. In order to reduce uncertainty due to noisy individual spectrum from each individual transect, spectra were averaged for both regions.

The horizontal SSS coherency spectra refer to the coherency of the SSS horizontal variability between the co-located TSG SSS and CCI+SSS products, i.e. the level of correlation of the SSS signal for a given wavelength range. This allows to assess the actual capability of CCI+SSS products to observe and resolve mesoscale features (>50 km).

In the Subtropical North Atlantic (Figure 39), in spite of slightly less energy between 50-1000 km wavelength, CCI+SSS horizontal variance spectrum, both TSG and CCI+SSS spectra show good agreement, i.e. comparable spectral slopes between 50-1000 km are observed. This suggests that for this range of wavelength the variance of mesoscale features are probably smoothed in CCI+SSS products. Interestingly, the coherency exhibits quasi-linear decrease from large scale (coherency>0.75 for wavelength > 1000 km) to mesoscale

(coherency \sim 0.30 for wavelength \sim 300 km). The significance (at 95%) is lost for wavelength below 200 km. This suggests that wavelengths smaller than 300 km are poorly represented in the CCI+SSS product. This is consistent with a previous study investigating the SMOS LOCEAN CEC L3 product (*Boutin et al., 2018*) in the same region, however with a slightly better coherency for CCI+SSS product.

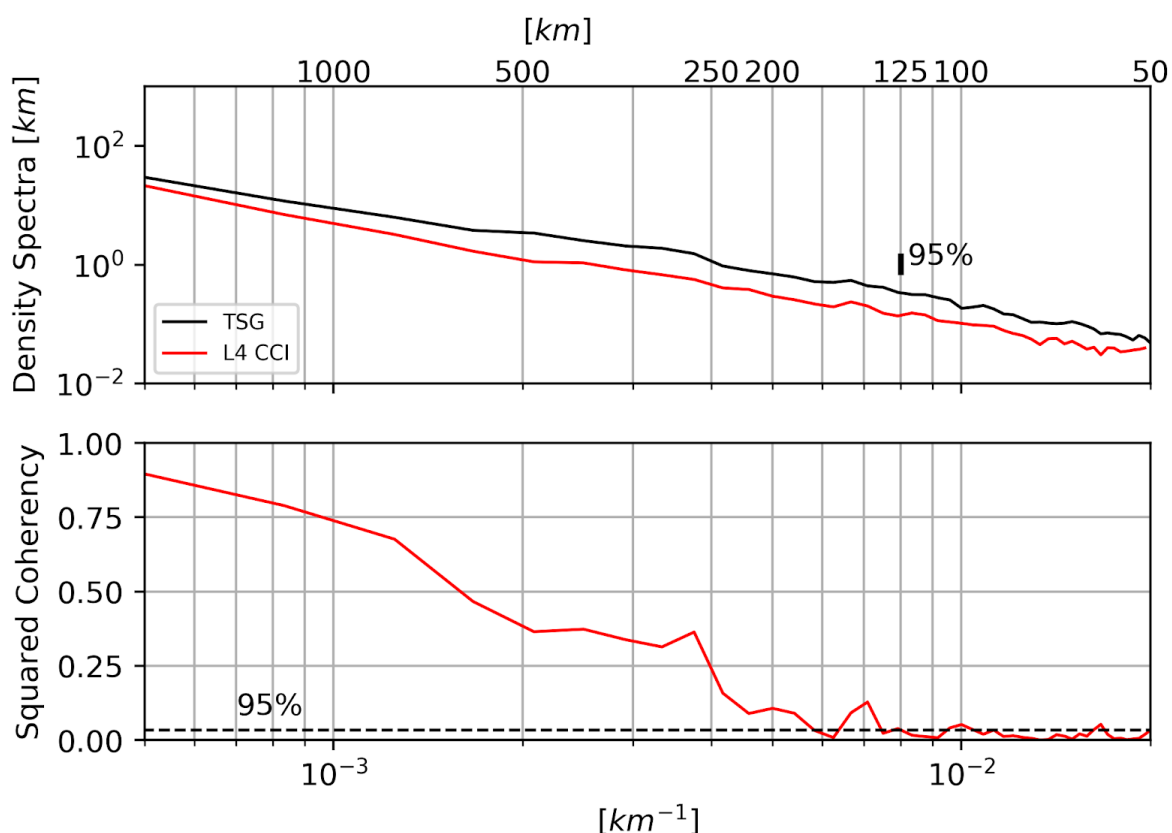


Figure 39: Upper panel: Density spectra from from 88 co-located TSG(black)/CCI+SSS(red) SSS transects in Subtropical North Atlantic. Vertical thick black bar is the level of confidence at 95%. Lower panel: Coherency between the TSG and CCI+SSS SSS transects. Dashed line is the level of significance at 95%.

In the Tropical Atlantic (Figure 40), TSG and CCI+SSS spectra show very comparable behaviors, the level of variance and slope have comparable values. Furthermore, both spectra also show a relatively high level of coherence at wavelengths larger than 300 km (coherency $>$ 0.5). In the Tropical Atlantic region, the coherency drops at wavelengths smaller than 200 km. It suggests that the CCI+SSS product is not able to consistently resolve scales smaller than 100 km.

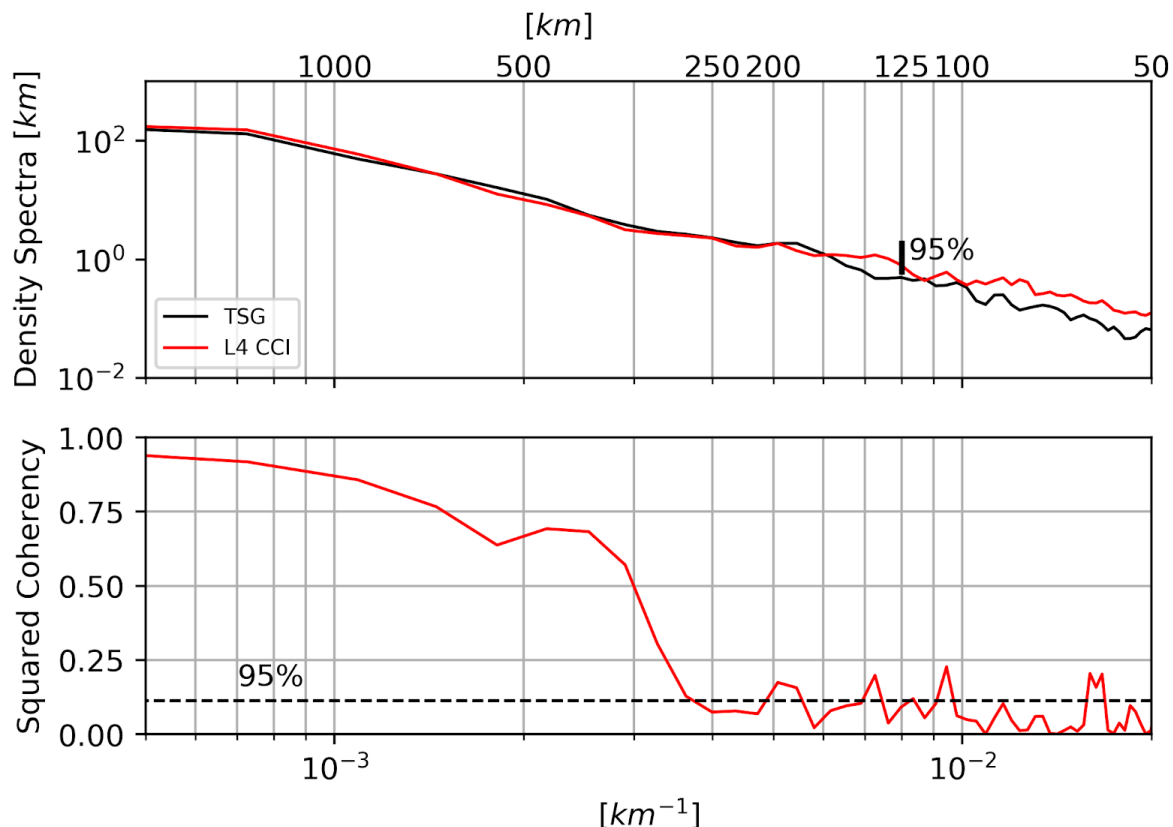


Figure 40: Upper panel: Density spectra from 26 colocated TSG(black)/CCI+SSS(red) SSS transects in Tropical Atlantic. Vertical thick black bar is the level of confidence at 95%. Lower panel: Coherency between the TSG and CCI+SSS SSS transects. Dashed line is the level of significance at 95%.

In conclusion, in the subtropical Atlantic, the CCI+SSS product is able to resolve wavelengths of the order of 300 km. This wavelength corresponds to horizontal mesoscale features of the order of about 150 km (such as large gradient or eddy). However, the level of coherency between TSG SSS horizontal variability and CCI+SSS drop rapidly at mesoscale. In the tropics the level of coherency remains high up to 300 km wavelength, then drop dramatically.

The loss of coherency at smaller horizontal wavelength could be explained by i) the limited resolution of SSS satellite mission (>50 km), ii) the remaining noise and artefacts in the CCI+SSS data, and iii) smoothing from objective analysis procedure of the CCI+SSS products. Nevertheless, it is worth pointing that inconsistency between instantaneous and point-wise measurements from the TSG data and co-localized CCI+SSS products (7 days, 50 km) may be responsible for shift and lag between TSG SSS measurements and CCI+SSS products SSS along transects, resulting in loss of coherency for the smaller and faster SSS mesoscale structures.



Climate Change Initiative+ (CCI+)
Phase 1
Product Validation and
Intercomparison Report

Ref.: ESA-CCI-PRGM-EOPS-SW-17-0032
Date: 07/04/2020
Version : v1.1
Page: 69 of 115

5.4.2 Validation of SSS+CCI products in the Gulf of Guinea

Gulf of Guinea is a key region for the regional climate variability. A noticeable regional climate feature is the Western African Monsoon, which is strongly influenced by sea surface temperature and subsurface conditions in the Gulf of Guinea, including stratification, mixing and circulation. Large river runoffs have strong impacts on the near surface stratification and mixing in the Gulf of Guinea. In return, the river plume extensions are strongly influenced by seasonal and interannual wind driven surface circulation. In the eastern Gulf of Guinea, historical in situ dataset suffers from sparse sampling providing little information on the river plume variability (*Da-Allada et al., 2013*). On the other hand, few model studies have focused on Eastern Gulf of Guinea SSS dynamics (*Camara et al., 2015*). SSS satellite missions offer a new opportunity to investigate the eastern Gulf of Guinea river plume dynamics. Furthermore, the recent enhancement of available in situ measurements in the Gulf of Guinea (Argo, TSG, CTD...) provides new perspective to investigate the stratification and small scale vertical structure within river plumes of the Gulf of Guinea region.

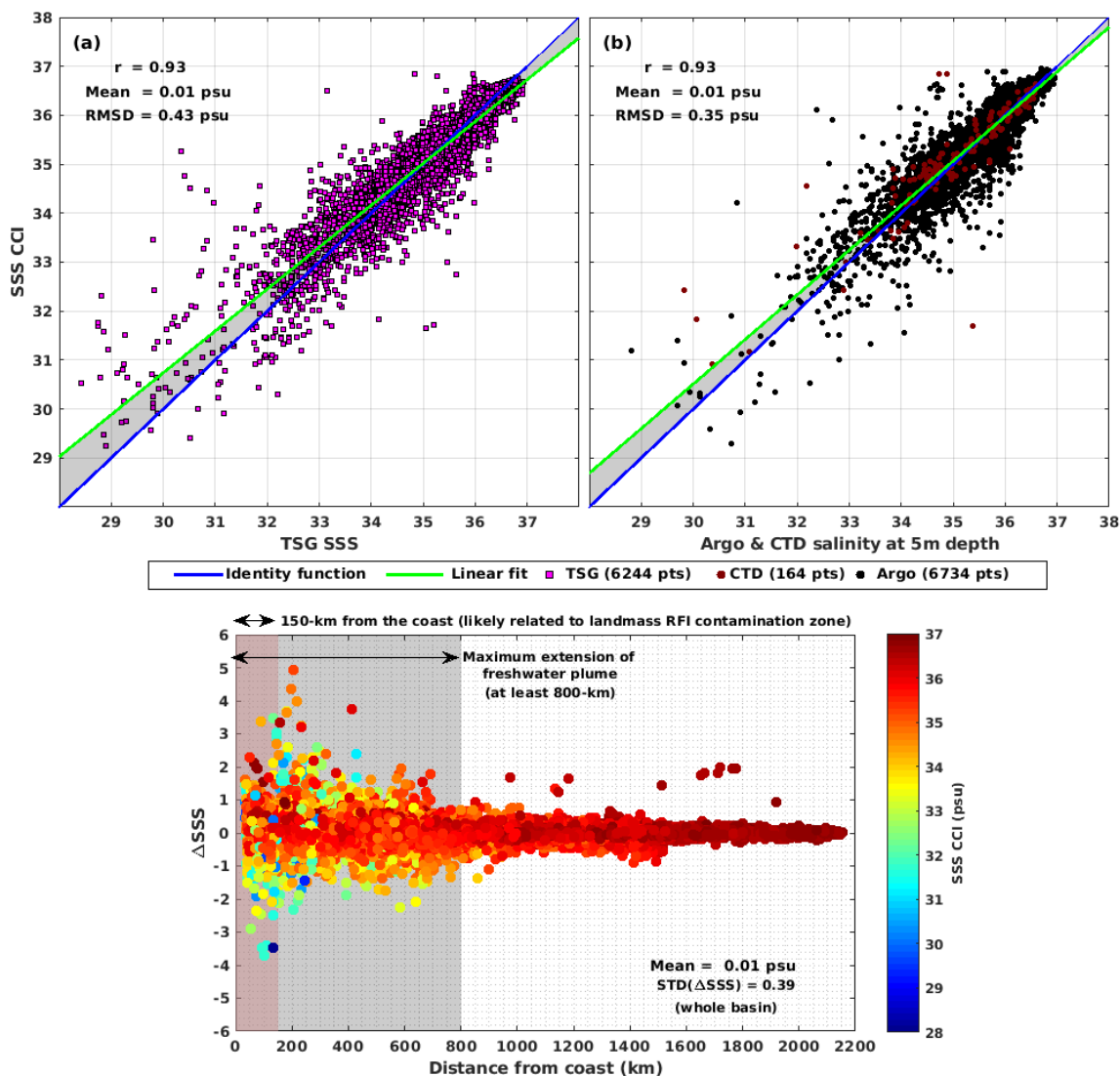


Figure 41: Upper panel: scatter plot of TSG SSS measurements (left) and Argo/CTD data (right) with the CCI+SSS products in the Gulf of Guinea (15°S-10°N/10°W-15°E) over the period 2011-2017. Lower panel: distribution of the difference of co-located in situ/CCI+SSS (in psu) as a function of the distance from the coast.

A first step is to validate the CCI+SSS products in the Eastern Gulf of Guinea. In the Gulf of Guinea (15°S-10°N/10°W-15°E), the available in situ SSS observation in the upper 10 m depth (TSG, Argo, CTD casts) have been co-located with CCI+SSS products (Figure 41; upper panel). Scatter plot for TSG and Argo/CTD products reveals a very good agreement with CCI+SSS products: with an insignificant bias (~0.01 psu), and a RMSD ranging from 0.43 psu for the comparison with TSG data and 0.35 psu for the comparison with the Argo and CTD data. This difference can be explained by the larger spread of the in situ/CCI+SSS products near coast (Figure 41; Lower panel). Indeed TSG measurements are generally carried out closer to the coast where residual coastal bias and RFI contamination can enhance the noise in the satellite measurements. Moreover, near coast the river plume signal generates



**Climate Change Initiative+ (CCI+)
Phase 1
Product Validation and
Intercomparison Report**

Ref.: ESA-CCI-PRGM-EOPS-SW-17-0032
Date: 07/04/2020
Version : v1.1
Page: 71 of 115

stronger SSS horizontal gradients and sharp surface salinity stratification, thus it implies larger difference when discrepancy exists between in situ observations and satellite products (Table 3).

Table 3: Statistics from in situ/CCI+SSS products difference for co-localisation in the Gulf of Guinea over the period 2011-2017.

Distance from the coast to offshore	150-km	800-km	whole basin (~2200-km)
Mean bias (Δ SSS)	- 0.03 <i>psu</i>	0.03 <i>psu</i>	0.01 <i>psu</i>
Mean absolute bias ($ \Delta$ SSS)	0.72 <i>psu</i>	0.47 <i>psu</i>	0.24 <i>psu</i>
STD (Δ SSS)	0.72	0.47	0.39
RMSD	0.72 <i>psu</i>	0.47 <i>psu</i>	0.39 <i>psu</i>
Correlation coefficient	0.84	0.90	0.94

References:

- Boutin J, J.L. Vergely, S. Marchand, F. D'Amico, A. Hasson, N. Kolodziejczyk, N. Reul, G. Reverdin and J. Vialard (2018): New SMOS Sea Surface Salinity with reduced systematic errors and improved variability. *Remote sensing of the Environment*, 214, 115-134. doi:10.1016/j.rse.2018.05.022.
- Callies, J., and R. Ferrari, (2013), Interpreting energy and tracer spectra of upper-ocean turbulence in the submesoscale range (1–200 km), *J. Phys. Oceanogr.*, 43, 2456–2474, doi:10.1175/JPO-D-13-063.1.
- Camara, I., N. Kolodziejczyk, J. Mignot, A. Lazar, and A. T. Gaye (2015), On the seasonal variations of salinity of the tropical Atlantic mixed layer, *J. Geophys. Res. Oceans*, 120, 4441–4462, doi:10.1002/2015JC010865.
- Chelton, D. B., R. A. de Szoeke, and M. G. Schlax (1998), Geographical variability of the first Rossby braoclinic radius of deformation, *J. Phys. Oceanogr.*, 28, 433–460.
- Da-Allada, C. Y., G. Alory, Y. du Penhoat, E. Kestenare, F. Durand, and N. M. Hounkonnou (2013), Seasonal mixed-layer salinity balance in the tropical Atlantic Ocean: Mean state and seasonal cycle, *J. Geophys. Res. Oceans*, 118, 332–345, doi:10.1029/2012JC008357.
- Fox-Kemper, B., R. Ferrari, and R. Halberg (2008), Parametrization of the mixed layer eddies. Part I: Theory and diagnosis, *J. Phys. Oceanogr.*, 38(6), 1145–1165.
- Kilpatrick, K. A., G. Podestá, S. Walsh, E. Williams, V. Halliwell, M. Szczodrak, O. B. Brown, P. J. Minnett, and R. Evans (2015). A decade of sea surface temperature from MODIS. *Remote Sensing of Environment*, 165, 27-41. <http://dx.doi.org/10.1016/j.rse.2015.04.023>.
- Kolodziejczyk, N., O. Hernandez, J. Boutin, and G. Reverdin (2015), SMOS salinity in the subtropical north Atlantic salinity maximum. Part II: Horizontal thermohaline variability, *J. Geophys. Res. Oceans*, 120, 972–987, doi:10.1002/2014JC010103.



Climate Change Initiative+ (CCI+)
Phase 1
**Product Validation and
Intercomparison Report**

Ref.: ESA-CCI-PRGM-EOPS-SW-17-0032

Date: 07/04/2020

Version : v1.1

Page: 72 of 115

Kolodziejczyk, N., G. Reverdin, J. Boutin, and O. Hernandez (2015), Observation of the surface horizontal thermohaline variability at mesoscale to submesoscale in the north-eastern subtropical Atlantic Ocean, *J. Geophys. Res. Oceans*, 120, doi:10.1002/2014JC010455.

Levy, M., and A. P. Martin (2013), The influence of mesoscale and submesoscale heterogeneity on ocean biogeochemical reactions, *Global Biogeochem. Cycles*, 27, doi:10.1002/2012GB004518

Reul, N., B. Chapron, T. Lee, C. Donlon, J. Boutin, and G. Alory (2014), Sea Surface Salinity structure of the meandering Gulf Stream revealed by SMOS sensor, *Geophys. Res. Lett.*, 41, 3141–3148, doi:10.1002/2014GL059215.

5.5 Case study 5: Comparing salinity variability between observations and models (D. Stammer, J. Köhler, M. Sena-Martins, A. Köhl; UHAM)

We aim to investigate the quality of the new CCI+SSS ECV product through a comparison of the satellite retrieved salinity variability with other in situ and model information both spatially and temporally. Available for such a comparison is a collection of in situ data which include all in situ data available. Also available is the access to own model simulations and those available from climate coupled models. All available data sets will be used together to investigate the salinity variability of the Atlantic, but also the Indian and the Pacific Ocean.

To compare the level of salinity signal to the level of background noise, the signal to noise ratio (SNR) was calculated by assuming random white noise for the CCI+SSS product. On average, the CCI+SSS product has a SNR above 4dB with highest SNR found in the tropical regions, often exceeding 6 dB meaning that the signal is at least 6 times the power of white noise (Figure 42).

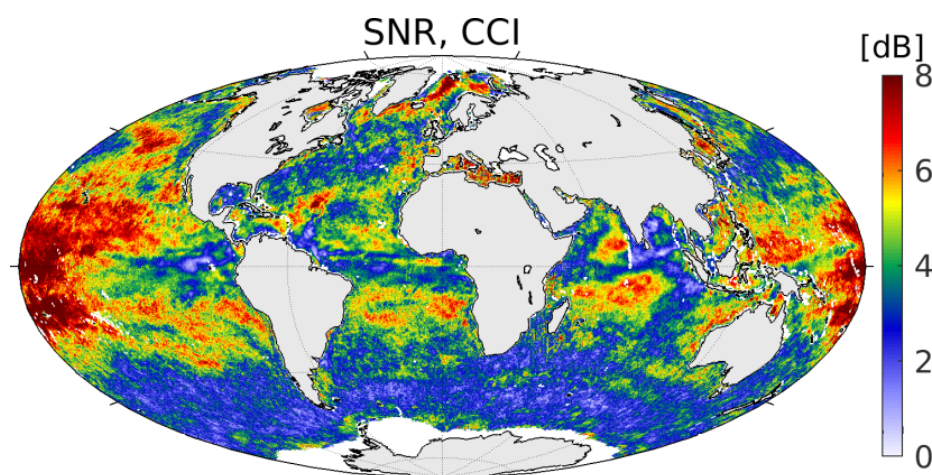


Figure 42: Signal to noise ratio (SNR) by assuming random white noise for the CCI+SSS product. The higher the value, the larger the signal. $SNR < 1$ means that noise is higher than signal.

The ratio of the annual amplitude of the difference between satellite CCI+SSS and EN4 uppermost salinity and the annual amplitude of the EN4 uppermost salinity is shown in Figure 43 right. High values (>1) indicate that the annual cycle of the differences is larger than the annual salinity cycle. This can be observed in the high latitudes, subtropical regions and in a small band at the equator. This could be an indicator of enhanced salinity stratification, unresolved salinity spatial features in EN4 maps (see case study 4 validation, PVIR) as well as data errors. All in all, the comparisons to the EN4 data show that satellite SSS show the expected patterns, but more finer structures in frontal regions etc., so that this data, with its higher temporal and spatial resolution, represents a gain for research.

Presented in Figure 43 left is the correlation of the seasonal CCI+SSS and in situ uppermost (approx. 5 m) salinity over the 2011-2018 period, reaching values larger than 0.8 in the

tropical and subtropical regions of all oceans. The correlation is, on the other hand, low in the Amazon outflow region and in the Bay of Bengal, where we have a strong annual signal but less accordance between SSS and uppermost salinity (compare section 5.2.3 and 5.2.4). Correlations are also low in subpolar and Polar Regions or in the western Arabian Sea.

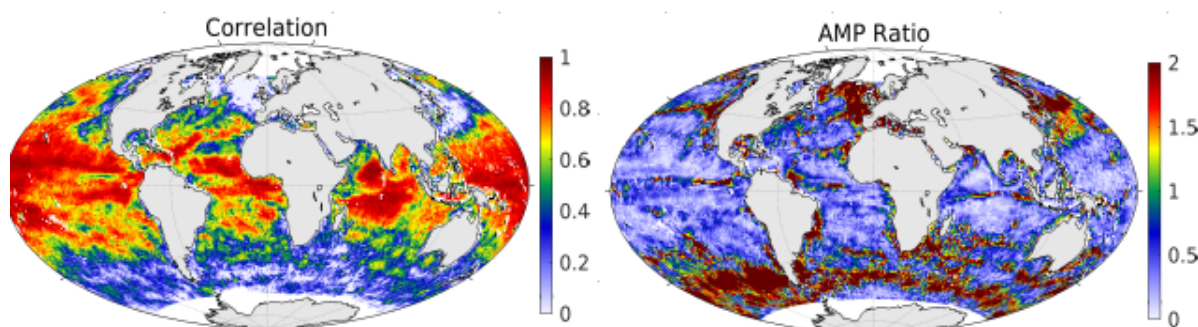


Figure 43: (left) Correlation of seasonal satellite SSS and uppermost EN4 salinity and (right) ratio of the annual amplitude of the difference between satellite CCI+SSS and EN4 uppermost salinity and the annual amplitude of the EN4 uppermost salinity. High values indicate that the annual cycle of differences between satellite and EN4 uppermost salinities is larger than the annual salinity cycle. This could be due to salinity stratification but also due to land-ice-contamination, RFI or sample errors in the in situ fields. The ratio shows high values in high latitudes, but also in subtropical/mid-latitude regions, where the amplitude of the annual cycle is generally low.

Many factors can cause the observed low correlations in these areas, like low SSS and uppermost salinity variance which leads to a computed low SNR (compare Figure 42), measurement errors in the satellite SSS (e.g., land contamination and RFI) and representative errors in the in situ fields. Strong rain events and salinity stratification in the upper layers can also cause low correlations, which could be of importance in the river outlet regions like the Amazon outflow and Bay of Bengal. Many studies, e.g. Köhler et al. (2018), Wilson and Riser (2016), Akhil et al. (2014), show the importance of stratification in the northern Bay of Bengal. Therefore, the ratio of the annual amplitude of the difference between satellite CCI+SSS and EN4 uppermost salinity and the annual amplitude of the EN4 uppermost salinity is shown in Figure 43 (right). High values (>1) indicate, that the annual cycle of the differences is larger than the annual salinity cycle, which can be observed in the high latitudes, subtropical regions and a small band at the equator due to reasons already discussed or in general a low annual signal. In the following, the focus is on high-frequency salinity variability.

Figure 44 shows the standard deviation of the high-pass filtered (< 3 month) in situ, CCI+SSS and model SSS data. From here it is clearly observable, that the higher temporal and spatial resolution of the satellite data leads to a more comprehensive impression of small-scale high-frequency variability than the in-situ data does.



Climate Change Initiative+ (CCI+)
Phase 1
**Product Validation and
Intercomparison Report**

Ref.: ESA-CCI-PRGM-EOPS-SW-17-0032

Date: 07/04/2020

Version : v1.1

Page: 75 of 115

The magnitude of variability is approximately 1.5 times higher for CCI+SSS than for EN4 and larger differences between the spatial patterns are clearly observable in the gulf stream region, Amazon outflow, eastern tropical Pacific, north-eastern Indian Ocean and around the maritime continent. Interestingly, high-frequency variability is also enhanced in a band around the equator, reflecting the surface salinity changes due to the Madden Julian Oscillation (MJO), not so clearly seen in the EN4 data. High-frequency and sub-seasonal variability is enhanced in regions of river outflow, due to strong stratification, and in regions where the unique vertical structure of the upper meters of the water column gives rise to small-scale advection processes (e.g. eastern Indian Ocean (Köhler,2018)).

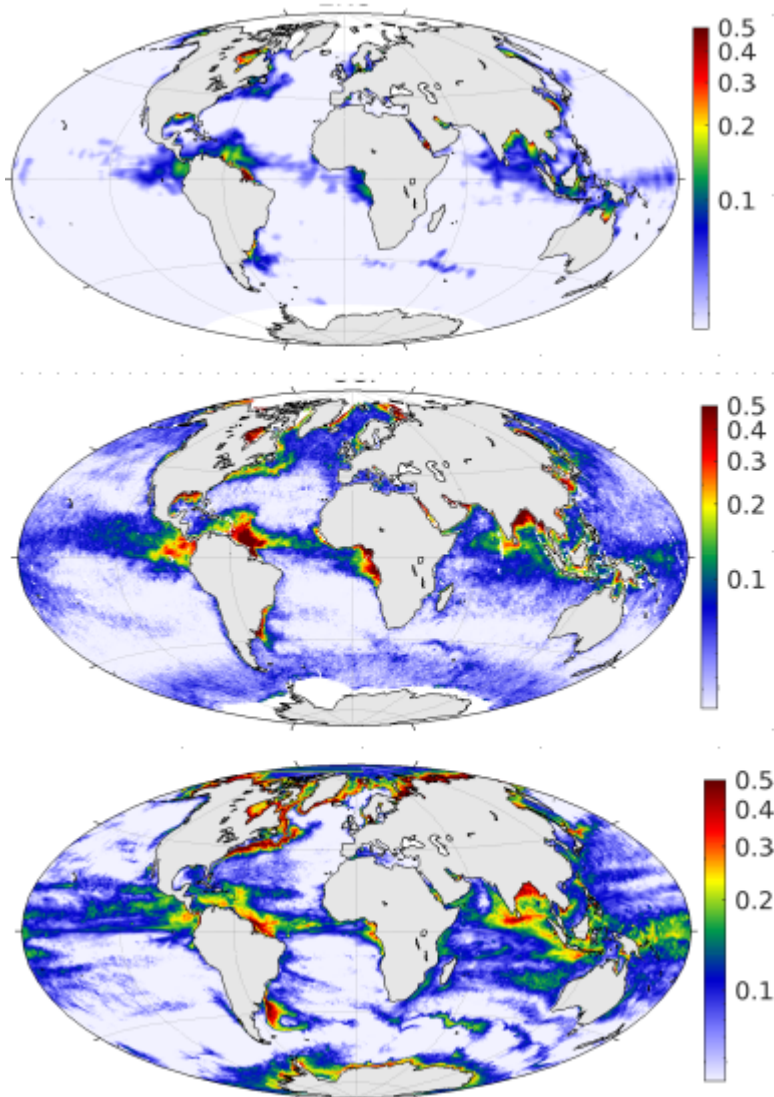


Figure 44: STD in high-pass (<3 months) filtered time series of each grid point in the EN4 data (top), the high-pass filtered CCI data (middle); the high-pass filtered model SSS data (bottom).

References:

- Akhil, V. P., Durand, F., Lengaigne, M., Vialard, J., Keerthi, M. G., Gopalakrishna, V. V., Boyer Montégut, C. (2014). A modeling study of the processes of surface salinity seasonal cycle in the Bay of Bengal. *Journal of Geophysical Research: Oceans*, 119, 3926– 3947.



Climate Change Initiative+ (CCI+)
Phase 1
Product Validation and
Intercomparison Report

Ref.: ESA-CCI-PRGM-EOPS-SW-17-0032

Date: 07/04/2020

Version : v1.1

Page: 77 of 115

- Köhl, A., D. Stammer, and M. Sena-Martins, 2014: Impact of Assimilating Surface Salinity from SMOS on Ocean Circulation Estimates. *J. Geophysical Res.*, 119, 5449-5464, doi: 10.1002/2014JC010040.
- Köhler, j., N. Serra, F. Bryan, B. K. Johnson and D. Stammer, 2017: Mechanisms of Mixed-Layer Salinity Seasonal Variability in the Indian Ocean, *J. Geophys Res.*, in revision
- Sena Martins, M., N. Serra, and D. Stammer, 2015: Sea surface salinity variability in the Atlantic Ocean. *J. Geophys. Res.*, 120, 4306-432, 3 DOI: 10.1002/2014JC010649.
- Wilson, E. A., & Riser, S. C. (2016). An assessment of the seasonal salinity budget for the upper Bay of Bengal. *Journal of Physical Oceanography*, 46, 1361– 1376.



Climate Change Initiative+ (CCI+)
Phase 1

**Product Validation and
Intercomparison Report**

Ref.: ESA-CCI-PRGM-EOPS-SW-17-0032

Date: 07/04/2020

Version : v1.1

Page: 78 of 115

Page Intentionally Blank



Climate Change Initiative+ (CCI+)
Phase 1
**Product Validation and
Intercomparison Report**

Ref.: ESA-CCI-PRGM-EOPS-SW-17-0032

Date: 07/04/2020

Version : v1.1

Page: 79 of 115

Annex A:Pi-MEP validation report againts Argo

This Annex reproduces one of the systematic report from Pi-MEP with validation against Argo:

https://pimep.ifremer.fr/diffusion/analyses/mdb-database/GO/cci-l4-esa-merged-oi-v1.8-30dr/argo/report/pimep-mdb-report_GO_cci-l4-esa-merged-oi-v1.8-30dr_argo_20190915.pdf

Summary of the analysis are report in the executive summary in section 2.



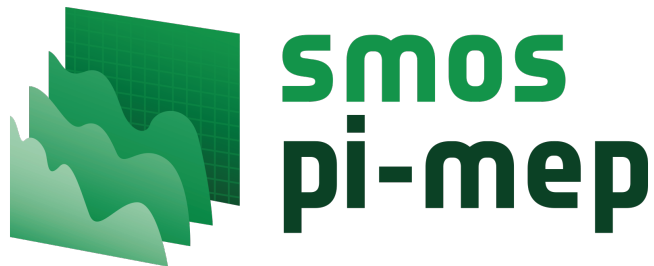
**Climate Change Initiative+ (CCI+)
Phase 1**
Product Validation and
Intercomparison Report

Ref.: ESA-CCI-PRGM-EOPS-SW-17-0032

Date: 07/04/2020

Version : v1.1

Page: 80 of 115



Match-up database Analyses Report

CCI-L4-ESA-MERGED-OI-V1.5-MONTHLY

Argo

Global Ocean

prepared by the Pi-MEP Consortium

March 15, 2019



**Climate Change Initiative+ (CCI+)
Phase 1
Product Validation and
Intercomparison Report**

Ref.: ESA-CCI-PRGM-EOPS-SW-17-0032
Date: 07/04/2020
Version : v1.1
Page: 81 of 115

Contents

1 Overview	5
2 The MDB file datasets	6
2.1 Satellite SSS product	6
2.1.1 CCI-L4-ESA-MERGED-OI-V1.5-MONTHLY	6
2.2 In situ SSS dataset	6
2.3 Auxiliary geophysical datasets	6
2.3.1 CMORPH	7
2.3.2 ASCAT	7
2.3.3 ISAS	8
2.3.4 World Ocean Atlas Climatology	8
2.4 Overview of the Match-ups generation method	9
2.4.1 In Situ/Satellite data filtering	9
2.4.2 In Situ/Satellite Co-localization	9
2.4.3 MDB pair Co-localization with auxiliary data and complementary information	10
2.4.4 Content of the Match-Up NetCDF files	11
2.5 MDB characteristics for the particular in situ/satellite pairs	18
2.5.1 Number of paired SSS data as a function of time and distance to coast	18
2.5.2 Histograms of the SSS match-ups	18
2.5.3 Distribution of in situ SSS depth measurements	19
2.5.4 Spatial Distribution of Match-ups	19
2.5.5 Histograms of the spatial and temporal lags of the match-ups pairs	20
3 MDB file Analyses	20
3.1 Spatial Maps of the Temporal mean and Std of in situ and satellite SSS and of the difference (Δ SSS)	20
3.2 Time series of the monthly averaged mean and Std of in situ and satellite SSS and of the (Δ SSS)	21
3.3 Zonally-averaged Time-mean and temporal Std of in situ and satellite SSS and of the Δ SSS	22
3.4 Scatterplots of satellite vs in situ SSS by latitudinal bands	24
3.5 Time series of the monthly averaged mean and Std of the Δ SSS sorted by latitudinal bands	25
3.6 Δ SSS sorted as function of geophysical parameters	25
3.7 Δ SSS maps and statistics for different geophysical conditions	26
4 Summary	28

List of Figures

1	Number of match-ups between Argo and CCI-L4-ESA-MERGED-OI-V1.5-MONTHLY SSS as a function of time (a) and as function of the distance to coast (b) over the Global Ocean Pi-MEP region and for the full satellite product period.	18
2	Histograms of SSS from Argo (a) and CCI-L4-ESA-MERGED-OI-V1.5-MONTHLY (b) considering all match-up pairs per bins of 0.1 over the Global Ocean Pi-MEP region and for the full satellite product period.	18



Climate Change Initiative+ (CCI+)
Phase 1
Product Validation and
Intercomparison Report

Ref.: ESA-CCI-PRGM-EOPS-SW-17-0032
 Date: 07/04/2020
 Version : v1.1
 Page: 82 of 115

3	Histograms of the depth of the upper level SSS measurements from Argo in the Match-up DataBase for the Global Ocean Pi-MEP region (a) and temporal mean spatial distribution of pressure of the in situ SSS data over 1°x1° boxes and for the full satellite product period (b).	19
4	Number of SSS match-ups between Argo SSS and the CCI-L4-ESA-MERGED-OI-V1.5-MONTHLY SSS product for the Global Ocean Pi-MEP region over 1°x1° boxes and for the full satellite product period.	19
5	Histograms of the spatial (a) and temporal (b) lags between the time of the Argo measurements and the date of the corresponding CCI-L4-ESA-MERGED-OI-V1.5-MONTHLY SSS product.	20
6	Temporal mean (left) and Std (right) of SSS from CCI-L4-ESA-MERGED-OI-V1.5-MONTHLY (top), Argo (middle), and of ΔSSS (Satellite - Argo). Only match-up pairs are used to generate these maps.	21
7	Time series of the monthly averaged mean SSS (top), mean ΔSSS (Satellite - Argo) and Std of ΔSSS (Satellite - Argo) over the Global Ocean Pi-MEP region considering all match-ups collected by the Pi-MEP platform.	22
8	Left panel: Zonally averaged time mean SSS from CCI-L4-ESA-MERGED-OI-V1.5-MONTHLY (black) and from Argo (blue). Right panel: zonally averaged time-mean ΔSSS (Satellite - Argo) for all the collected Pi-MEP match-up pairs estimated over the full satellite product period.	23
9	Contour maps of the concentration of CCI-L4-ESA-MERGED-OI-V1.5-MONTHLY SSS (y-axis) versus Argo SSS (x-axis) at match-up pairs for different latitude bands. For each plot, the red line shows x=y. The black thin and dashed lines indicate a linear fit through the data cloud and the ±95% confidence levels, respectively. The number match-up pairs <i>n</i> , the slope and R ² coefficient of the linear fit, the root mean square (RMS) and the mean bias between satellite and in situ data are indicated for each latitude band in each plots.	24
10	Monthly-average mean (red curves) ΔSSS (Satellite - Argo) and ±1 Std (black vertical thick bars) as function of time for all the collected Pi-MEP match-up pairs estimated over the Global Ocean Pi-MEP region and for the full satellite product period are shown for different latitude bands: (a) Latitude band 80°S-80°N, (b) latitude band 20°S-20°N, (c) Mid Latitude bands 40°S-20°S and 20°N-40°N and (d) Latitude bands 60°S-40°S and 40°N-60°N.	25
11	ΔSSS (Satellite - Argo) sorted as function of Argo SSS values a), Argo SST b), ASCAT Wind speed c), CMORPH rain rate d) and distance to coast (e). In all plots the mean and Std of ΔSSS for each bin is indicated by the red curves and black vertical thick bars (±1 Std).	26
12	Temporal mean gridded over spatial boxes of size 1°x1° of ΔSSS (CCI-L4-ESA-MERGED-OI-V1.5-MONTHLY - Argo) for 6 different subdatasets corresponding to: RR=0 mm/h, 3< U ₁₀ <12 m/s, SST>5°C, distance to coast > 800 km (a), RR=0 mm/h, 3< U ₁₀ <12 m/s (b), RR>1mm/h and U ₁₀ <4m/s (c),MLD<20m (d),WOA2013 SSS Std<0.2 (e),WOA2013 SSS Std>0.2 (f).	27
13	Normalized histogram of ΔSSS (CCI-L4-ESA-MERGED-OI-V1.5-MONTHLY - Argo) for 6 different subdatasets corresponding to: RR=0 mm/h, 3< U ₁₀ <12 m/s, SST>5°C, distance to coast > 800 km (a), RR=0 mm/h, 3< U ₁₀ <12 m/s (b), RR>1mm/h and U ₁₀ <4m/s (c), MLD<20m (d), WOA2013 SSS Std<0.2 (e), WOA2013 SSS Std>0.2 (f).	28



Climate Change Initiative+ (CCI+)
Phase 1
Product Validation and
Intercomparison Report

Ref.: ESA-CCI-PRGM-EOPS-SW-17-0032

Date: 07/04/2020

Version : v1.1

Page: 83 of 115



Match-up database Analyses Report

Acronym

Aquarius	NASA/CONAE Salinity mission
ASCAT	Advanced Scatterometer
ATBD	Algorithm Theoretical Baseline Document
BLT	Barrier Layer Thickness
CMORPH	CPC MORPHing technique
CTD	Instrument used to measure the conductivity, temperature, and pressure of seawater
DM	Delayed Mode
EO	Earth Observation
ESA	European Space Agency
FTP	File Transfer Protocol
GOSUD	Global Ocean Surface Underway Data
GTMBA	The Global Tropical Moored Buoy Array
Ifremer	Institut français de recherche pour l'exploitation de la mer
IPEV	Institut polaire français Paul-Émile Victor
IQR	Interquartile range
ISAS	In Situ Analysis System
Kurt	Kurtosis (fourth central moment divided by fourth power of the standard deviation)
L2	Level 2
LEGOS	Laboratoire d'Etudes en Géophysique et Océanographie Spatiales
LOCEAN	Laboratoire d'Océanographie et du Climat : Expérimentations et Approches Numériques
LOPS	Laboratoire d'Océanographie Physique et Spatiale
MDB	Match-up Data Base
MEOP	Marine Mammals Exploring the Oceans Pole to Pole
MLD	Mixed Layer Depth
NCEI	National Centers for Environmental Information
NRT	Near Real Time
NTAS	Northwest Tropical Atlantic Station
OI	Optimal interpolation
Pi-MEP	Pilot Mission Exploitation Platform
PIRATA	Prediction and Researched Moored Array in the Atlantic
QC	Quality control
R_{sat}	Spatial resolution of the satellite SSS product
RAMA	Research Moored Array for African-Asian-Australian Monsoon Analysis and Prediction
r^2	Square of the Pearson correlation coefficient
RMS	Root mean square
RR	Rain rate
SAMOS	Shipboard Automated Meteorological and Oceanographic System
Skew	Skewness (third central moment divided by the cube of the standard deviation)
SMAP	Soil Moisture Active Passive (NASA mission)
SMOS	Soil Moisture and Ocean Salinity (ESA mission)
SPURS	Salinity Processes in the Upper Ocean Regional Study
SSS	Sea Surface Salinity
SSS_{insitu}	In situ SSS data considered for the match-up



Climate Change Initiative+ (CCI+)
Phase 1
Product Validation and
Intercomparison Report

Ref.: ESA-CCI-PRGM-EOPS-SW-17-0032

Date: 07/04/2020

Version : v1.1

Page: 84 of 115



Match-up database Analyses Report

SSS_{SAT}	Satellite SSS product considered for the match-up
ΔSSS	Difference between satellite and in situ SSS at colocalized point ($\Delta SSS = SSS_{SAT} - SSS_{insitu}$)
SST	Sea Surface Temperature
Std	Standard deviation
Std*	Robust Standard deviation = $\text{median}(\text{abs}(x - \text{median}(x))) / 0.67$ (less affected by outliers than Std)
Stratus	Surface buoy located in the eastern tropical Pacific
Survostral	SURveillance de l'Océan AuSTRAL (Monitoring the Southern Ocean)
TAO	Tropical Atmosphere Ocean
TSG	ThermoSalinoGraph
WHOI	Woods Hole Oceanographic Institution
WHOTS	WHOI Hawaii Ocean Time-series Station
WOA	World Ocean Atlas



Climate Change Initiative+ (CCI+)
Phase 1
Product Validation and
Intercomparison Report

Ref.: ESA-CCI-PRGM-EOPS-SW-17-0032
Date: 07/04/2020
Version : v1.1
Page: 85 of 115



Match-up database Analyses Report

1 Overview

In this report, we present systematic analyses of the Match-up DataBase (MDB) files generated by the Pi-MEP platform within the following Pi-MEP region and for the below pair of Satellite/In situ SSS data:

- Pi-MEP region: Global Ocean (download the corresponding mask [here](#))
- SSS satellite product (SSS_{SAT}): CCI-L4-ESA-MERGED-OI-V1.5-MONTHLY
- In situ dataset ($SSS_{In situ}$): Argo (download the corresponding report [here](#))

In the following, $\Delta SSS = SSS_{SAT} - SSS_{In situ}$ denotes the difference between the satellite and in situ SSS at the colocalized points that form the MDB.

This report presents successively:

The MDB file DataSets (Section 2)

- A short description of the satellite SSS product considered in the match-up (2.1)
- A short description of the In situ SSS dataset considered in the match-up (2.2)
- A short description of the auxiliary geophysical datasets co-localized with SSS pairs (2.3)
- An overview of how the Match-ups were evaluated (2.4)
- An overview of the MDB characteristics for the particular in situ/satellite pairs (2.5)

The major results of the MDB file Analyses (Section 3)

- Spatial Maps of the Time-mean and temporal Std of in situ and satellite SSS and of the ΔSSS (3.1)
- Time series of the monthly averaged mean and Std of in situ and satellite SSS and of the ΔSSS (3.2)
- Zonally-averaged Time-mean and temporal Std of in situ and satellite SSS and of the ΔSSS (3.3)
- Scatterplots of satellite vs in situ SSS by latitudinal bands (3.4)
- Time series of the monthly averaged mean and Std of the ΔSSS sorted by latitudinal bands (3.5)
- ΔSSS sorted as function of geophysical parameters (3.6)
- ΔSSS maps and statistics for different geophysical conditions (3.7)

All analyses are conducted over the Pi-MEP Region specified above and over the full satellite SSS product period.



Climate Change Initiative+ (CCI+)
Phase 1
Product Validation and
Intercomparison Report

Ref.: ESA-CCI-PRGM-EOPS-SW-17-0032
Date: 07/04/2020
Version : v1.1
Page: 86 of 115



Match-up database Analyses Report

2 The MDB file datasets

2.1 Satellite SSS product

2.1.1 CCI-L4-ESA-MERGED-OI-V1.5-MONTHLY

Table 1: Satellite SSS product characteristics

CCI-L4-ESA-MERGED-OI-V1.5-MONTHLY	
Spatial resolution	25 km
Temporal resolution	Monthly (file every 15 days)
Temporal coverage	From 2010-01-01 to 2018-11-01
Data Provider	CCI-SSS
Release Date	2019-03
Version	1.5
Data access	
DOI	
Documentation	

2.2 In situ SSS dataset

Argo is a global array of 3,000 free-drifting profiling floats that measures the temperature and salinity of the upper 2000 m of the ocean. This allows continuous monitoring of the temperature and salinity of the upper ocean, with all data being relayed and made publicly available within hours after collection. The array provides around 100,000 temperature/salinity profiles per year distributed over the global oceans at an average of 3-degree spacing. Only Argo salinity and temperature float data with quality index set to 1 or 2 and data mode set to real time (RT), real time adjusted (RTA) and delayed mode (DM) are considered in the Pi-MEP. Argo floats which may have problems with one or more sensors appearing in the [grey list](#) maintained at the Coriolis/GDACs are discarded. Furthermore, Pi-MEP provides an additional [list](#) of ~1000 "suspicious" argo salinity profiles that are also removed before analysis. The upper ocean salinity and temperature values recorded between 0m and 10m depth are considered as Argo sea surface salinities (SSS) and sea surface temperatures (SST). These data were collected and made freely available by the international Argo project and the national programs that contribute to it ([Argo \(2000\)](#)).

2.3 Auxiliary geophysical datasets

Additional EO datasets are used to characterize the geophysical conditions at the in situ/satellite SSS pair measurement locations and time, and 10 days prior the measurements to get an estimate of the geophysical condition and history. As discussed in [Boutin et al. \(2016\)](#), the presence of vertical gradients in, and horizontal variability of, sea surface salinity indeed complicates comparison of satellite and in situ measurements. The additional EO data are used here to get a first estimates of conditions for which L-band satellite SSS measured in the first centimeters of the upper ocean within a 50-150 km diameter footprint might differ from pointwise in situ measurements performed in general between 10 and 5 m depth below the surface. The spatio-temporal variability of SSS within a satellite footprint (50-150 km) is a major issue for satellite SSS validation in the vicinity of river plumes, frontal zones, and significant precipitation. Rainfall



Climate Change Initiative+ (CCI+)
Phase 1
**Product Validation and
Intercomparison Report**

Ref.: ESA-CCI-PRGM-EOPS-SW-17-0032

Date: 07/04/2020

Version : v1.1

Page: 87 of 115



**Climate Change Initiative+ (CCI+)
Phase 1
Product Validation and
Intercomparison Report**

Ref.: ESA-CCI-PRGM-EOPS-SW-17-0032

Date: 07/04/2020

Version : v1.1

Page: 88 of 115



Match-up database Analyses Report

can in some cases produce vertical salinity gradients exceeding 1 pss m^{-1} ; consequently, it is recommended that satellite and in situ SSS measurements less than 3–6 h after rain events should be considered with care when used in satellite calibration/validation analyses. To identify such situation, the Pi-MEP test platform is first using CMORPH products to characterize the local value and history of rain rate and ASCAT gridded data are used to characterize the local surface wind speed and history. For validation purpose, the ISAS monthly SSS in situ analysed fields at 5 m depth are collocated and compared with the satellite SSS products. The use of ISAS is motivated by the fact that it is used in the SMOS L2 official validation protocol in which systematic comparisons of SMOS L2 retrieved SSS with ISAS are done. In complement to ISAS, monthly std climatological fields from the World Ocean Atlas (WOA13) at the match-up pairs location and date are also used to have an a priori information of the local SSS variability.

2.3.1 CMORPH

Precipitation are estimated using the CMORPH 3-hourly products at $1/4^\circ$ resolution (Joyce et al. (2004)). CMORPH (CPC MORPHing technique) produces global precipitation analyses at very high spatial and temporal resolution. This technique uses precipitation estimates that have been derived from low orbiter satellite microwave observations exclusively, and whose features are transported via spatial propagation information that is obtained entirely from geostationary satellite IR data. At present NOAA incorporate precipitation estimates derived from the passive microwaves aboard the DMSP 13, 14 and 15 (SSM/I), the NOAA-15, 16, 17 and 18 (AMSU-B), and AMSR-E and TMI aboard NASA's Aqua, TRMM and GPM spacecraft, respectively. These estimates are generated by algorithms of Ferraro (1997) for SSM/I, Ferraro et al. (2000) for AMSU-B and Kummerow et al. (2001) for TMI. Note that this technique is not a precipitation estimation algorithm but a means by which estimates from existing microwave rainfall algorithms can be combined. Therefore, this method is extremely flexible such that any precipitation estimates from any microwave satellite source can be incorporated.

With regard to spatial resolution, although the precipitation estimates are available on a grid with a spacing of 8 km (at the equator), the resolution of the individual satellite-derived estimates is coarser than that - more on the order of 12 x 15 km or so. The finer "resolution" is obtained via interpolation.

In effect, IR data are used as a means to transport the microwave-derived precipitation features during periods when microwave data are not available at a location. Propagation vector matrices are produced by computing spatial lag correlations on successive images of geostationary satellite IR which are then used to propagate the microwave derived precipitation estimates. This process governs the movement of the precipitation features only. At a given location, the shape and intensity of the precipitation features in the intervening half hour periods between microwave scans are determined by performing a time-weighting interpolation between microwave-derived features that have been propagated forward in time from the previous microwave observation and those that have been propagated backward in time from the following microwave scan. NOAA refer to this latter step as "morphing" of the features.

For the present Pi-MEP products, we only considered the 3-hourly products at $1/4$ degree resolution. The entire CMORPH record (December 2002-present) for 3-hourly, $1/4$ degree lat/lon resolution can be found at: ftp://ftp.cpc.ncep.noaa.gov/precip/CMORPH_V1.0/RAW/. CMORPH estimates cover a global belt (-180°W to 180°E) extending from 60°S to 60°N latitude and are available for the complete period of the Pi-MEP core datasets (Jan 2010-now).



Climate Change Initiative+ (CCI+)
Phase 1
Product Validation and
Intercomparison Report

Ref.: ESA-CCI-PRGM-EOPS-SW-17-0032
Date: 07/04/2020
Version : v1.1
Page: 89 of 115



Match-up database Analyses Report

2.3.2 ASCAT

Advanced SCATterometer (ASCAT) daily data produced and made available at [Ifremer/CERSAT](#) on a $0.25^\circ \times 0.25^\circ$ resolution grid ([Bentamy and Fillon \(2012\)](#)) since March 2007 are used to characterize the mean daily wind at the match-up pair location as well as the wind history during the 10-days period preceding the in situ measurement date. These wind fields are calculated based on a geostatistical method with external drift. Remotely sensed data from ASCAT are considered as observations while those from numerical model analysis (ECMWF) are associated with the external drift. The spatial and temporal structure functions for wind speed, zonal and meridional wind components are estimated from ASCAT retrievals. Furthermore, the new procedure includes a temporal interpolation of the retrievals based on the complex empirical orthogonal function (CEOF) approach, in order to enhance the sampling length of the scatterometer observations. The resulting daily wind fields involves the main known surface wind patterns as well as some variation modes associated with temporal and spatial moving features. The accuracy of the gridded winds was investigated through comparisons with moored buoy data in [Bentamy et al. \(2012\)](#) and resulted in rms differences for wind speed and direction are about 1.50 m.s^{-1} and 20° .

2.3.3 ISAS

The In Situ Analysis System (ISAS), as described in [Gaillard et al. \(2016\)](#) is a data based re-analysis of temperature and salinity fields over the global ocean. It was initially designed to synthesize the temperature and salinity profiles collected by the Argo program. It has been later extended to accommodate all type of vertical profile as well as time series. ISAS gridded fields are entirely based on in-situ measurements. The methodology and configuration have been conceived to preserve as much as possible the data information content and resolution. ISAS is developed and run in a research laboratory (LOPS) in close collaboration with Coriolis, one of Argo Global Data Assembly Center and unique data provider for the Mercator operational oceanography system. At the moment the period covered starts in 2002 and only the upper 2000 m are considered. The gridded fields were produced over the global ocean 70°N – 70°S on a $1/2^\circ$ grid by the ISAS project with datasets downloaded from the Coriolis data center (for more details on ISAS see [Gaillard et al. \(2009\)](#)). In the Pi-MEP, the product in used is the [INSITU_GLO_TS_OA_NRT_OBSERVATIONS.013.002_a v6.2](#) NRT derived at the Coriolis data center and provided by Copernicus (www.marine.copernicus.eu/documents/PUM/CMEMS-INS-PUM-013-002-ab.pdf). The major contribution to the data set is from Argo array of profiling floats, reaching an approximate resolution of one profile every 10-days and every 3-degrees over the satellite SSS period (<http://www.umr-lops.fr/SNO-Argo/Products/ISAS-T-S-fields/>); in this version SSS from ship of opportunity thermosalinographs are not used, so that we can consider SMOS SSS validation using these measurements independent of ISAS. The ISAS optimal interpolation involves a structure function modeled as the sum of two Gaussian functions, each associated with specific time and space scales, resulting in a smoothing over typically 3 degrees. The smallest scale which can be retrieved with ISAS analysis is not smaller than 300–500 km ([Kolodziejczyk et al. \(2015\)](#)). For validation purpose, the ISAS monthly SSS fields at 5 m depth are collocated and compared with the satellite SSS products and included in the Pi-MEP Match-up files. In addition, the “percentage of variance” fields (PCTVAR) contained in the ISAS analyses provide information on the local variability of in situ SSS measurements within $1/2^\circ \times 1/2^\circ$ boxes.



**Climate Change Initiative+ (CCI+)
Phase 1
Product Validation and
Intercomparison Report**

Ref.: ESA-CCI-PRGM-EOPS-SW-17-0032
Date: 07/04/2020
Version : v1.1
Page: 90 of 115



2.3.4 World Ocean Atlas Climatology

The World Ocean Atlas 2013 version 2 (**WOA13 V2**) is a set of objectively analyzed (1° grid) climatological fields of in situ temperature, salinity and other variables provided at standard depth levels for annual, seasonal, and monthly compositing periods for the World Ocean. It also includes associated statistical fields of observed oceanographic profile data interpolated to standard depth levels on 5° , 1° , and 0.25° grids. We use these fields in complement to ISAS to characterize the climatological fields (annual mean and std) at the match-up pairs location and date.

2.4 Overview of the Match-ups generation method

The match-up production is basically a three steps process:

1. preparation of the input in situ and satellite data, and,
2. co-localization of satellite products with in situ SSS measurements.
3. co-localization of the in situ/satellite pair with auxiliary information.

In the following, we successively detail the approaches taken for these different steps.

2.4.1 In Situ/Satellite data filtering

The first step consist in filtering Argoin situ dataset using the quality flags as described in 2.2 so that only valid salinity data remains in the produced match-ups.

For high-spatial resolution in situ SSS measurements such as the Thermo-SalinoGraph (TSG) SSS data from research vessels, Voluntary Observing Ships (VOS) or sailing ships, as well as SSS data from surface drifters, an additional spatial-filtering step is performed on the in situ data that will be in fine compared to the satellite SSS products. If R_{sat} is the spatial resolution of the satellite SSS product (L2 to L3-L4), we keep the in situ data at the original spatial resolution but we also estimate for all spatio-temporal samples a running median filtered SSS applied to all neighbouring in situ SSS data acquired within a distance of $R_{sat}/2$ from a given in situ acquisition. Both the original and the filtered data are finally stored in the MDB files.

Only for satellite L2 SSS data, a third step consist in filtering spurious data using the flags and associated recommendation as provided by the official data centers and described in 2.1.

2.4.2 In Situ/Satellite Co-localization

In this step, each SSS satellite acquisition is co-localized with the filtered in situ measurements. The method used for co-localization differ if the satellite SSS is a swath product (so-called Level 2-types) or a time-space composite product (so-called Level 3/level 4-types).

- For L2 SSS swath data :

If R_{sat} is the spatial resolution of the satellite swath SSS product, for each in situ data sample collected in the Pi-MEP database, the platform searches for all satellite SSS data found at grid nodes located within a radius of $R_{sat}/2$ from the in situ data location and acquired with a time-lag from the in situ measurement date that is less or equal than ± 12 hours. If several satellite SSS samples are found to meet these criteria, the final satellite SSS match-up point is selected to be the closest in time from the in situ data measurement date. The final spatial and temporal lags between the in situ and satellite data are stored in the MDB files.



Climate Change Initiative+ (CCI+)
Phase 1
Product Validation and
Intercomparison Report

Ref.: ESA-CCI-PRGM-EOPS-SW-17-0032

Date: 07/04/2020

Version : v1.1

Page: 91 of 115



Match-up database Analyses Report

- For L3 and L4 composite SSS products :

If R_{sat} is the spatial resolution of the composite satellite SSS product and D the period over which the composite product was built (e.g., periods of 1, 7, 8, 9, 10, 18 days, 1 month, etc..) with central time t_0 , for each in situ data sample collected in the Pi-MEP database during period D, the platform searches for all satellite SSS data of the composite product found at grid nodes located within a radius of $R_{sat}/2$ from the in situ data location. If several satellite SSS product samples are found to meet these criteria, the final satellite SSS match-up point is chosen to be the composite SSS with central time to which is the closest in time from the in situ data measurement date. The final spatial and temporal lags between the in situ and satellite data are stored in the MDB files.

2.4.3 MDB pair Co-localization with auxiliary data and complementary information

MDB data consist of satellite and in-situ SSS pair datasets but also of auxiliary geophysical parameters such as local and history of wind speed and rain rates, as well as various information (climatology, distance to coast, mixed layer depth, barrier layer thickness, etc) that can be derived from in situ data and which are included in the final match-up files. The collocation of auxiliary parameters and additional information is done for each filtered in-situ SSS measurement contained in the match-up files as follows :

If t_{insitu} is the time/date at which the in situ measurement is performed, we collect:

- The **ASCAT** wind speed product of the same day than t_{insitu} found at the ASCAT $1/4^\circ$ grid node with closest distance from the in situ data location and the time series of the ASCAT wind speed at the same node for the 10 days prior the in situ measurement day.
- If the in situ data is located within the 60°N - 60°S band, we select the **CMORPH** 3-hourly product the closest in time from in situ and found at the CMORPH $1/4^\circ$ grid node with closest distance from the in situ data location. We then store the time series of the CMORPH rain rate at the same node for the 10 days prior the in situ measurement time.

For the given month/year of the in situ data, we select the **ISAS** and **WOA** fields for the same month (and same year for ISAS fields) and take the SSS analysis (monthly mean, std) found at the closest grid node from the in situ measurement.

The distance from the in situ SSS data location to the nearest coast is evaluated and provided in km. We use a distance-to-coast map at $1/4^\circ$ resolution where small islands have been removed.

When vertical profiles of salinity (S) and temperature (T) are made available from the in situ measurements used to build the match-up (Argo or sea mammals), the following variables are included into each satellite/in situ match-up file:

1. The vertical distribution of pressure at which the profile were measured,
2. The vertical $S(z)$ and $T(z)$ profiles,
3. The vertical potential density anomaly profile $\sigma_0(z)$,
4. The Mixed Layer Depth (MLD). The MLD is defined here as the depth where the potential density has increased from the reference depth (10 meter) by a threshold equivalent to 0.2°C decrease in temperature at constant salinity: $\sigma_0 = \sigma_{010m} + \Delta\sigma_0$ with $\Delta\sigma_0 = \sigma_0(\theta_{10m} - 0.2, S_{10m}) - \sigma_0(\theta_{10m}, S_{10m})$ where θ_{10m} and S_{10m} are the temperature and salinity at the reference depth (i.e. 10 m) (de Boyer Montégut et al. (2004), de Boyer Montégut et al. (2007)).



Climate Change Initiative+ (CCI+)
Phase 1
Product Validation and
Intercomparison Report

Ref.: ESA-CCI-PRGM-EOPS-SW-17-0032
Date: 07/04/2020
Version : v1.1
Page: 92 of 115



Match-up database Analyses Report

5. The Top of the Thermocline Depth (TTD) is defined as the depth at which temperature decreases from its 10 m value by 0.2°C.
6. The Barrier Layer if present, is defined as the intermediate layer between the top of the thermocline and the bottom of the density mixed-layer and its thickness (BLT) is defined as the difference between the MLD and the TTD.
7. The vertical profile of the buoyancy frequency $N^2(z)$

The resulting match-ups files are serialized as NetCDF-4 files whose structure depends on the origin of the in-situ data they contain.

2.4.4 Content of the Match-Up NetCDF files

```
netcdf pimep-mdb_cci-l4-esa-merged-oi-v1.5-1m_argo_TIMEID_v01 {  
dimensions:
```

```
    N_prof = 944 ;  
    N_LEVELS = 499 ;  
    N_DAYS_WIND = 10 ;  
    N_3H_RAIN = 80 ;  
    TIME_Sat = UNLIMITED ; // (1 currently)
```

variables:

```
float DATE_ARGO(N_prof) ;  
    DATE_ARGO:long_name = "Date of Argo profile" ;  
    DATE_ARGO:units = "days since 1990-01-01 00:00:00" ;  
    DATE_ARGO:standard_name = "time" ;  
    DATE_ARGO:_FillValue = -999.f ;  
float LATITUDE_ARGO(N_prof) ;  
    LATITUDE_ARGO:long_name = "Latitude of Argo profile" ;  
    LATITUDE_ARGO:units = "degrees_north" ;  
    LATITUDE_ARGO:valid_min = -90. ;  
    LATITUDE_ARGO:valid_max = 90. ;  
    LATITUDE_ARGO:standard_name = "latitude" ;  
    LATITUDE_ARGO:_FillValue = -999.f ;  
float LONGITUDE_ARGO(N_prof) ;  
    LONGITUDE_ARGO:long_name = "Longitude of Argo profile" ;  
    LONGITUDE_ARGO:units = "degrees_east" ;  
    LONGITUDE_ARGO:valid_min = -180. ;  
    LONGITUDE_ARGO:valid_max = 180. ;  
    LONGITUDE_ARGO:standard_name = "longitude" ;  
    LONGITUDE_ARGO:_FillValue = -999.f ;  
float SSS_DEPTH_ARGO(N_prof) ;  
    SSS_DEPTH_ARGO:long_name = "Sea water pressure at Argo float location (equals 0 at  
sea level)" ;  
    SSS_DEPTH_ARGO:units = "decibar" ;  
    SSS_DEPTH_ARGO:standard_name = "sea_water_pressure" ;  
    SSS_DEPTH_ARGO:_FillValue = -999.f ;  
float SSS_ARGO(N_prof) ;  
    SSS_ARGO:long_name = "Argo SSS" ;  
    SSS_ARGO:units = "1" ;
```



Climate Change Initiative+ (CCI+)
Phase 1
Product Validation and
Intercomparison Report

Ref.: ESA-CCI-PRGM-EOPS-SW-17-0032
Date: 07/04/2020
Version : v1.1
Page: 93 of 115



Match-up database Analyses Report

```
SSS_ARGO:salinity_scale = "Practical Salinity Scale(PSS-78)" ;
SSS_ARGO:standard_name = "sea_water_salinity" ;
SSS_ARGO:FillValue = -999.f ;
float SST_ARGO(N_prof) ;
SST_ARGO:long_name = "Argo SST" ;
SST_ARGO:units = "degree Celsius" ;
SST_ARGO:standard_name = "sea_water_temperature" ;
SST_ARGO:FillValue = -999.f ;
float DELAYED_MODE_ARGO(N_prof) ;
DELAYED_MODE_ARGO:long_name = "Argo data mode (delayed mode = 1, real time
=0) " ;
DELAYED_MODE_ARGO:units = "1" ;
DELAYED_MODE_ARGO:FillValue = -999.f ;
float DISTANCE_TO_COAST_ARGO(N_prof) ;
DISTANCE_TO_COAST_ARGO:long_name = "Distance to coasts at Argo float location"
;
DISTANCE_TO_COAST_ARGO:units = "km" ;
DISTANCE_TO_COAST_ARGO:FillValue = -999.f ;
float PLATFORM_NUMBER_ARGO(N_prof) ;
PLATFORM_NUMBER_ARGO:long_name = "Argo float unique identifier" ;
PLATFORM_NUMBER_ARGO:conventions = "WMO float identifier : A9IIIII" ;
PLATFORM_NUMBER_ARGO:units = "1" ;
PLATFORM_NUMBER_ARGO:FillValue = -999.f ;
float PSAL_ARGO(N_prof, N_LEVELS) ;
PSAL_ARGO:long_name = "Argo salinity profile" ;
PSAL_ARGO:units = "1" ;
PSAL_ARGO:salinity_scale = "Practical Salinity Scale (PSS-78)" ;
PSAL_ARGO:standard_name = "sea_water_salinity" ;
PSAL_ARGO:FillValue = -999.f ;
float TEMP_ARGO(N_prof, N_LEVELS) ;
TEMP_ARGO:long_name = "Argo temperature profile" ;
TEMP_ARGO:units = "degree Celsius" ;
TEMP_ARGO:standard_name = "sea_water_temperature" ;
TEMP_ARGO:FillValue = -999.f ;
float PRES_ARGO(N_prof, N_LEVELS) ;
PRES_ARGO:long_name = "Argo pressure profile" ;
PRES_ARGO:units = "decibar" ;
PRES_ARGO:standard_name = "sea_water_pressure" ;
PRES_ARGO:FillValue = -999.f ;
float RHO_ARGO(N_prof, N_LEVELS) ;
RHO_ARGO:long_name = "Argo in-situ density profile" ;
RHO_ARGO:units = "kg/m" ;
RHO_ARGO:FillValue = -999.f ;
float SIGMA0_ARGO(N_prof, N_LEVELS) ;
SIGMA0_ARGO:long_name = "Argo potential density anomaly profile" ;
SIGMA0_ARGO:units = "kg/m3" ;
SIGMA0_ARGO:FillValue = -999.f ;
float N2_ARGO(N_prof, N_LEVELS) ;
N2_ARGO:long_name = "Argo buoyancy frequency profile" ;
```



Climate Change Initiative+ (CCI+)
Phase 1
Product Validation and
Intercomparison Report

Ref.: ESA-CCI-PRGM-EOPS-SW-17-0032
Date: 07/04/2020
Version : v1.1
Page: 94 of 115



Match-up database Analyses Report

```
N2_ARGO:units = "1/s2" ;
N2_ARGO:_FillValue = -999.f ;
float MLD_ARGO(N_prof) ;
  MLD_ARGO:long_name = "Mixed Layer Depth (MLD) calculated from Argo profile (depth
where  $\sigma_0 = \sigma_{010m} + \Delta\sigma_0$  with  $\Delta\sigma_0 = \sigma_0(\theta_{10m} - 0.2, S_{10m}) - \sigma_0(\theta_{10m}, S_{10m})$ )" ;
  MLD_ARGO:units = "m" ;
  MLD_ARGO:_FillValue = -999.f ;
float TTD_ARGO(N_prof) ;
  TTD_ARGO:long_name = "Top of Thermocline Depth (TTD) calculated from Argo profile
(depth where  $\theta = \theta_{10m} - 0.2$ )" ;
  TTD_ARGO:units = "m" ;
  TTD_ARGO:_FillValue = -999.f ;
float BLT_ARGO(N_prof) ;
  BLT_ARGO:long_name = "Barrier Layer Thickness (TTD-MLD)" ;
  BLT_ARGO:units = "m" ;
  BLT_ARGO:_FillValue = -999.f ;
float DATE_Satellite_product(TIME_Sat) ;
  DATE_Satellite_product:long_name = "Central time of satellite SSS file" ;
  DATE_Satellite_product:units = "days since 1990-01-01 00:00:00" ;
  DATE_Satellite_product:standard_name = "time" ;
float LATITUDE_Satellite_product(N_prof) ;
  LATITUDE_Satellite_product:long_name = "Satellite product latitude at Argo float loca-
tion" ;
  LATITUDE_Satellite_product:units = "degrees_north" ;
  LATITUDE_Satellite_product:valid_min = -90. ;
  LATITUDE_Satellite_product:valid_max = 90. ;
  LATITUDE_Satellite_product:standard_name = "latitude" ;
  LATITUDE_Satellite_product:_FillValue = -999.f ;
float LONGITUDE_Satellite_product(N_prof) ;
  LONGITUDE_Satellite_product:long_name = "Satellite product longitude at Argo float lo-
cation" ;
  LONGITUDE_Satellite_product:units = "degrees_east" ;
  LONGITUDE_Satellite_product:valid_min = -180. ;
  LONGITUDE_Satellite_product:valid_max = 180. ;
  LONGITUDE_Satellite_product:standard_name = "longitude" ;
  LONGITUDE_Satellite_product:_FillValue = -999.f ;
float SSS_Satellite_product(N_prof) ;
  SSS_Satellite_product:long_name = "Satellite product SSS at Argo float location" ;
  SSS_Satellite_product:units = "1" ;
  SSS_Satellite_product:salinity_scale = "Practical Salinity Scale(PSS-78)" ;
  SSS_Satellite_product:standard_name = "sea_surface_salinity" ;
  SSS_Satellite_product:_FillValue = -999.f ;
float SST_Satellite_product(N_prof) ;
  SST_Satellite_product:long_name = "Satellite product SST at Argo float location" ;
  SST_Satellite_product:units = "degree_Celsius" ;
  SST_Satellite_product:standard_name = "sea_surface_temperature" ;
  SST_Satellite_product:_FillValue = -999.f ;
float Spatial_lags(N_prof) ;
  Spatial_lags:long_name = "Spatial lag between Argo float location and satellite SSS product
```



Climate Change Initiative+ (CCI+)
Phase 1
Product Validation and
Intercomparison Report

Ref.: ESA-CCI-PRGM-EOPS-SW-17-0032
Date: 07/04/2020
Version : v1.1
Page: 95 of 115



Match-up database Analyses Report

```
pixel center" ;
    Spatial_lags:units = "km" ;
    Spatial_lags:FillValue = -999.f ;
float Time_lags(N_prof) ;
    Time_lags:long_name = "Temporal lag between Argo float time and satellite SSS product
central time" ;
    Time_lags:units = "days" ;
    Time_lags:FillValue = -999.f ;
float ROSSBY_RADIUS_at_ARGO(N_prof) ;
    ROSSBY_RADIUS_at_ARGO:long_name = "Baroclinic Rossby radius of deformation (Chel-
ton et al., 1998) at Argo float location" ;
    ROSSBY_RADIUS_at_ARGO:units = "km" ;
    ROSSBY_RADIUS_at_ARGO:FillValue = -999.f ;
float Ascat_daily_wind_at_ARGO(N_prof) ;
    Ascat_daily_wind_at_ARGO:long_name = "Daily Ascat wind speed module at Argo float
location" ;
    Ascat_daily_wind_at_ARGO:units = "m/s" ;
    Ascat_daily_wind_at_ARGO:FillValue = -999.f ;
float CMORPH_3h_Rain_Rate_at_ARGO(N_prof) ;
    CMORPH_3h_Rain_Rate_at_ARGO:long_name = "3-hourly CMORPH rain rate at Argo
float location" ;
    CMORPH_3h_Rain_Rate_at_ARGO:units = "mm/3h" ;
    CMORPH_3h_Rain_Rate_at_ARGO:FillValue = -999.f ;
float Ascat_10_prior_days_wind_at_ARGO(N_prof, N_DAYS_WIND) ;
    Ascat_10_prior_days_wind_at_ARGO:long_name = "Prior 10 days time series of Ascat wind
speed module at Argo float location" ;
    Ascat_10_prior_days_wind_at_ARGO:units = "m/s" ;
    Ascat_10_prior_days_wind_at_ARGO:FillValue = -999.f ;
float CMORPH_10_prior_days_Rain_Rate_at_ARGO(N_prof, N_3H_RAIN) ;
    CMORPH_10_prior_days_Rain_Rate_at_ARGO:long_name = "Prior 10 days times series of
3-hourly CMORPH Rain Rate at Argo float location" ;
    CMORPH_10_prior_days_Rain_Rate_at_ARGO:units = "mm/3h" ;
    CMORPH_10_prior_days_Rain_Rate_at_ARGO:FillValue = -999.f ;
float SSS_ISAS_at_ARGO(N_prof) ;
    SSS_ISAS_at_ARGO:long_name = "ISAS SSS (5m depth) at Argo float location" ;
    SSS_ISAS_at_ARGO:units = "1" ;
    SSS_ISAS_at_ARGO:salinity_scale = "Practical Salinity Scale(PSS-78)" ;
    SSS_ISAS_at_ARGO:standard_name = "sea_water_salinity" ;
    SSS_ISAS_at_ARGO:FillValue = -999.f ;
float SSS_PCTVAR_ISAS_at_ARGO(N_prof) ;
    SSS_PCTVAR_ISAS_at_ARGO:long_name = "Error on ISAS SSS (5m depth) at Argo float
location (% variance)" ;
    SSS_PCTVAR_ISAS_at_ARGO:units = "%" ;
    SSS_PCTVAR_ISAS_at_ARGO:FillValue = -999.f ;
float SSS_WOA13_at_ARGO(N_prof) ;
    SSS_WOA13_at_ARGO:long_name = "WOA 2013 (DECAV-1deg) SSS (0m depth) at Argo
float location" ;
    SSS_WOA13_at_ARGO:units = "1" ;
    SSS_WOA13_at_ARGO:salinity_scale = "Practical Salinity Scale(PSS-78)" ;
```



Climate Change Initiative+ (CCI+)
Phase 1
Product Validation and
Intercomparison Report

Ref.: ESA-CCI-PRGM-EOPS-SW-17-0032
Date: 07/04/2020
Version : v1.1
Page: 96 of 115



Match-up database Analyses Report

```
SSS_WOA13_at_ARGO:standard_name = "sea_surface_salinity" ;
SSS_WOA13_at_ARGO:FillValue = -999.f ;
float SSS_STD_WOA13_at_ARGO(N_prof) ;
SSS_STD_WOA13_at_ARGO:long_name = "WOA 2013 (DECAV-1deg) SSS STD (0m depth)
at Argo float location" ;
SSS_STD_WOA13_at_ARGO:units = "1" ;
SSS_STD_WOA13_at_ARGO:FillValue = -999.f ;
float SSS_ISAS15_at_ARGO(N_prof) ;
SSS_ISAS15_at_ARGO:long_name = "Monthly ISAS-15 SSS (5m depth) at Argo float loca-
tion" ;
SSS_ISAS15_at_ARGO:units = "1" ;
SSS_ISAS15_at_ARGO:salinity_scale = "Practical Salinity Scale (PSS-78)" ;
SSS_ISAS15_at_ARGO:standard_name = "sea_water_salinity" ;
SSS_ISAS15_at_ARGO:FillValue = -999.f ;
float SSS_PCTVAR_ISAS15_at_ARGO(N_prof) ;
SSS_PCTVAR_ISAS15_at_ARGO:long_name = "Error on monthly ISAS-15 SSS (5m depth)
at Argo float location (% variance)" ;
SSS_PCTVAR_ISAS15_at_ARGO:units = "%" ;
SSS_PCTVAR_ISAS15_at_ARGO:FillValue = -999.f ;
float SSS_WOA18_at_ARGO(N_prof) ;
SSS_WOA18_at_ARGO:long_name = "Monthly WOA 2018 (DECAV-1deg) SSS (0m depth)
at Argo float location" ;
SSS_WOA18_at_ARGO:units = "1" ;
SSS_WOA18_at_ARGO:salinity_scale = "Practical Salinity Scale (PSS-78)" ;
SSS_WOA18_at_ARGO:standard_name = "sea_surface_salinity" ;
SSS_WOA18_at_ARGO:FillValue = -999.f ;
float SSS_STD_WOA18_at_ARGO(N_prof) ;
SSS_STD_WOA18_at_ARGO:long_name = "Monthly WOA 2018 (DECAV-1deg) SSS STD
(0m depth) at Argo float location" ;
SSS_STD_WOA18_at_ARGO:units = "1" ;
SSS_STD_WOA18_at_ARGO:FillValue = -999.f ;
float SEA_ICE_CONCENTRATION_at_ARGO(N_prof) ;
SEA_ICE_CONCENTRATION_at_ARGO:long_name = "Daily sea ice area fraction (EU-
METSAT OSI-SAF OSI-450) at Argo float location (%)" ;
SEA_ICE_CONCENTRATION_at_ARGO:units = "1" ;
SEA_ICE_CONCENTRATION_at_ARGO:standard_name = "sea_ice_area_fraction" ;
SEA_ICE_CONCENTRATION_at_ARGO:FillValue = -999.f ;
float CCMP_6h_Wind_Speed_at_ARGO(N_prof) ;
CCMP_6h_Wind_Speed_at_ARGO:long_name = "6-hourly CCMP wind speed at Argo float
location" ;
CCMP_6h_Wind_Speed_at_ARGO:units = "m s-1" ;
CCMP_6h_Wind_Speed_at_ARGO:standard_name = "wind_speed" ;
CCMP_6h_Wind_Speed_at_ARGO:FillValue = -999.f ;
float CCMP_10_prior_days_Wind_Speed_at_ARGO(N_prof, N_DAYS_WIND_CCMP) ;
CCMP_10_prior_days_Wind_Speed_at_ARGO:long_name = "Prior 10 days time series of
CCMP wind speed at Argo float location" ;
CCMP_10_prior_days_Wind_Speed_at_ARGO:units = "m s-1" ;
CCMP_10_prior_days_Wind_Speed_at_ARGO:standard_name = "wind_speed" ;
CCMP_10_prior_days_Wind_Speed_at_ARGO:FillValue = -999.f ;
```




Climate Change Initiative+ (CCI+)
Phase 1
Product Validation and
Intercomparison Report

Ref.: ESA-CCI-PRGM-EOPS-SW-17-0032
Date: 07/04/2020
Version : v1.1
Page: 97 of 115



Match-up database Analyses Report

```
float CDM_GLOBCOLOUR_at_ARGO(N_prof) ;
    CDM_GLOBCOLOUR_at_ARGO:long_name = "8-day Coloured dissolved and detrital or-
organic materials - mean of the binned pixels at Argo float location" ;
    CDM_GLOBCOLOUR_at_ARGO:units = "m-1" ;
    CDM_GLOBCOLOUR_at_ARGO:standard_name = "volume_absorption_coefficient_of_radiative_flux_in_sea_wate
;
    CDM_GLOBCOLOUR_at_ARGO:FillValue = -999.f ;
float CHL1_GLOBCOLOUR_at_ARGO(N_prof) ;
    CHL1_GLOBCOLOUR_at_ARGO:long_name = "8-day Chlorophyll concentration - mean
of the binned pixels at Argo float location" ;
    CHL1_GLOBCOLOUR_at_ARGO:units = "mg m-3" ;
    CHL1_GLOBCOLOUR_at_ARGO:standard_name = "mass_concentration_of_chlorophyll_a_in_sea_water"
;
    CHL1_GLOBCOLOUR_at_ARGO:FillValue = -999.f ;
float EVAPORATION_OAFLUX_at_ARGO(N_prof) ;
    EVAPORATION_OAFLUX_at_ARGO:long_name = "Daily mean evaporation rate (OAFlux)
at Argo float location" ;
    EVAPORATION_OAFLUX_at_ARGO:units = "cm year-1" ;
    EVAPORATION_OAFLUX_at_ARGO:FillValue = -999.f ;
float SSS_SCRIPPS_at_ARGO(N_prof) ;
    SSS_SCRIPPS_at_ARGO:long_name = "Argo gridded monthly mean SSS (0m depth) from
SCRIPPS (Roemmich-Gilson) at Argo float location" ;
    SSS_SCRIPPS_at_ARGO:units = "1" ;
    SSS_SCRIPPS_at_ARGO:salinity_scale = "Practical Salinity Scale (PSS-78)" ;
    SSS_SCRIPPS_at_ARGO:standard_name = "sea_water_salinity" ;
    SSS_SCRIPPS_at_ARGO:FillValue = -999.f ;
float SSS_IPRC_at_ARGO(N_prof) ;
    SSS_IPRC_at_ARGO:long_name = "Argo gridded monthly mean SSS (0m depth) from
IPRC at Argo float location" ;
    SSS_IPRC_at_ARGO:units = "1" ;
    SSS_IPRC_at_ARGO:salinity_scale = "Practical Salinity Scale (PSS-78)" ;
    SSS_IPRC_at_ARGO:standard_name = "sea_water_salinity" ;
    SSS_IPRC_at_ARGO:FillValue = -999.f ;
float SST_AVHRR_at_ARGO(N_prof) ;
    SST_AVHRR_at_ARGO:long_name = "Daily OI AVHRR-only v2 SST (Reynolds et al.,
2007) at Argo float location" ;
    SST_AVHRR_at_ARGO:units = "degree Celsius" ;
    SST_AVHRR_at_ARGO:standard_name = "sea_water_temperature" ;
    SST_AVHRR_at_ARGO:FillValue = -999.f ;
float U_EKMAN_GLOBCURRENT_at_ARGO(N_prof) ;
    U_EKMAN_GLOBCURRENT_at_ARGO:long_name = "15m depth Ekman current veloc-
ity: zonal component at Argo float location" ;
    U_EKMAN_GLOBCURRENT_at_ARGO:units = "m s-1" ;
    U_EKMAN_GLOBCURRENT_at_ARGO:FillValue = -999.f ;
float V_EKMAN_GLOBCURRENT_at_ARGO(N_prof) ;
    V_EKMAN_GLOBCURRENT_at_ARGO:long_name = "15m depth Ekman current veloc-
ity: meridian component at Argo float location" ;
    V_EKMAN_GLOBCURRENT_at_ARGO:units = "m s-1" ;
    V_EKMAN_GLOBCURRENT_at_ARGO:FillValue = -999.f ;
```



Climate Change Initiative+ (CCI+)
Phase 1
Product Validation and
Intercomparison Report

Ref.: ESA-CCI-PRGM-EOPS-SW-17-0032
Date: 07/04/2020
Version : v1.1
Page: 98 of 115



Match-up database Analyses Report

```
float U_GEOSTROPHIC_GLOBCURRENT_at_ARGO(N_prof) ;
    U_GEOSTROPHIC_GLOBCURRENT_at_ARGO:long_name = "Absolute geostrophic ve-
    locity: zonal component at Argo float location" ;
    U_GEOSTROPHIC_GLOBCURRENT_at_ARGO:units = "m s-1" ;
    U_GEOSTROPHIC_GLOBCURRENT_at_ARGO:FillValue = -999.f ;
float V_GEOSTROPHIC_GLOBCURRENT_at_ARGO(N_prof) ;
    V_GEOSTROPHIC_GLOBCURRENT_at_ARGO:long_name = "Absolute geostrophic ve-
    locity: meridian component at Argo float location" ;
    V_GEOSTROPHIC_GLOBCURRENT_at_ARGO:units = "m s-1" ;
    V_GEOSTROPHIC_GLOBCURRENT_at_ARGO:FillValue = -999.f ;

// global attributes:
:Conventions = "CF-1.6" ;
:title = "ARGO Match-Up Database" ;
:Satellite_product_name = "CCI-L4-ESA-MERGED-OI-V1.5-MONTHLY" ;
:Satellite_product_spatial_resolution = "25 km" ;
:Satellite_product_temporal_resolution = "Monthly" ;
:Satellite_product_filename = "14/v01.05/monthly/2010/ESACCI-SSS-L4-SSS-MERGED-OI-Monthly-CENTRED-15Day-
25km-20100101-fv1.5.nc" ;
:Match-Up_spatial_window_radius_in_km = 12.5;
:Match-Up_temporal_window_radius_in_days = 7.5;
:start_time = "20100114T000005Z" ;
:stop_time = "20100118T235026Z" ;
:northernmost_latitude = 77.676f ;
:southernmost_latitude = -66.423f ;
:westernmost_longitude = -179.219f ;
:easternmost_longitude = 179.199f ;
:geospatial_lat_units = "degrees north" ;
:geospatial_lat_resolution = "25 km" ;
:geospatial_lon_units = "degrees east" ;
:geospatial_lon_resolution = "25 km" ;
:institution = "ESA-IFREMER-ODL" ;
:project_name = "SMOS Pilote Mission Exploitation Platfrom (Pi-MEP) for salinity" ;
:project_url = "https://pimep-project.odl.bzh" ;
:license = "Pi-MEP data use is free and open" ;
:product_version = "1.0" ;
:keywords = "Oceans > Ocean Salinity > Sea Surface Salinity" ;
:acknowledgment = "Please acknowledge the use of these data with the following statement:
These data were provided by SMOS Pilote Mission Exploitation Platfrom (Pi-MEP) for salinity"
;
;
:SOURCE = "14/v01.05/monthly/2010/ESACCI-SSS-L4-SSS-MERGED-OI-Monthly-CENTRED-15Day-25km-20100101-fv1.5.nc"
;
;
:In_situ_data_source = "ftp://ftp.ifremer.fr/ifremer/argo/geo/" ;
:references = "https://pimep-project.odl.bzh" ;
:history = "Processed on 2018-04-18 using MDB.generator" ;
:date_created = "2018-04-18 17:09:30" ;
}
```

2.5 MDB characteristics for the particular in situ/satellite pairs

2.5.1 Number of paired SSS data as a function of time and distance to coast

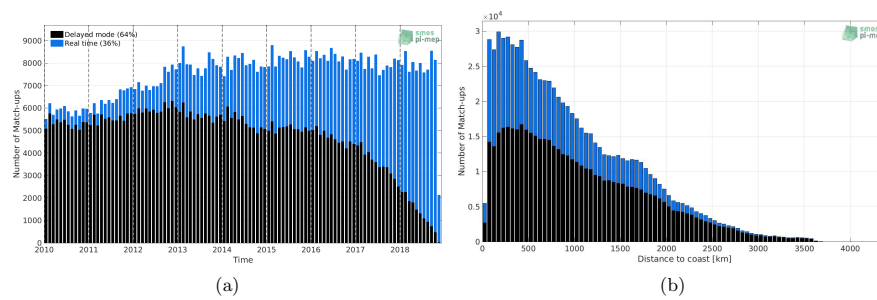


Figure 1: Number of match-ups between Argo and CCI-L4-ESA-MERGED-OI-V1.5-MONTHLY SSS as a function of time (a) and as function of the distance to coast (b) over the Global Ocean Pi-MEP region and for the full satellite product period.

2.5.2 Histograms of the SSS match-ups

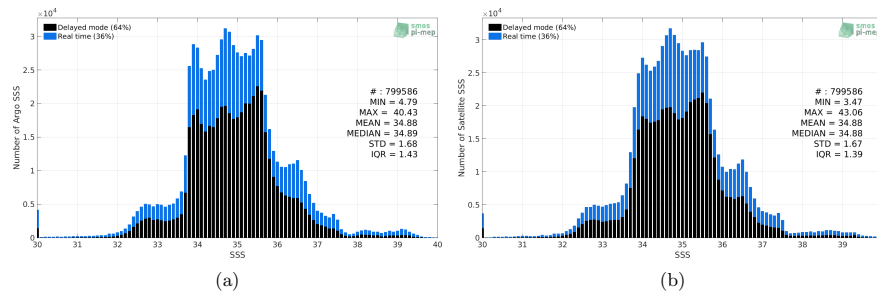


Figure 2: Histograms of SSS from Argo (a) and CCI-L4-ESA-MERGED-OI-V1.5-MONTHLY (b) considering all match-up pairs per bins of 0.1 over the Global Ocean Pi-MEP region and for the full satellite product period.

2.5.3 Distribution of in situ SSS depth measurements

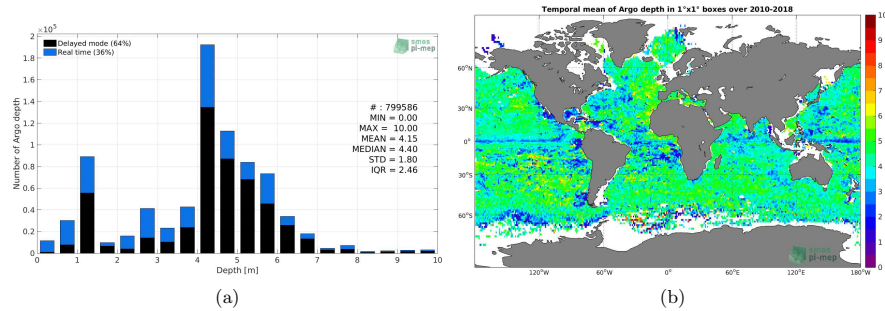


Figure 3: Histograms of the depth of the upper level SSS measurements from Argo in the Match-up DataBase for the Global Ocean Pi-MEP region (a) and temporal mean spatial distribution of pressure of the in situ SSS data over $1^\circ \times 1^\circ$ boxes and for the full satellite product period (b).

2.5.4 Spatial Distribution of Match-ups

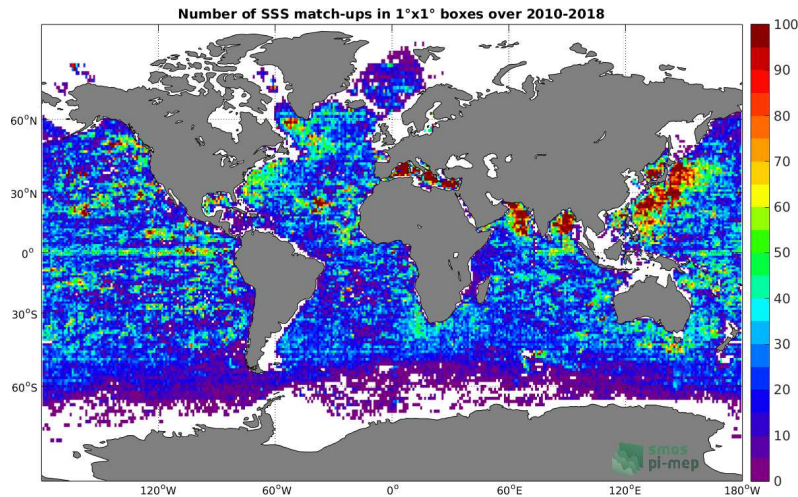


Figure 4: Number of SSS match-ups between Argo SSS and the CCI-L4-ESA-MERGED-OL-V1.5-MONTHLY SSS product for the Global Ocean Pi-MEP region over $1^\circ \times 1^\circ$ boxes and for the full satellite product period.



**Climate Change Initiative+ (CCI+)
Phase 1
Product Validation and
Intercomparison Report**

Ref.: ESA-CCI-PRGM-EOPS-SW-17-0032
Date: 07/04/2020
Version : v1.1
Page: 101 of 115



Match-up database Analyses Report

2.5.5 Histograms of the spatial and temporal lags of the match-ups pairs

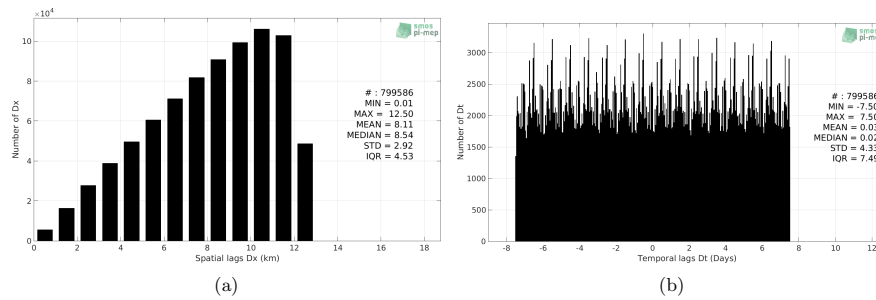


Figure 5: Histograms of the spatial (a) and temporal (b) lags between the time of the Argo measurements and the date of the corresponding CCI-L4-ESA-MERGED-OI-V1.5-MONTHLY SSS product.

3 MDB file Analyses

3.1 Spatial Maps of the Temporal mean and Std of in situ and satellite SSS and of the difference (Δ SSS)

In Figure 6, we show maps of temporal mean (left) and standard deviation (right) of the CCI-L4-ESA-MERGED-OI-V1.5-MONTHLY satellite SSS product (top) and of the Argo in situ dataset at the collected Pi-MEP match-up pairs. The temporal mean and std are gridded over the full satellite product period and over spatial boxes of size $1^\circ \times 1^\circ$.

At the bottom of Figure 6, the temporal mean (left) and standard deviation (right) of the differences between the satellite SSS product and in situ data found at match-up pairs, namely Δ SSS(Satellite -Argo), is also gridded over the full satellite product period and over spatial boxes of size $1^\circ \times 1^\circ$.

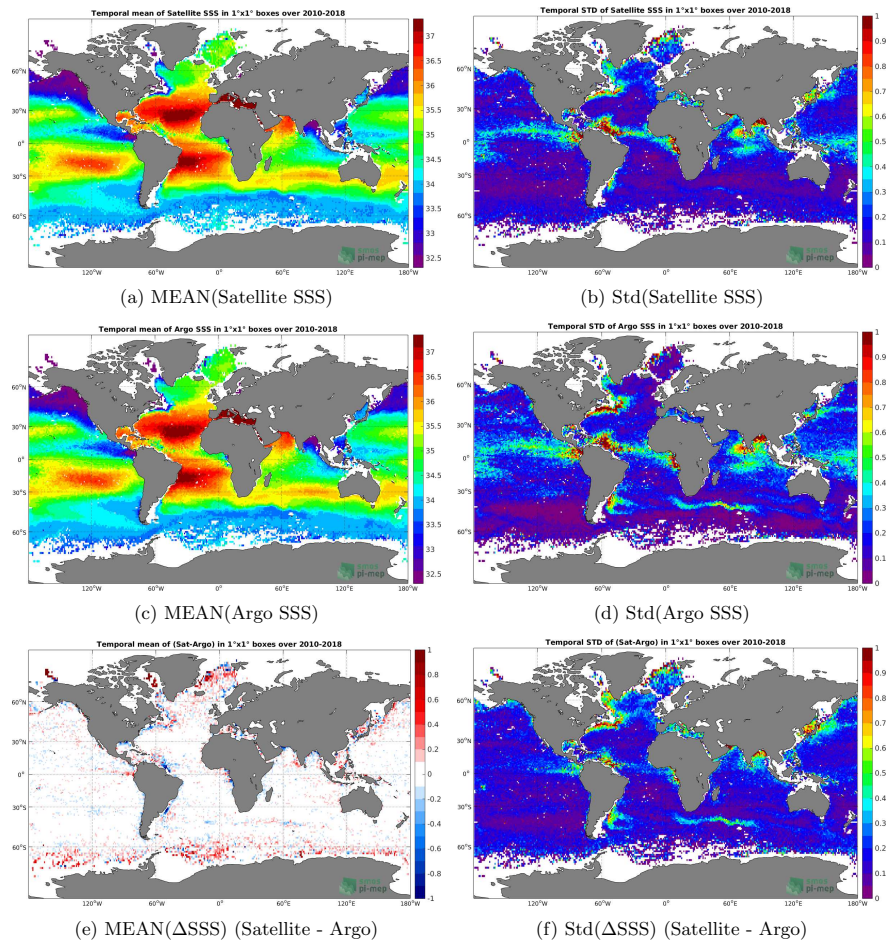


Figure 6: Temporal mean (left) and Std (right) of SSS from CCI-L4-ESA-MERGED-OI-V1.5-MONTHLY (top), Argo (middle), and of Δ SSS (Satellite - Argo). Only match-up pairs are used to generate these maps.

3.2 Time series of the monthly averaged mean and Std of in situ and satellite SSS and of the (Δ SSS)

In the top panel of Figure 7, we show the time series of the monthly averaged SSS estimated over the full Global Ocean Pi-MEP region for both CCI-L4-ESA-MERGED-OI-V1.5-MONTHLY satellite SSS product (in black) and the Argo in situ dataset (in blue) at the collected Pi-MEP match-up pairs.

In the middle panel of Figure 7, we show the time series of the monthly averaged ΔSSS (Satellite - Argo) for the collected Pi-MEP match-up pairs and estimated over the full Global Ocean Pi-MEP region.

In the bottom panel of Figure 7, we show the time series of the monthly averaged standard deviation of the ΔSSS (Satellite - Argo) for the collected Pi-MEP match-up pairs and estimated over the full Global Ocean Pi-MEP region.

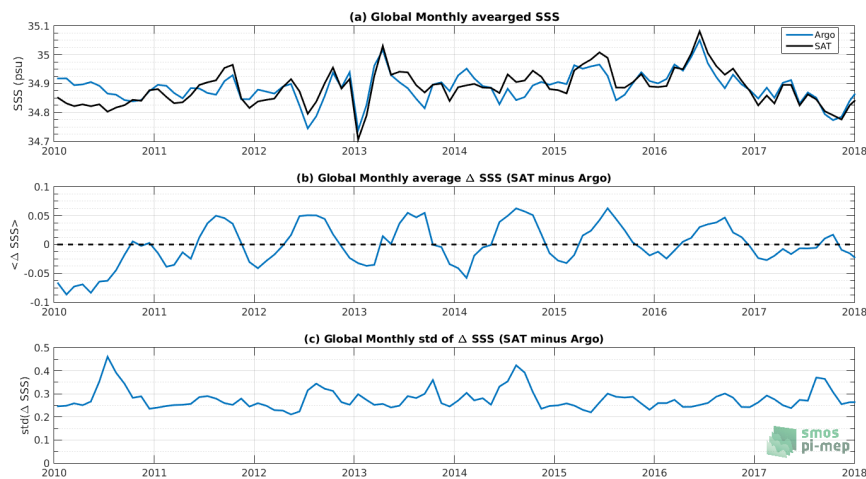


Figure 7: Time series of the monthly averaged mean SSS (top), mean ΔSSS (Satellite - Argo) and Std of ΔSSS (Satellite - Argo) over the Global Ocean Pi-MEP region considering all match-ups collected by the Pi-MEP platform.

3.3 Zonally-averaged Time-mean and temporal Std of in situ and satellite SSS and of the ΔSSS

In Figure 8 left panel, we show the zonally averaged time-mean SSS estimated at the collected Pi-MEP match-up pairs for both CCI-L4-ESA-MERGED-OI-V1.5-MONTHLY satellite SSS product (in black) and the Argo in situ dataset (in blue). The time mean is evaluated over the full satellite SSS product period.

In the right panel of Figure 8, we show the zonally averaged time-mean ΔSSS (Satellite - Argo) for all the collected Pi-MEP match-up pairs estimated over the full satellite product period.



**Climate Change Initiative+ (CCI+)
Phase 1
Product Validation and
Intercomparison Report**

Ref.: ESA-CCI-PRGM-EOPS-SW-17-0032
Date: 07/04/2020
Version : v1.1
Page: 104 of 115



Match-up database Analyses Report

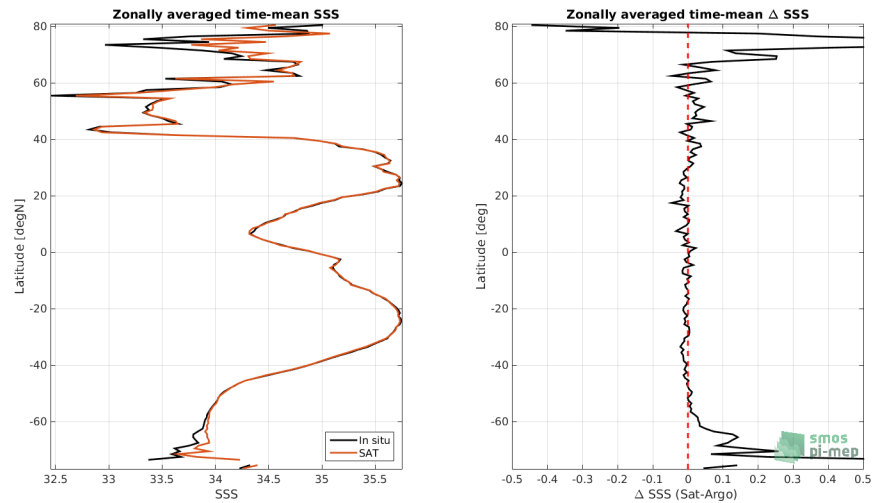


Figure 8: Left panel: Zonally averaged time mean SSS from CCI-L4-ESA-MERGED-OI-V1.5-MONTHLY (black) and from Argo (blue). Right panel: zonally averaged time-mean Δ SSS (Satellite - Argo) for all the collected Pi-MEP match-up pairs estimated over the full satellite product period.

3.4 Scatterplots of satellite vs in situ SSS by latitudinal bands

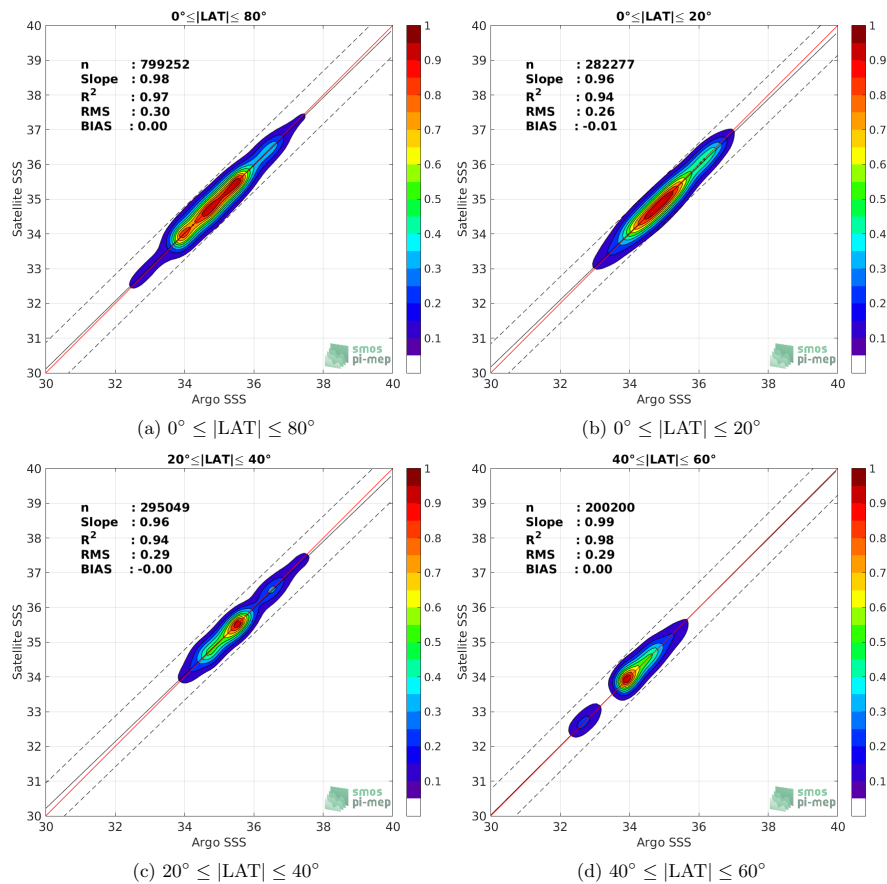


Figure 9: Contour maps of the concentration of CCI-L4-ESA-MERGED-OI-V1.5-MONTHLY SSS (y-axis) versus Argo SSS (x-axis) at match-up pairs for different latitude bands. For each plot, the red line shows $x=y$. The black thin and dashed lines indicate a linear fit through the data cloud and the $\pm 95\%$ confidence levels, respectively. The number match-up pairs n , the slope and R^2 coefficient of the linear fit, the root mean square (RMS) and the mean bias between satellite and in situ data are indicated for each latitude band in each plots.

3.5 Time series of the monthly averaged mean and Std of the Δ SSS sorted by latitudinal bands

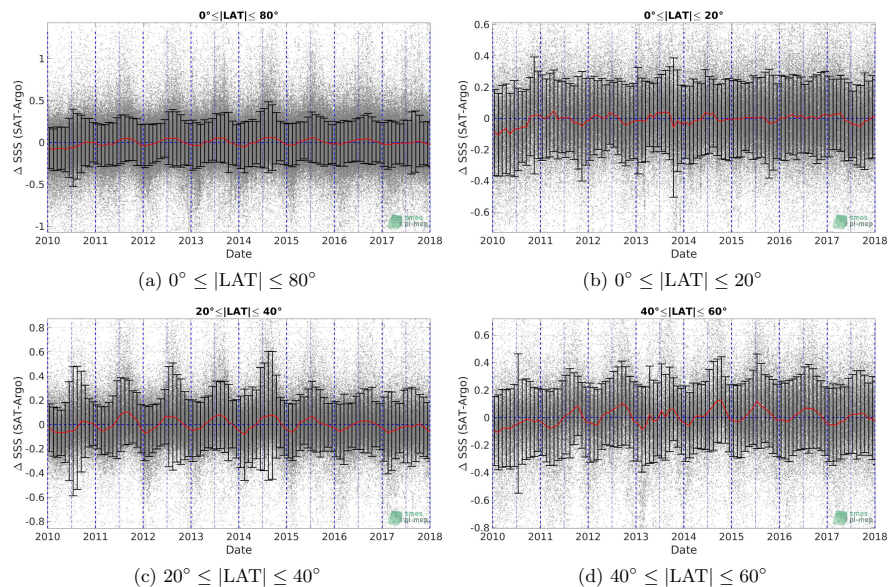


Figure 10: Monthly-average mean (red curves) Δ SSS (Satellite - Argo) and ± 1 Std (black vertical thick bars) as function of time for all the collected Pi-MEP match-up pairs estimated over the Global Ocean Pi-MEP region and for the full satellite product period are shown for different latitude bands: (a) Latitude band 80°S-80°N, (b) latitude band 20°S-20°N, (c) Mid Latitude bands 40°S-20°S and 20°N-40°N and (d) Latitude bands 60°S-40°S and 40°N-60°N.

3.6 Δ SSS sorted as function of geophysical parameters

In Figure 11, we classify the match-up differences Δ SSS (Satellite - in situ) between CCI-L4-ESA-MERGED-OI-V1.5-MONTHLY and Argo SSS as function of the geophysical conditions at match-up points. The mean and std of Δ SSS (Satellite - Argo) is thus evaluated as function of the

- in situ SSS values per bins of width 0.2,
- in situ SST values per bins of width 1°C,
- ASCAT daily wind values per bins of width 1 m/s,
- CMORPH 3-hourly rain rates per bins of width 1 mm/h, and,
- distance to coasts per bins of width 50 km.



Match-up database Analyses Report

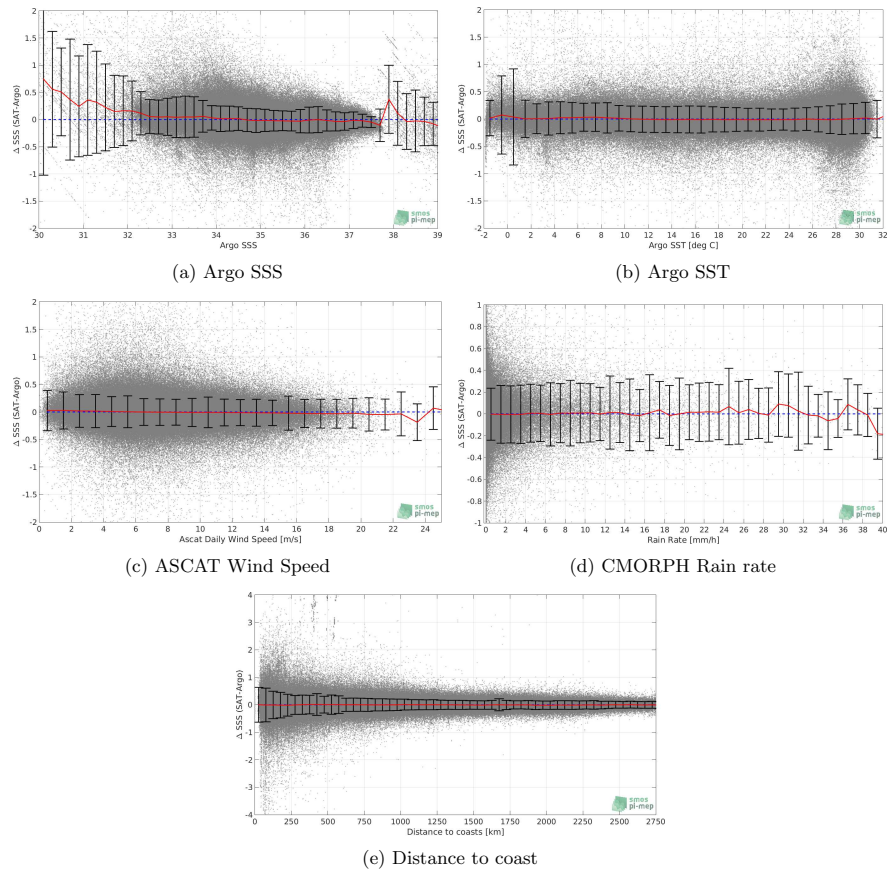


Figure 11: Δ SSS (Satellite - Argo) sorted as function of Argo SSS a), Argo SST b), ASCAT Wind speed c), CMORPH rain rate d) and distance to coast (e). In all plots the mean and Std of Δ SSS for each bin is indicated by the red curves and black vertical thick bars (± 1 Std)

3.7 Δ SSS maps and statistics for different geophysical conditions

In Figures 12 and 13, we focus on sub-datasets of the match-up differences Δ SSS (Satellite - in situ) between CCI-L4-ESA-MERGED-OI-V1.5-MONTHLY and Argo for the following specific geophysical conditions:

- **C1**:if the local value at in situ location of estimated rain rate is zero, mean daily wind is in the range [3, 12] m/s, the SST is $> 5^{\circ}\text{C}$ and distance to coast is > 800 km.
- **C2**:if the local value at in situ location of estimated rain rate is zero, mean daily wind is in the range [3, 12] m/s.

- **C3**:if the local value at in situ location of estimated rain rate is high (ie. > 1 mm/h) and mean daily wind is low (ie. < 4 m/s).
- **C4**:if the mixed layer is shallow with depth < 20 m.
- **C5**:if the in situ data is located where the climatological SSS standard deviation is low (ie. above < 0.2).
- **C6**:if the in situ data is located where the climatological SSS standard deviation is high (ie. above > 0.2).

For each of these conditions, the temporal mean (gridded over spatial boxes of size $1^\circ \times 1^\circ$) and the histogram of the difference Δ SSS (Satellite - in situ) are presented.

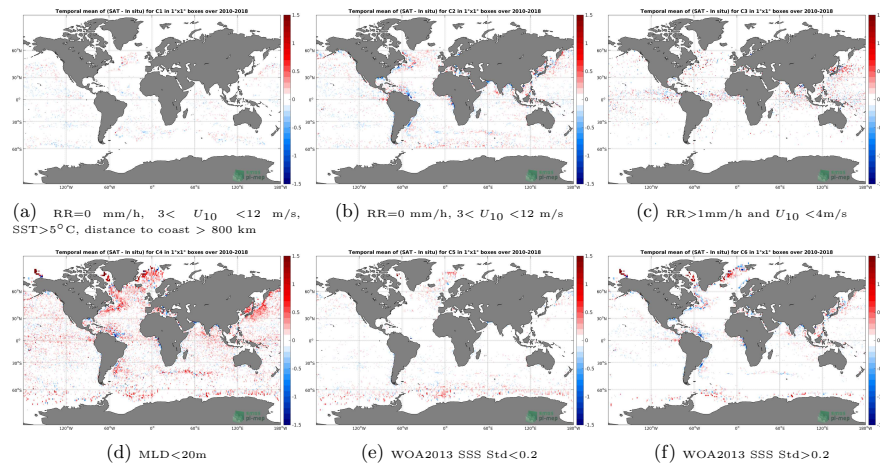


Figure 12: Temporal mean gridded over spatial boxes of size $1^\circ \times 1^\circ$ of Δ SSS (CCI-L4-ESAMERGED-OI-V1.5-MONTHLY - Argo) for 6 different subdatasets corresponding to:RR=0 mm/h, $3 < U_{10} < 12$ m/s, SST $>5^\circ$ C, distance to coast > 800 km (a), RR=0 mm/h, $3 < U_{10} < 12$ m/s (b), RR >1 mm/h and $U_{10} < 4$ m/s (c),MLD <20 m (d),WOA2013 SSS Std <0.2 (e),WOA2013 SSS Std >0.2 (f).

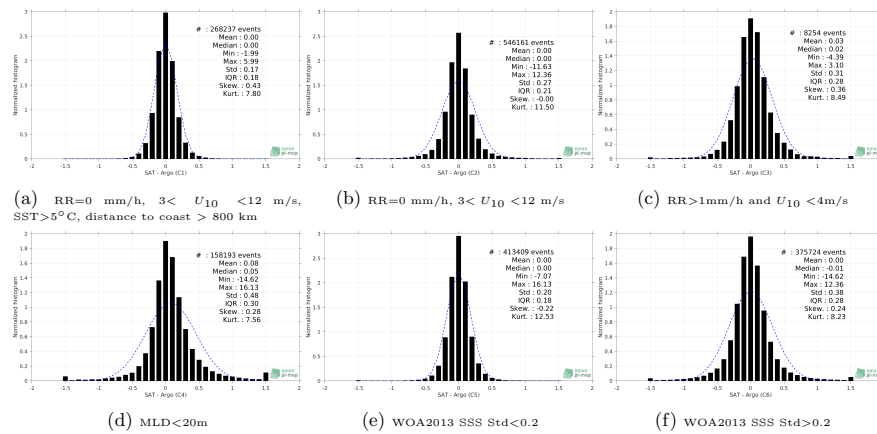


Figure 13: Normalized histogram of Δ SSS (CCI-L4-ESA-MERGED-OI-V1.5-MONTHLY - Argo) for 6 different subdatasets corresponding to: RR=0 mm/h, $3 < U_{10} < 12$ m/s, SST > 5°C, distance to coast > 800 km (a), RR=0 mm/h, $3 < U_{10} < 12$ m/s (b), RR > 1mm/h and $U_{10} < 4$ m/s (c), MLD < 20m (d), WOA2013 SSS Std < 0.2 (e), WOA2013 SSS Std > 0.2 (f).

4 Summary

Table 1 shows the mean, median, standard deviation (Std), root mean square (RMS), interquartile range (IQR), correlation coefficient (r^2) and robust standard deviation (Std*) of the match-up differences Δ SSS (Satellite - in situ) between CCI-L4-ESA-MERGED-OI-V1.5-MONTHLY and Argo derived over the Global Ocean Pi-MEP region and for the full satellite product period and for the following conditions:

- all: All the match-up pairs satellite/in situ SSS are used to derive the statistics
- C1: only pairs where RR=0 mm/h, $3 < U_{10} < 12$ m/s, SST > 5°C, distance to coast > 800 km
- C2: only pairs where RR=0 mm/h, $3 < U_{10} < 12$ m/s
- C3: only pairs where RR > 1mm/h and $U_{10} < 4$ m/s
- C4: only pairs where MLD < 20m
- C5: only pairs where WOA2013 SSS Std < 0.2
- C6: only pairs at WOA2013 SSS Std > 0.2
- C7a: only pairs where distance to coast is < 150 km.
- C7b: only pairs where distance to coast is in the range [150, 800] km.
- C7c: only pairs where distance to coast is > 800 km.
- C8a: only pairs where in situ SST is < 5°C.



**Climate Change Initiative+ (CCI+)
Phase 1
Product Validation and
Intercomparison Report**

Ref.: ESA-CCI-PRGM-EOPS-SW-17-0032
Date: 07/04/2020
Version : v1.1
Page: 110 of 115



Match-up database Analyses Report

- C8b: only pairs where in situ SST is in the range [5, 15]°C.
- C8c: only pairs where in situ SST is > 15°C.
- C9a: only pairs where in situ SSS is < 33.
- C9b: only pairs where in situ SSS is in the range [33, 37].
- C9c: only pairs where in situ SSS is > 37.

Table 1: Statistics of Δ SSS (Satellite - Argo)

Condition	#	Median	Mean	Std	RMS	IQR	r ²	Std*
all	799586	0.00	0.00	0.30	0.30	0.22	0.97	0.17
C1	268237	0.00	0.00	0.17	0.17	0.18	0.97	0.13
C2	546161	0.00	0.00	0.27	0.27	0.21	0.97	0.16
C3	8254	0.02	0.03	0.31	0.31	0.28	0.96	0.21
C4	158193	0.05	0.08	0.48	0.49	0.30	0.97	0.22
C5	413409	0.00	0.00	0.20	0.20	0.18	0.97	0.14
C6	375724	-0.01	0.00	0.38	0.38	0.28	0.97	0.21
C7a	61651	-0.01	-0.02	0.57	0.57	0.40	0.98	0.30
C7b	338211	0.00	0.01	0.34	0.34	0.25	0.94	0.19
C7c	399093	0.00	0.00	0.18	0.18	0.19	0.97	0.14
C8a	55941	0.02	0.05	0.47	0.47	0.26	0.84	0.20
C8b	159673	0.00	0.00	0.27	0.27	0.22	0.98	0.17
C8c	583640	-0.01	0.00	0.28	0.28	0.22	0.96	0.16
C9a	42529	0.08	0.16	0.67	0.68	0.35	0.98	0.26
C9b	720774	0.00	-0.01	0.25	0.25	0.22	0.92	0.16
C9c	36283	-0.02	-0.02	0.39	0.39	0.26	0.79	0.19

Table 2 presents statistics of Δ SSS (Satellite - Argo) as Table 1 but for Argo delayed mode only.

Table 2: Statistics of Δ SSS (Satellite - Argo) - Delayed mode

Condition	#	Median	Mean	Std	RMS	IQR	r ²	Std*
all	509675	0.00	0.00	0.25	0.25	0.21	0.96	0.16
C1	186489	0.00	0.00	0.16	0.16	0.18	0.97	0.13
C2	348988	0.00	0.00	0.24	0.24	0.20	0.97	0.15
C3	5040	0.01	0.03	0.28	0.28	0.26	0.95	0.20
C4	91522	0.04	0.05	0.40	0.40	0.27	0.96	0.20
C5	283946	0.00	0.00	0.19	0.19	0.18	0.97	0.13
C6	218757	-0.01	0.00	0.32	0.32	0.26	0.96	0.20
C7a	30490	0.00	-0.02	0.56	0.56	0.36	0.98	0.27
C7b	200829	0.00	0.00	0.28	0.28	0.23	0.94	0.17
C7c	277856	0.00	0.00	0.17	0.17	0.18	0.97	0.14
C8a	34673	0.02	0.02	0.28	0.28	0.25	0.71	0.18
C8b	109674	0.01	0.01	0.24	0.24	0.20	0.97	0.15
C8c	365251	-0.01	-0.01	0.26	0.26	0.21	0.96	0.15
C9a	21585	0.06	0.08	0.47	0.48	0.30	0.98	0.22
C9b	472734	0.00	0.00	0.23	0.23	0.20	0.92	0.15
C9c	15356	-0.04	-0.05	0.37	0.38	0.24	0.79	0.18



Climate Change Initiative+ (CCI+)
Phase 1
Product Validation and
Intercomparison Report

Ref.: ESA-CCI-PRGM-EOPS-SW-17-0032
Date: 07/04/2020
Version : v1.1
Page: 111 of 115



Match-up database Analyses Report

For the same conditions, Table 3 presents statistics of Δ SSS (Satellite - ISAS). Only ISAS SSS values with PCTVAR<80% are used to derive the statistics.

Table 3: Statistics of Δ SSS (Satellite - ISAS)

Condition	#	Median	Mean	Std	RMS	IQR	r ²	Std*
all	787870	0.00	0.00	0.25	0.25	0.18	0.96	0.14
C1	266574	0.00	0.00	0.13	0.13	0.14	0.98	0.11
C2	540000	0.00	0.00	0.24	0.24	0.18	0.96	0.13
C3	8174	0.00	0.01	0.26	0.26	0.23	0.94	0.17
C4	154114	0.03	0.04	0.40	0.40	0.24	0.93	0.18
C5	409374	0.00	0.00	0.18	0.18	0.15	0.97	0.11
C6	369916	0.00	0.00	0.31	0.31	0.23	0.94	0.17
C7a	57750	0.00	-0.01	0.54	0.54	0.36	0.93	0.27
C7b	334170	0.00	0.01	0.27	0.27	0.21	0.95	0.16
C7c	395950	0.00	0.00	0.14	0.14	0.15	0.98	0.11
C8a	53470	0.01	0.01	0.33	0.33	0.24	0.71	0.18
C8b	156480	0.00	0.00	0.22	0.22	0.19	0.95	0.14
C8c	577592	0.00	0.00	0.25	0.25	0.18	0.95	0.13
C9a	38478	0.03	0.03	0.49	0.49	0.30	0.60	0.23
C9b	713282	0.00	0.00	0.22	0.22	0.18	0.94	0.13
C9c	36110	0.00	0.01	0.37	0.37	0.23	0.81	0.17

Numerical values can be downloaded as csv files for [Table 1](#), [Table 2](#) and [Table 3](#).

References

- Argo. Argo float data and metadata from Global Data Assembly Centre (Argo GDAC), 2000. doi: [10.17882/42182](https://doi.org/10.17882/42182).
- Abderrahim Bentamy and Denis Croize Fillon. Gridded surface wind fields from Metop/ASCAT measurements. *Int. J. Remote Sens.*, 33(6):1729–1754, March 2012. ISSN 1366-5901. doi: [10.1080/01431161.2011.600348](https://doi.org/10.1080/01431161.2011.600348).
- Abderrahim Bentamy, Semyon A. Grodsky, James A. Carton, Denis Croizé-Fillon, and Bertrand Chapron. Matching ASCAT and QuikSCAT winds. *J. Geophys. Res.*, 117(C2), February 2012. ISSN 0148-0227. doi: [10.1029/2011JC007479](https://doi.org/10.1029/2011JC007479). C02011.
- Jaqueline Boutin, Y. Chao, W. E. Asher, T. Delcroix, R. Drucker, K. Drushka, N. Kolodziejczyk, T. Lee, N. Reul, G. Reverdin, J. Schanze, A. Soloviev, L. Yu, J. Anderson, L. Brucker, E. Dinnat, A. S. Garcia, W. L. Jones, C. Maes, T. Meissner, W. Tang, N. Vinogradova, and B. Ward. Satellite and In Situ Salinity: Understanding Near-Surface Stratification and Sub-footprint Variability. *Bull. Am. Meteorol. Soc.*, 97(8):1391–1407, 2016. ISSN 1520-0477. doi: [10.1175/bams-d-15-00032.1](https://doi.org/10.1175/bams-d-15-00032.1).
- Clément de Boyer Montégut, Gurvan Madec, A. S. Fischer, A. Lazar, and D. Ludicone. Mixed layer depth over the global ocean: An examination of profile data and a profile-based climatology. *J. Geophys. Res.*, 109(C12):C12003, December 2004. ISSN 0148-0227. doi: [10.1029/2004jc002378](https://doi.org/10.1029/2004jc002378).
- Clément de Boyer Montégut, Juliette Mignot, Alban Lazar, and Sophie Cravatte. Control of salinity on the mixed layer depth in the world ocean: 1. General description. *J. Geophys. Res.*, 112(C6):C06011, June 2007. ISSN 0148-0227. doi: [10.1029/2006jc003953](https://doi.org/10.1029/2006jc003953).



Climate Change Initiative+ (CCI+)
Phase 1
Product Validation and
Intercomparison Report

Ref.: ESA-CCI-PRGM-EOPS-SW-17-0032
Date: 07/04/2020
Version : v1.1
Page: 112 of 115



Match-up database Analyses Report

- Ralph R. Ferraro. SSM/I derived global rainfall estimates for climatological applications. *J. Geophys. Res.*, 1021:16715–16736, 07 1997. doi: [10.1029/97JD01210](https://doi.org/10.1029/97JD01210).
- Ralph R. Ferraro, Fuzhong Weng, Norman C. Grody, and Limin Zhao. Precipitation characteristics over land from the NOAA-15 AMSU sensor. *Geophys. Res. Lett.*, 27(17):2669–2672, 2000. doi: [10.1029/2000GL011665](https://doi.org/10.1029/2000GL011665).
- Fabienne Gaillard, E. Autret, V. Thierry, P. Galaup, C. Coatanoan, and T. Loubrieu. Quality Control of Large Argo Datasets. *J. Atmos. Oceanic Technol.*, 26(2):337–351, 2012/10/10 2009. doi: [10.1175/2008JTECHO552.1](https://doi.org/10.1175/2008JTECHO552.1).
- Fabienne Gaillard, Thierry Reynaud, Virginie Thierry, Nicolas Kolodziejczyk, and Karina von Schuckmann. In Situ-Based Reanalysis of the Global Ocean Temperature and Salinity with ISAS: Variability of the Heat Content and Steric Height. *J. Clim.*, 29(4):1305–1323, February 2016. ISSN 1520-0442. doi: [10.1175/jcli-d-15-0028.1](https://doi.org/10.1175/jcli-d-15-0028.1).
- Robert J. Joyce, John E. Janowiak, Phillip A. Arkin, and Pingping Xie. CMORPH: A Method that Produces Global Precipitation Estimates from Passive Microwave and Infrared Data at High Spatial and Temporal Resolution. *J. Hydrometeorol.*, 5(3):487–503, June 2004. ISSN 1525-7541. doi: [10.1175/1525-7541\(2004\)005\(0487:camtpg\)2.0.co;2](https://doi.org/10.1175/1525-7541(2004)005(0487:camtpg)2.0.co;2).
- Nicolas Kolodziejczyk, Gilles Reverdin, and Alban Lazar. Interannual Variability of the Mixed Layer Winter Convection and Spice Injection in the Eastern Subtropical North Atlantic. *J. Phys. Oceanogr.*, 45(2):504–525, Feb 2015. ISSN 1520-0485. doi: [10.1175/jpo-d-14-0042.1](https://doi.org/10.1175/jpo-d-14-0042.1).
- Christian Kummerow, Y. Hong, W. S. Olson, S. Yang, R. F. Adler, J. McCollum, R. Ferraro, G. Petty, D-B. Shin, and T. T. Wilheit. The Evolution of the Goddard Profiling Algorithm (GPROF) for Rainfall Estimation from Passive Microwave Sensors. *J. Appl. Meteorol.*, 40(11):1801–1820, 2001. doi: [10.1175/1520-0450\(2001\)040\(1801:TEOTGP\)2.0.CO;2](https://doi.org/10.1175/1520-0450(2001)040(1801:TEOTGP)2.0.CO;2).



Annex B: Pi-MEP Satellite precision comparison against Argo

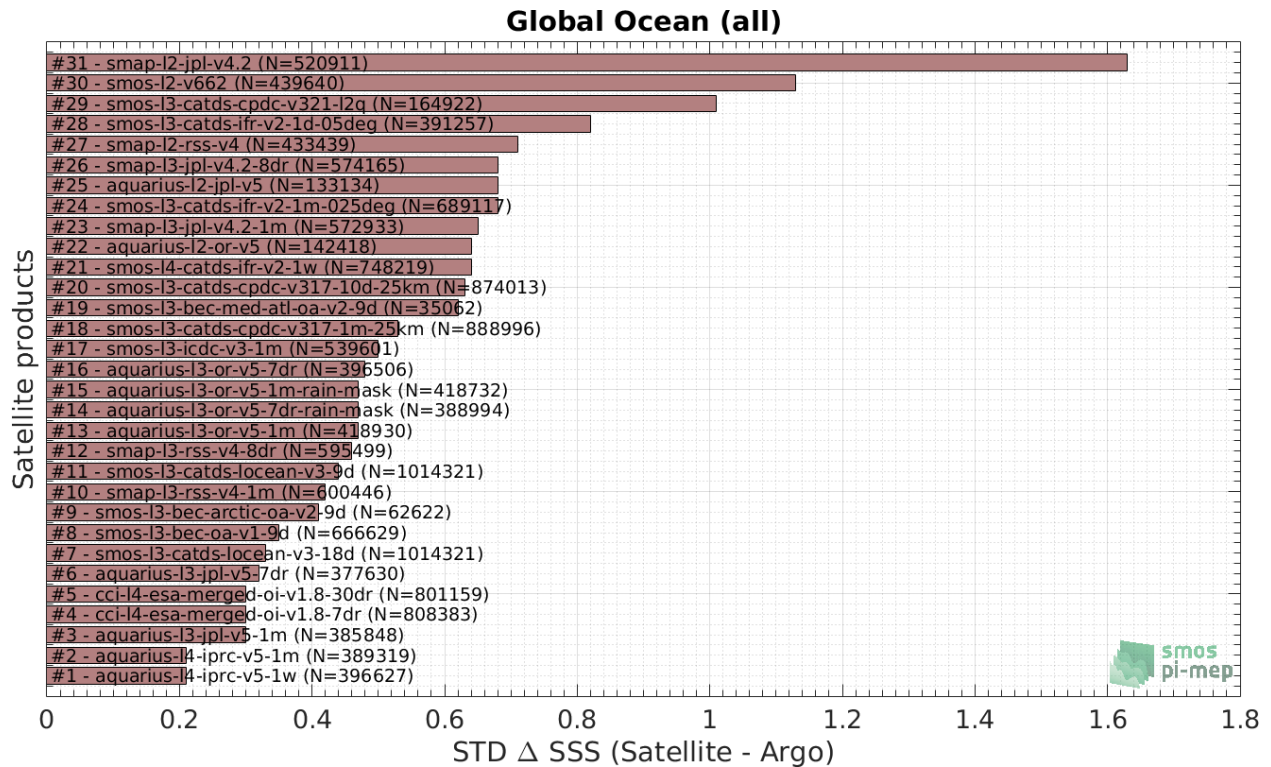


Figure 45: Pi-MEP comparison of satellite precision (standard deviation) against Argo of a wide range of satellite products.

Annex C: Pi-MEP

Below are reproduced Figure 3 and 4 of Pi-MEP Match-up report with moorings for the:

- Weekly: https://pimep.ifremer.fr/diffusion/analyses/mdb-database/GO/cci-l4-esa-merged-oi-v1.8-7dr/mooring/report/pimep-mdb-report_GO_cci-l4-esa-merged-oi-v1.8-7dr_mooring_20190915.pdf
- Monthly: https://pimep.ifremer.fr/diffusion/analyses/mdb-database/GO/cci-l4-esa-merged-oi-v1.8-30dr/mooring/report/pimep-mdb-report_GO_cci-l4-esa-merged-oi-v1.8-30dr_mooring_20190915.pdf

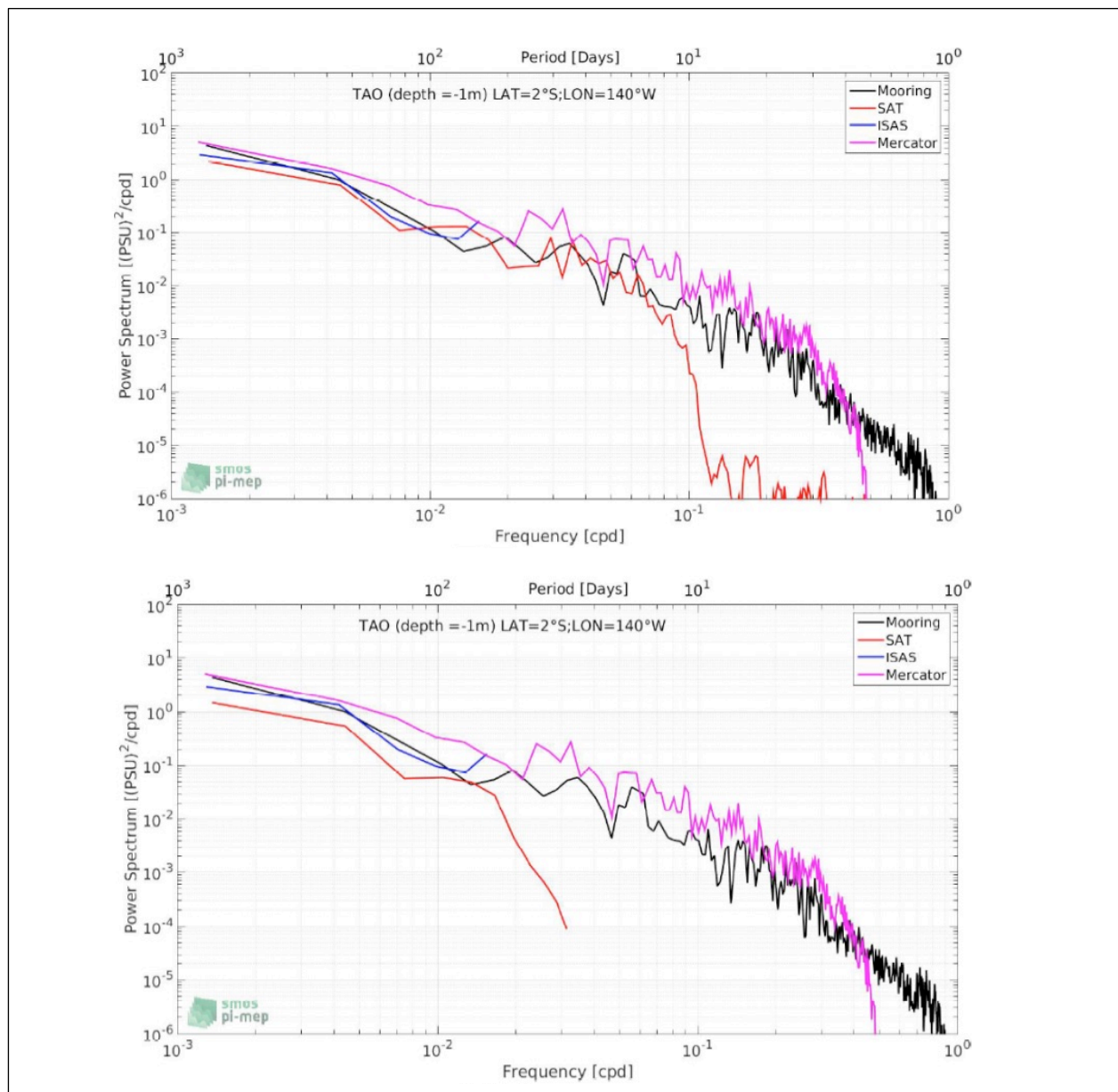


Figure 46: Pi-MEP CCI comparison report with moorings. Power spectrum of SSS from moorings, CCI (top; weekly), (bottom; monthly) products, ISAS and Mercator for the TAO mooring/match-up time series at 2°S; 140°W.

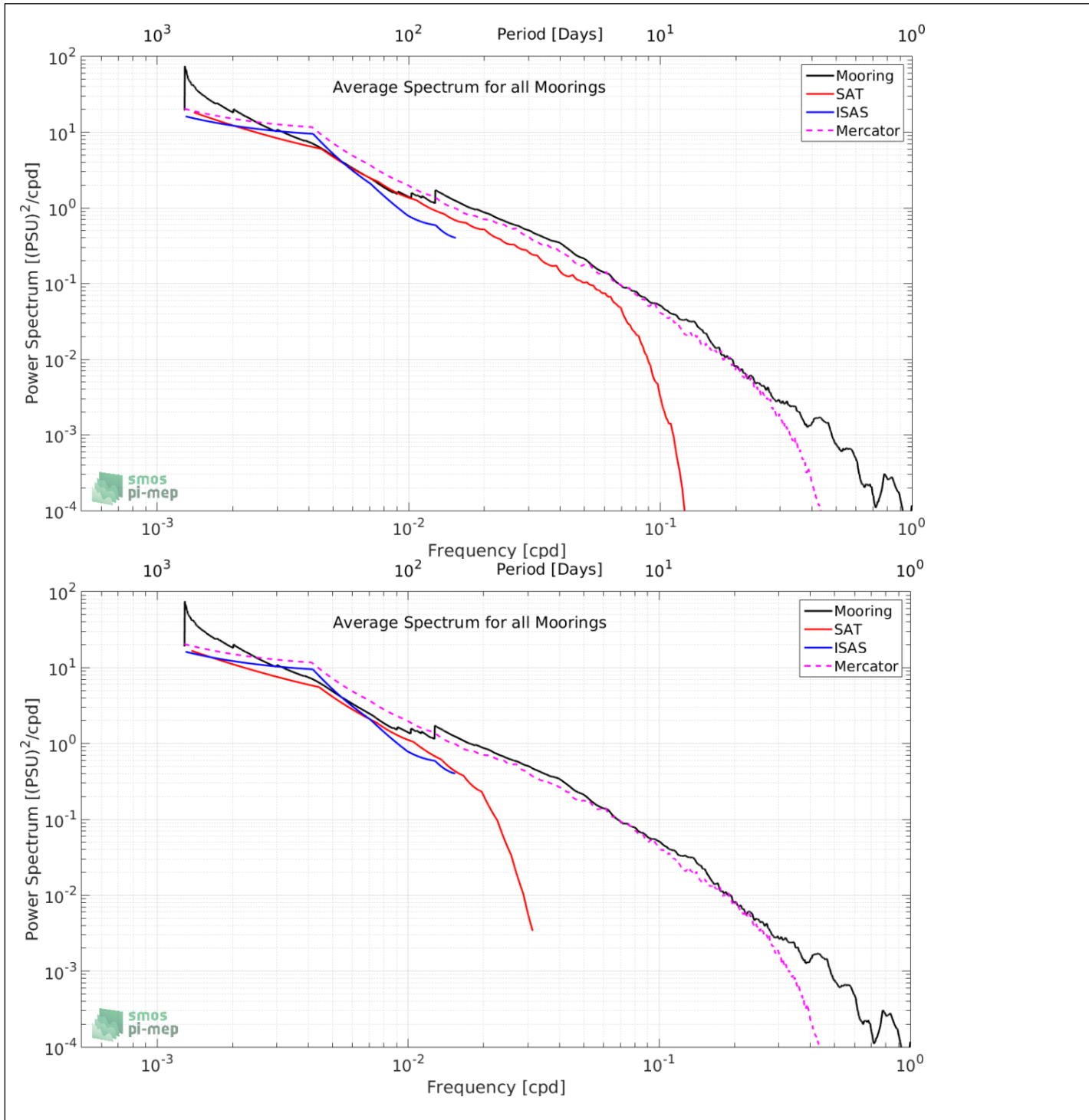


Figure 47: Pi-MEP CCI comparison report with moorings. Average of all SSS power spectra for all moorings/match-up from moorings, CCI (top; weekly), (bottom; monthly) products, ISAS and Mercator.